SPRINGER BRIEFS IN PHYSICS

Francesco Knechtli
Michael Günther
Michael Peardon

# Lattice Quantum Chromodynamics

## Practical Essentials

Springer

# SpringerBriefs in Physics

More information about this series at http://www.springer.com/series/8902

Francesco Knechtli · Michael Günther
Michael Peardon

# Lattice Quantum Chromodynamics

## Practical Essentials

Springer

Francesco Knechtli
Department of Physics, School of Mathematics and Natural Sciences
University of Wuppertal
Wuppertal
Germany

Michael Günther
Department of Mathematics, School of Mathematics and Natural Sciences
University of Wuppertal
Wuppertal
Germany

Michael Peardon
School of Mathematics
Trinity College Dublin
Dublin 2
Ireland

ISSN 2191-5423 ISSN 2191-5431 (electronic)
SpringerBriefs in Physics
ISBN 978-94-024-0997-0 ISBN 978-94-024-0999-4 (eBook)
DOI 10.1007/978-94-024-0999-4

Library of Congress Control Number: 2016954543



Printed on acid-free paper

This Springer imprint is published by Springer Nature
The registered company is Springer Science+Business Media B.V.
The registered company address is: Van Godewijckstraat 30, 3311 GX Dordrecht, The Netherlands

*To our wives and children*

# Preface

More than 40 years after its invention, lattice field theory has developed into an interdisciplinary research area, with close connections between physics, mathematics and informatics. Monte Carlo simulations of lattice Quantum Chromodynamics (QCD) describe the physics of hadrons from their constituents: quarks and gluons. These studies are computationally challenging. In this book we provide an overview of the techniques central to lattice QCD, including modern developments. The book has four chapters. The first chapter explains the formulation of quarks and gluons on a Euclidean lattice. The second chapter introduces Monte Carlo methods and details the numerical algorithms to simulate lattice gauge fields. The third chapter explains the mathematical and numerical techniques needed to study quark fields and the computation of quark propagators. The fourth chapter is devoted to the physical observables constructed from lattice fields and explains how to measure them in simulations. The book is aimed at enabling graduate students who are new to the field to carry out explicitly the first steps and prepare them for research in lattice QCD.

Wuppertal, Germany — Francesco Knechtli
Wuppertal, Germany — Michael Günther
Dublin, Ireland — Michael Peardon

# Acknowledgements

We thank Peter Weisz for reading the first version of the book and providing many constructive comments to improve it. We thank Ulli Wolff for the permission to use the material from his lecture "Quantum Field Theory" Ref. [1].

The work on this book has been motivated and supported by the Collaborative Research Centre SFB/TRR-55 "Hadron Physics from Lattice QCD" funded by the Deutsche Forschungsgemeinschaft.

## Reference

1. U. Wolff, *Quantum Field Theory* (Lecture note, HU Berlin, Unpublished, 2010)

# Contents

# Chapter 1
# Quantum Field Theory (QFT) on the Lattice

## 1.1 A Brief History of Quarks and Gluons

In 1964, Gell-Mann [1] and Zweig [2] proposed that hadrons, the particles which experience strong interactions, are made of quarks. Quarks are confined within hadrons and never seen in isolation. Electron-nucleon scattering experiments at large momentum transfer could be explained by assuming the nucleon is made of almost-free point-like constituents called partons [3–5]. Later partons were identified with quarks. Quantum chromodynamics (QCD) was proposed in 1973 to describe these properties in a unified way [6]. QCD is a gauge theory based on the group $SU(3)_c$. In QCD, quarks $q^i$ exist in six different species $q = u, d, s, c, b, t$ and have colour $i = 1, 2, 3$. The quark species are called in order of ascending mass "up", "down", "strange", "charm", "bottom" and "top". The gauge principle [7] introduces the gluon fields, which carry the interactions between quarks. Gluons are described by eight real vector fields $A^a_\nu$ with colour label $a = 1, 2, \ldots, 8$. Since gluons have colour they interact both with quarks and with each other. The coupling $g$, which determines the strength of these interactions depends through loop effects and after renormalisation on the magnitude $\mu$ of the energy-momentum transferred. The renormalised running coupling is denoted by $\bar{g}(\mu)$ and the strong coupling

$$\alpha_s(\mu) \equiv \frac{\bar{g}(\mu)^2}{4\pi} = \frac{c}{\ln(\mu/\Lambda)} + \ldots \tag{1.1}$$

decays logarithmically for large $\mu$ ($c$ is some computable constant). This property is called asymptotic freedom [8–10] and is observed in high-energy scattering experiments. Asymptotic freedom enables a perturbative expansion in the coupling $\alpha_s(\mu)$ for high energies $\mu$, where the coupling is small. The existence of the gluons was confirmed experimentally in 1979 at the electron-positron collider PETRA at DESY



F. Knechtli et al., *Lattice Quantum Chromodynamics*,
SpringerBriefs in Physics, DOI 10.1007/978-94-024-0999-4_1

[11]. While asymptotic freedom can be shown using perturbation theory, the confinement of quarks and gluons into hadrons requires a non-perturbative formulation of QCD on the lattice. Since Wilson's original formulation [12], the field has advanced [13]. It is the aim of this book to cover the essentials of these developments.

## 1.2 Classical Fields and Gauge Invariance

In the continuum, the gauge potential $A_\mu(x)$ is an element of the Lie algebra $\mathfrak{su}(N)$ of the gauge group $SU(N)$. A summary of properties of $SU(N)$ Lie groups is given in Sect. A.1. The gauge potential satisfies the following properties

$$A_\mu^\dagger = -A_\mu, \quad \mathrm{tr}\,\{A_\mu\} = 0, \tag{1.2}$$

where $A_\mu^\dagger$ is the Hermitian transpose of $A_\mu$. For QCD, the gauge group is $SU(3)$. A gauge transformation is defined by a set of $SU(N)$ matrices $\Omega(x)$. It transforms the gauge potential according to

$$A_\mu^{(\mathrm{g})}(x) = \Omega(x) A_\mu(x) \Omega(x)^{-1} + \Omega(x) \partial_\mu \Omega(x)^{-1}. \tag{1.3}$$

Consider a $N$ component complex matter field $\chi(x) = (\chi_1(x), \ldots, \chi_N(x))^T \in \mathbb{C}^N$ which transforms in the fundamental representation of the gauge group $SU(N)$. This means under a gauge transformation, the field becomes

$$\chi^{(\mathrm{g})}(x) = \Omega(x) \chi(x). \tag{1.4}$$

The transformations of Eqs. (1.3) and (1.4) are such that the expression

$$D_\mu \chi(x) = (\partial_\mu + A_\mu(x)) \chi(x), \tag{1.5}$$

transforms in the same way as $\chi$, namely $(D_\mu \chi)^{(\mathrm{g})}(x) = \Omega(x) D_\mu \chi(x)$. Therefore $D_\mu \chi(x)$ is called the *gauge covariant derivative*.

The continuum Yang–Mills action for a pure $SU(N)$ gauge field is

$$S_{\mathrm{YM}} = \frac{1}{4 g_0^2} \int \mathrm{d}^4 x \; F_{\mu\nu}^i(x) \; F_{\mu\nu}^i(x). \tag{1.6}$$

The parameter $g_0$ is the bare gauge coupling constant. The field strength tensor $F_{\mu\nu}$ is defined as

$$[D_\mu, D_\nu] \chi(x) = F_{\mu\nu}(x) \; \chi(x). \tag{1.7}$$

The *commutator* of two operators $A$ and $B$ is defined as $[A, B] = AB - BA$. In terms of the gauge potential $A_\mu$, the field strength tensor is given by

$$F_{\mu\nu} = \partial_\mu A_\nu - \partial_\nu A_\mu + [A_\mu, A_\nu]. \tag{1.8}$$

It is an element of the Lie algebra with components $F_{\mu\nu} = F^i_{\mu\nu} T^i, i = 1, \ldots, N^2 - 1$. It follows from Eq. (1.7) that under gauge transformation $F_{\mu\nu}$ transforms as

$$F_{\mu\nu}(x) \to \Omega(x)\, F_{\mu\nu}(x)\, \Omega^{-1}(x). \tag{1.9}$$

Quarks in QCD-like theories are spin-$\frac{1}{2}$ fermion fields $\psi^\alpha_i(x)$. Their components are Grassmann variables (see Sect. A.2) which carry a Dirac spinor index $\alpha = 1, \ldots, 4$ and a gauge group index $i = 1, \ldots, N$ in the fundamental representation of $SU(N)$. An antiquark field $\bar\psi^\alpha_i$ is an independent Grassmann field in the complex conjugate representation. Under gauge transformations, quark and antiquark fields become

$$(\psi^{(g)})^\alpha_i(x) = [\Omega(x)_{ij}]\psi^\alpha_j(x) \quad \text{and} \quad (\bar\psi^{(g)})^\alpha_i(x) = \bar\psi^\alpha_j[\Omega(x)^{-1}]_{ji}. \tag{1.10}$$

The classical quark fields satisfy the anticommutation relations

$$\{\psi^\alpha_i(x), \psi^\beta_j(y)\} = 0, \quad \{\bar\psi^\alpha_i(x), \bar\psi^\beta_j(y)\} = 0, \quad \{\psi^\alpha_i(x), \bar\psi^\beta_j(y)\} = 0, \tag{1.11}$$

for any $x, y, \alpha, \beta, i$ and $j$. The *anticommutator* of two operators $A$ and $B$ is defined as $\{A, B\} = AB + BA$. The classical continuum Euclidean action of a quark field is

$$S_F = \int \mathrm{d}^4x\ \bar\psi^\alpha_i(x)[\not{D} + m_0]^{\alpha\beta}_{ij}\psi^\beta_j(x), \tag{1.12}$$

where $[\not{D} + m_0]^{\alpha\beta}_{ij} = (\gamma_\mu)^{\alpha\beta}[\partial_\mu\delta_{ij} + (A_\mu)_{ij}] + m_0\delta^{\alpha\beta}\delta_{ij}$ and $m_0$ is the bare mass parameter of the quark field. The Euler–Lagrange equation yields the Dirac equation

$$(\gamma_\mu D_\mu + m_0)\psi(x) = 0. \tag{1.13}$$

The $\gamma$ matrices acting on the spinor indices are defined in Sect. A.2.

## 1.3 Hamiltonian and Path Integral Formulations of Quantum Mechanics

In this section we describe the relation between the Hamiltonian and Feynman path integral formulation for a simple system, that of one oscillator. The partition function

$$Z(\beta) = \mathrm{Tr}_{\mathscr{H}}\, \mathrm{e}^{-\beta\hat H} = \sum_{\text{states } n} \mathrm{e}^{-\beta E_n}, \tag{1.14}$$

is a probe of the statistical mechanical properties of the system at inverse temperature $\beta$. $\hat{H}$ is the Hamilton operator for the system and $E_n$ the energies of the states. The trace $\mathrm{Tr}_{\mathscr{H}}$ is computed in the Hilbert space $\mathscr{H}$ in which the operator $\hat{H}$ acts. We use Dirac's notation $|\psi\rangle$ to represent vectors in the Hilbert space. We evaluate the trace using the basis spanned by the eigenstates $\hat{H}|n\rangle = E_n|n\rangle$. The Hamilton operator is Hermitian and its eigenvalues $E_n$ are therefore real.

### 1.3.1 One Bosonic Oscillator

One bosonic oscillator of frequency $\omega$ is described in terms of an annihilation $\hat{a}$ and creation $\hat{a}^\dagger$ operator with

$$[\hat{a}, \hat{a}^\dagger] = 1, \qquad \hat{H} = \omega \left( \hat{a}^\dagger \hat{a} + \frac{1}{2} \right). \tag{1.15}$$

The space of states $|n\rangle$ with $n \in \mathbb{N}$ is called the Fock space and is constructed starting from the vacuum state defined by $\hat{a}|0\rangle = 0$ using the creation operator

$$|n\rangle = \frac{(\hat{a}^\dagger)^n}{\sqrt{n!}}|0\rangle, \quad n = 1, 2, 3, \ldots. \tag{1.16}$$

Recall that the vacuum state is non-trivial in quantum mechanics. The path integral representation of Eq. (1.14) can be derived by introducing position and momentum operators

$$\hat{x} = \frac{1}{\sqrt{2}}(\hat{a} + \hat{a}^\dagger), \qquad \hat{p} = \frac{-i}{\sqrt{2}}(\hat{a} - \hat{a}^\dagger). \tag{1.17}$$

They fulfill the commutation relation $[\hat{x}, \hat{p}] = i$ and so the momentum operator acting on a function of the coordinate $x$ can be represented as $\hat{p} = -i\frac{\partial}{\partial x}$. Using the operators in Eq. (1.17) the Hamilton operator Eq. (1.15) becomes

$$\hat{H} = \frac{\omega}{2}\left(\hat{p}^2 + \hat{x}^2\right). \tag{1.18}$$

If we introduce a "time" step $\tau$ through $\beta = N\tau$, where $N$ is an integer, the partition function Eq. (1.14) can be written as

$$Z(\beta) = \mathrm{Tr}\left(\mathrm{e}^{-\tau\hat{H}}\right)^N. \tag{1.19}$$

The operator $\mathrm{e}^{-\tau\hat{H}}$ describes the evolution in Euclidean time over a time step $\tau$. Here, the trace can be evaluated in the basis of eigenstates $|x_0\rangle$ of the operator $\hat{x}$ such that $\hat{x}|x_0\rangle = x_0|x_0\rangle$. They fulfill the completeness relation $1 = \int \mathrm{d}x_0 |x_0\rangle\langle x_0|$.

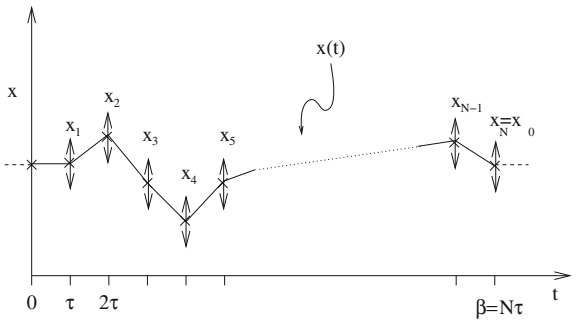


**Fig. 1.1** Representation of the bosonic partition function. The set of intermediate states $|x_1\rangle, \ldots, |x_{N-1}\rangle$ inserted in the trace Eq. (1.20) leads to a sum over all possible paths which start and end at $x_0$, see Eq. (1.22)

We introduce between each consecutive factor of $\mathrm{e}^{-\tau\hat{H}}$ in Eq. (1.19) a complete set of states to obtain

$$Z(\beta) = \int \prod_{k=0}^{N-1} \mathrm{d}x_k \, \langle x_0|\mathrm{e}^{-\tau\hat{H}}|x_1\rangle\langle x_1|\mathrm{e}^{-\tau\hat{H}}|x_2\rangle \ldots \langle x_{N-1}|\mathrm{e}^{-\tau\hat{H}}|x_0\rangle. \tag{1.20}$$

This expression is schematically represented in Fig. 1.1. We define the transfer matrix operator $\mathbb{T} = \mathrm{e}^{-\tau\hat{x}^2/4}\mathrm{e}^{-\tau\hat{p}^2/2}\mathrm{e}^{-\tau\hat{x}^2/4}$ and note that $\mathbb{T} = \mathrm{e}^{-\tau\hat{H}} + \mathrm{O}(\tau^3)$. The matrix elements $\langle x_k|\mathbb{T}|x_{k+1}\rangle$ can be computed by changing to the momentum basis

$$\langle x|p\rangle = \mathrm{e}^{ipx}, \qquad 1 = \int \frac{\mathrm{d}p}{2\pi}|p\rangle\,\langle p|. \tag{1.21}$$

Neglecting $\mathrm{O}(\tau^3)$ terms, we arrive at the result

$$Z(\beta) = \int \prod_{k=0}^{N-1} \mathrm{d}x_k \, \mathrm{e}^{-S[x]}, \tag{1.22}$$

where $S[x]$ is the Euclidean action for one bosonic oscillator

$$S[x] = \frac{\omega\tau}{2}\sum_{k=0}^{N-1}\left[\left(\frac{x_{k+1}-x_k}{\tau}\right)^2 + x_k^2\right] \xrightarrow{\tau\to 0} \frac{\omega}{2}\int_0^\beta \mathrm{d}t\left[\left(\frac{\mathrm{d}x}{\mathrm{d}t}\right)^2 + x^2\right]. \tag{1.23}$$

$S[x]$ is a discretised form of the continuum action of the harmonic oscillator. The latter is recovered in the limit $\tau \to 0$. Equation (1.22) is the path-integral representation of the partition function for one bosonic oscillator. It integrates over all classical paths starting from arbitrary position $x_0$ at time 0 and ending at the same position $x_0 = x_N$ at time $\beta$, see Fig. 1.1.

### 1.3.2 One Fermionic Oscillator

Following a similar construction we now show the path-integral representation of the partition function for one fermionic oscillator of frequency $\omega$. This system is described in terms of an annihilation $\hat{c}$ and creation $\hat{c}^\dagger$ operator with the properties $\hat{c}^2 = 0$, $(\hat{c}^\dagger)^2 = 0$ and

$$\{\hat{c}, \hat{c}^\dagger\} = 1, \qquad \hat{H} = \omega\, \hat{c}^\dagger\, \hat{c}. \tag{1.24}$$

Since $(\hat{c}^\dagger)^2 = 0$, the Fock space contains only two states $|0\rangle$, $|1\rangle$ with

$$\hat{c}\,|0\rangle = 0, \qquad |1\rangle = \hat{c}^\dagger\,|0\rangle. \tag{1.25}$$

We use Grassmann numbers to derive a path-integral representation for this partition function. A coherent state $|\eta\rangle$ is defined as [14, 15] a linear combination of the Fock states in Eq. (1.25), whose coefficients contain a Grassmann variable $\eta$;

$$|\eta\rangle = \mathrm{e}^{\hat{c}^\dagger \eta}|0\rangle = (1 + \hat{c}^\dagger \eta)|0\rangle. \tag{1.26}$$

It fulfills $\hat{c}\,|\eta\rangle = \eta\,|\eta\rangle$. A dual coherent state is defined as

$$\langle\eta| = \langle 0|\mathrm{e}^{\bar{\eta}\hat{c}} = \langle 0|(1 + \bar{\eta}\hat{c}), \tag{1.27}$$

where $\bar{\eta}$ is a Grassmann variable independent of $\eta$. The scalar product of two coherent states is $\langle\eta|\eta'\rangle = \mathrm{e}^{\bar{\eta}\eta'}$. Coherent states fulfill the completeness relation

$$1 = \int \mathrm{d}\bar{\eta}\,\mathrm{d}\eta\,\mathrm{e}^{-\bar{\eta}\eta}\,|\eta\rangle\,\langle\eta|. \tag{1.28}$$

The trace of an operator can now be expressed as

$$\mathrm{Tr}\; O = \int \mathrm{d}\bar{\eta}\,\mathrm{d}\eta\,\mathrm{e}^{-\bar{\eta}\eta}\,\langle\eta|O|-\eta\rangle, \tag{1.29}$$

Using Eqs. (1.28) and (1.29) the partition function can be evaluated

$$Z(\beta) = \mathrm{Tr}\,\left(\mathrm{e}^{-\tau\hat{H}}\right)^N = \int \mathrm{d}\bar{\eta}\,\mathrm{d}\eta \prod_{i=1}^{N-1} \mathrm{d}\bar{\eta}_i\,\mathrm{d}\eta_i\,\mathrm{e}^{-\bar{\eta}\eta} \prod_{i=1}^{N-1} \mathrm{e}^{-\bar{\eta}_i\eta_i}$$
$$\langle\eta|\mathrm{e}^{-\tau\hat{H}}|\eta_1\rangle\langle\eta_1|\mathrm{e}^{-\tau\hat{H}}|\eta_2\rangle \ldots \langle\eta_{N-1}|\mathrm{e}^{-\tau\hat{H}}|-\eta\rangle.$$

With the result $\langle\eta_i|\exp(-\tau\hat{H})|\eta_j\rangle = \exp[\bar{\eta}_i \exp(-\omega\tau)\eta_j]$ we arrive at

$$Z(\beta) = \int \prod_{i=0}^{N-1} \mathrm{d}\bar{\eta}_i\,\mathrm{d}\eta_i\,\mathrm{e}^{-\sum_{i,j=0}^{N-1}\bar{\eta}_j \Delta_{ji}\eta_i} = \det(\Delta), \tag{1.30}$$

where $\eta_0 = \eta$ and $\bar{\eta}_0 = \bar{\eta}$ and

$$\Delta_{ji} = \delta_{ji} - \delta^{\mathrm{F}}_{j+1,i}\, \mathrm{e}^{-\omega\tau}, \quad i, j = 0, 1, \ldots, N-1. \tag{1.31}$$

The anti-periodic Kronecker symbol $\delta^{\mathrm{F}}_{ij}$ coincides with $\delta_{ij}$ if $i, j = 0, 1, \ldots, N-1$. Further it satisfies $\delta^{\mathrm{F}}_{N,0} = -\delta_{0,0}$ which is equivalent to the Grassmann numbers having anti-periodic boundary conditions in the time direction. The determinant in Eq. (1.30) comes from the Matthews-Salam formula Eq. (A.10). It is easy to check that $\det(\Delta)$ agrees with the direct evaluation of the trace in Eq. (1.14) $Z(\beta) = 1 + \mathrm{e}^{-\beta\omega}$. In the continuum limit $\tau \to 0$ ($\beta$ fixed) we obtain for the action of one bosonic oscillator

$$S[\eta, \bar{\eta}] = \sum_{i,j=0}^{N-1} \bar{\eta}_j \Delta_{ji} \eta_i \quad \stackrel{\tau\to 0}{\longrightarrow} \quad \int_0^\beta \mathrm{d}\tau\, \bar{\eta}(\tau) \left( \frac{\mathrm{d}}{\mathrm{d}\tau} + \omega \right) \eta(\tau). \tag{1.32}$$

## 1.4 Quantum Fields on a Lattice

In this section we discuss the construction of lattice quantum fields, starting with the path integral formulation of a bosonic field theory based on the harmonic oscillator introduced in Sect. 1.3.1. This motivates the generalisation to the path integral of lattice QCD. We explain how the fields and symmetries of classical continuum QCD which were introduced in Sect. 1.2 are defined on the lattice as proposed by Wilson [12]. The lattice discretisation of spin-$\frac{1}{2}$ fermion fields is closely related to chiral symmetry. We discuss this relation as well as alternative formulations to Wilson's fermions.

### *1.4.1 From One Oscillator to a Field*

This and the next section are based on Ref. [16]. Consider free particles of mass $m$ in a three-dimensional box of size $L^3$. The space is discretized on a cubic lattice of points $\underline{x}$ with coordinates $x_k = l_k\, a, l_k = 0, 1, \ldots, \frac{L}{a} - 1$ ($k = 1, 2, 3$). In total there are $(L/a)^3$ points. In Fourier space there is the same number of momenta $\underline{p}$ with components $p_k = l_k \frac{2\pi}{L}$, $l_k = 0, 1, \ldots, \frac{L}{a} - 1$. In order to construct a bosonic field theory to describe the particles, a bosonic oscillator is assigned to each momentum $\underline{p}$. The frequency of the oscillators is given by the energy $E(\underline{p})$ of the particle. In the continuum limit $a \to 0$ and infinite volume limit $L \to \infty$ the frequency is given by the relativistic formula

$$\omega(\underline{p}) = E(\underline{p}) = \sqrt{\underline{p}^2 + m^2}. \tag{1.33}$$

The Hamilton operator is the sum over the Hamilton operators for each momentum (cf. Eq. (1.15))

$$\hat{H} = \sum_{\underline{p}} \omega(\underline{p}) \left( \hat{a}^\dagger(\underline{p})\, \hat{a}(\underline{p}) + \frac{1}{2} \right). \tag{1.34}$$

Similarly to what we did for one bosonic oscillator, we transform the creation $\hat{a}^\dagger(\underline{p})$ and annihilation $\hat{a}(\underline{p})$ operators and define the field operators

$$\hat{\varphi}(\underline{p}) = \sqrt{\frac{1}{2E(\underline{p})}} \left[ \hat{A}^\dagger(-\underline{p}) + \hat{A}(\underline{p}) \right] = \hat{\varphi}^\dagger(-\underline{p}), \tag{1.35}$$

$$\hat{\pi}(\underline{p}) = i\sqrt{\frac{E(\underline{p})}{2}} \left[ \hat{A}^\dagger(\underline{p}) - \hat{A}(-\underline{p}) \right] = \hat{\pi}^\dagger(-\underline{p}), \tag{1.36}$$

where $\hat{A}(\underline{p}) = L^{3/2}\hat{a}(\underline{p})$. Through Fourier transformation we construct the field operators in position space

$$\hat{\varphi}(\underline{x}) = \frac{1}{L^3} \sum_{\underline{p}} \hat{\varphi}(\underline{p}) \mathrm{e}^{i\underline{x}\cdot\underline{p}}, \quad \hat{\pi}(\underline{x}) = \frac{1}{L^3} \sum_{\underline{p}} \hat{\pi}(\underline{p}) \mathrm{e}^{i\underline{x}\cdot\underline{p}}. \tag{1.37}$$

These operators are self-adjoint (or Hermitian)[1] : $\hat{\varphi}(\underline{x})^\dagger = \hat{\varphi}(\underline{x})$, $\hat{\pi}(\underline{x})^\dagger = \hat{\pi}(\underline{x})$. They satisfy the commutation relations $[\hat{\varphi}(\underline{x}), \hat{\pi}(\underline{y})] = i\frac{1}{a^3}\delta_{\underline{x},\underline{y}}$, $[\hat{\varphi}(\underline{x}), \hat{\varphi}(\underline{y})] = 0$ and $[\hat{\pi}(\underline{x}), \hat{\pi}(\underline{y})] = 0$. In terms of the field operators in position space the Hamilton operator Eq. (1.34) becomes

$$\hat{H} = a^3 \sum_{\underline{x}} \frac{1}{2} \left[ \hat{\pi}^2(\underline{x}) + (\partial_k \hat{\varphi}(\underline{x}))^2 + m^2 \hat{\varphi}^2(\underline{x}) \right], \tag{1.38}$$

where $\partial_k \hat{\varphi}(\underline{x}) = \frac{1}{a}[\hat{\varphi}(\underline{x} + a\hat{k}) - \hat{\varphi}(\underline{x})]$. To introduce interactions between the particles a point-like interaction term $\hat{\varphi}^4$ is added to the Hamilton operator Eq. (1.38) with a coupling $\lambda \geq 0$

$$\hat{H} = a^3 \sum_{\underline{x}} \frac{1}{2} \left[ \hat{\pi}^2(\underline{x}) + (\partial_k \hat{\varphi}(\underline{x}))^2 + m^2 \hat{\varphi}^2(\underline{x}) + \frac{\lambda}{12} \hat{\varphi}^4(\underline{x}) \right]. \tag{1.39}$$

Now let us turn to the evaluation of the partition function Eq. (1.14). We use a basis of states $\{|\varphi\rangle\}$ in which the field operators $\hat{\varphi}(\underline{x})$ are diagonal; $\hat{\varphi}(\underline{x})|\varphi\rangle = \varphi(\underline{x})|\varphi\rangle$. The basis defines a complete set $1 = \left[\prod_{\underline{x}} a \int \mathrm{d}\varphi(\underline{x})\right] |\varphi\rangle\langle\varphi|$, so we can express the partition function as

[1] In the space of complex fields $\varphi(\underline{x})$ the scalar product is defined as $(\varphi, \varphi') = a^3 \sum_{\underline{x}} \varphi(\underline{x})^* \varphi'(\underline{x})$. The adjoint $\hat{A}^\dagger$ of an operator $\hat{A}$ acting on the fields is defined as $(\varphi, \hat{A}\varphi') = (\hat{A}^\dagger\varphi, \varphi')$. A self-adjoint operator has $\hat{A}^\dagger = \hat{A}$.

$$Z = \left[\prod_{\underline{x}} a \int \mathrm{d}\varphi(\underline{x})\right] \langle\varphi|\mathrm{e}^{-\beta\hat{H}}|\varphi\rangle. \tag{1.40}$$

The trace is evaluated in a similar manner to Sect. 1.3.1. We factorize $\mathrm{e}^{-\beta\hat{H}} = \left(\mathrm{e}^{-\tau\hat{H}}\right)^N$ with $N = \beta/\tau$ and define the transfer matrix $\mathbb{T}$ as

$$\mathbb{T} = \mathrm{e}^{-\frac{\tau}{2}V}\,\mathrm{e}^{-\tau K}\,\mathrm{e}^{-\frac{\tau}{2}V}, \tag{1.41}$$

where

$$V[\hat{\varphi}] = \frac{a^3}{2}\sum_{\underline{x}}\left[(\partial_k\hat{\varphi}(\underline{x}))^2 + m^2\hat{\varphi}^2(\underline{x}) + \frac{\lambda}{12}\hat{\varphi}^4(\underline{x})\right], \quad K[\hat{\varphi}] = \frac{a^3}{2}\sum_{\underline{x}}\hat{\pi}^2(\underline{x}). \tag{1.42}$$

Using the Baker-Campbell-Hausdorff formula it can be shown that

$$\mathbb{T} = \mathrm{e}^{-\tau\hat{H}} + \mathrm{O}(\tau^3). \tag{1.43}$$

The matrix elements of the transfer operator are given by

$$\langle\varphi'|\mathbb{T}|\varphi\rangle = \left(\frac{2\pi\tau}{a}\right)^{-\frac{1}{2}(L/a)^3} \mathrm{e}^{-\frac{a^3}{2\tau}\sum_{\underline{x}}(\varphi'(\underline{x})-\varphi(\underline{x}))^2 - \frac{\tau}{2}(V[\varphi']+V[\varphi])}. \tag{1.44}$$

Introducing $N-1$ complete sets of field operators between the factors $\mathrm{e}^{-\tau\hat{H}}$ we arrive at the expression for the partition function

$$Z = \left[\prod_{n=0}^{N-1}\prod_{\underline{x}} a \int \mathrm{d}\varphi_n(\underline{x})\right] \langle\varphi_0|\mathbb{T}|\varphi_1\rangle \ldots \langle\varphi_{N-1}|\mathbb{T}|\varphi_0\rangle + \mathrm{O}(\tau^3), \tag{1.45}$$

where we have renamed the boundary field in the trace as $\varphi = \varphi_0$. We can now interpret the set of spatial fields $\varphi_n(\underline{x}) \equiv \varphi(t = n\tau, \underline{x})$ as one field defined on a four-dimensional Euclidean lattice. The lattice points are denoted by the four-dimensional coordinates $x_\mu$, $\mu = 0, 1, 2, 3$, with $x_0 = t$ and the other coordinates equal to $\underline{x}$. The metric on the lattice is Euclidean $x^2 \equiv x_\mu^2 = t^2 + \underline{x}^2$. If we identify the lattice spacings $\tau = a$ we arrive at the result

$$Z = \int \mathscr{D}\varphi\ \mathrm{e}^{-S[\varphi]}, \tag{1.46}$$

with the measure $\mathscr{D}\varphi = \prod_x \frac{a}{\sqrt{2\pi}}\mathrm{d}\varphi(x)$ and the action

$$S[\varphi] = \frac{a^4}{2} \sum_x \left[ \underbrace{(\partial_t \varphi)^2 + (\partial_k \varphi)^2}_{(\partial_\mu \varphi)^2} + m^2 \varphi^2 + \frac{\lambda}{12} \varphi^4 \right]. \tag{1.47}$$

Notice that the action $S[\varphi]$ is invariant under the hypercubic group in the four-dimensional Euclidean space. The symmetry transformations are rotations by a $\pi/2$ angle and reflections. In the formal continuum limit $a \to 0$ and infinite volume the symmetry group becomes the orthogonal group O(4) of four-dimensional rotations.

### 1.4.2 Correlation Functions

The path integral involves a high-dimensional integration over the values of the classical field $\varphi(x)$ at each lattice point $x$. The integration is weighted by the Boltzmann factor $\exp(-S[\varphi])$. The expectation value of a functional $\mathscr{O}[\varphi]$, which is called an observable is defined by

$$\langle \mathscr{O}[\varphi] \rangle = \frac{1}{Z} \int \mathscr{D}\varphi \, \mathrm{e}^{-S[\varphi]} \mathscr{O}[\varphi]. \tag{1.48}$$

As an example, consider a state resembling a boson at rest, $\underline{p} = 0$, which can be created by the interpolator $\Phi(t) = a^3 \sum_{\underline{x}} \varphi(t, \underline{x})$. The relevant two-point correlation function is defined as $\langle \Phi(t) \Phi(0) \rangle$. Following similar steps to the derivation of Eq. (1.46) we arrive at the result

$$\langle \Phi(t) \Phi(0) \rangle = \frac{1}{Z} \mathrm{Tr} \left[ \mathbb{T}^{(T-t)/a} \, \hat{\Phi} \, \mathbb{T}^{t/a} \, \hat{\Phi} \right], \tag{1.49}$$

which expresses the two point function in operator (or Hamiltonian) formalism where $\hat{\Phi} = a^3 \sum_{\underline{x}} \hat{\varphi}(\underline{x})$. The transfer matrix operator $\mathbb{T}$ is self-adjoint and positive and admits a spectral representation

$$\mathbb{T} = \sum_{\alpha \geq 0} \mathrm{e}^{-aE_\alpha} \, |\alpha\rangle\langle\alpha|, \quad E_\alpha \leq E_{\alpha+1}. \tag{1.50}$$

If we neglect the $\mathrm{O}(a^3)$ discretization errors in Eq. (1.43) then $\mathbb{T} \simeq \exp(-a\hat{H})$ and the real values $E_\alpha$ are identified with the eigenvalues of the Hamilton operator $\hat{H}$. The eigenstates $\{|\alpha\rangle\}$ form an orthonormal basis $\langle \alpha | \alpha' \rangle = \delta_{\alpha,\alpha'}$. Inserting the spectral representation Eq. (1.50) in Eq. (1.14) we get

$$Z \simeq \mathrm{Tr} \left[ \mathbb{T}^{T/a} \right] = \sum_\alpha \mathrm{e}^{-TE_\alpha}. \tag{1.51}$$

The trace in Eq. (1.49) can be similarly evaluated and gives

$$\mathrm{Tr}\left[\mathbb{T}^{(T-t)/a}\,\hat{\Phi}\,\mathbb{T}^{t/a}\,\hat{\Phi}\right] = \sum_{\alpha,\alpha'}\left|\langle\alpha|\hat{\Phi}|\alpha'\rangle\right|^2 \mathrm{e}^{-t(E_{\alpha'}-E_\alpha)}\,\mathrm{e}^{-TE_\alpha}. \tag{1.52}$$

If we assume that the Euclidean time extent of the lattice $T$ is large enough such that $(E_1 - E_0)T \gg 1$ then

$$Z \simeq \mathrm{e}^{-TE_0}. \tag{1.53}$$

If in addition $T \gg t$ then

$$\langle\Phi(t)\,\Phi(0)\rangle \simeq \sum_{\alpha}\left|\langle\alpha|\hat{\Phi}|0\rangle\right|^2 \mathrm{e}^{-t(E_\alpha-E_0)}. \tag{1.54}$$

Notice that only energy differences $E_\alpha - E_0$ appear in Eq. (1.54). The value of the vacuum energy $E_0$ is arbitrary, since a constant shift can be added to the Hamilton operator without affecting expectation values defined in Eq. (1.48). Therefore only energy differences have a physical meaning. The renormalized mass is defined as

$$m_\mathrm{R} = E_1 - E_0. \tag{1.55}$$

If there are no interaction terms ($\lambda = 0$ in Eq. (1.39)), it is clear from Eq. (1.34) that the renormalized mass is equal to the mass $m$. With interactions ($\lambda > 0$) we expect on dimensional grounds a relation $m_\mathrm{R} = m\,f(\lambda, am, Lm)$. If $(E_2 - E_1)t \gg 1$ then

$$\langle\Phi(t)\Phi(0)\rangle \simeq c_0 + c_1\,\mathrm{e}^{-m_\mathrm{R}t}, \tag{1.56}$$

where $c_0 = \left|\langle 0|\hat{\Phi}|0\rangle\right|^2$ and $c_1 = \left|\langle 1|\hat{\Phi}|0\rangle\right|^2$. If we consider the *connected* two point correlation function

$$\langle\Phi(t)\Phi(0)\rangle - \langle\Phi(t)\rangle\,\langle\Phi(0)\rangle \simeq c_1\,\mathrm{e}^{-m_\mathrm{R}t}, \tag{1.57}$$

the constant $c_0$ is cancelled and the mass $m_\mathrm{R}$ can be extracted from the exponential fall-off of the correlator in Euclidean time.

### 1.4.3 Analytic Continuation to Minkowski Space

In order to recover Eqs. (1.46) and (1.47) from the path integral formulation of a bosonic theory in Minkowski space, the Euclidean time $t$ has to be analytically continued to real time $x^0$ through $x^0 = -it$. The operator $\exp(-t\hat{H})$ is then replaced by $\exp(-ix^0\hat{H})$, which is the time evolution operator in quantum mechanics. After the analytic continuation, the symmetry group becomes the Lorentz group O(1, 3).

We illustrate the analytical continuation from Euclidean to Minkowski space by an example in the continuum. Consider a free scalar field in Euclidean space. Its action is the continuum version of Eq. (1.47) where we set $\lambda = 0$. The Euclidean two point correlation function of a free scalar field is given by

$$\mathscr{S}(x,0) = \langle \varphi(x)\varphi(0)\rangle = \int \frac{\mathrm{d}^4 p}{(2\pi)^4} \frac{\mathrm{e}^{ipx}}{p^2 + m^2}, \tag{1.58}$$

where we label for convenience the Euclidean coordinates by $x = (t = x_4, \underline{x})$ and $p = (p_4, \underline{p})$. The scalar products are given by $px = p_4 x_4 + \underline{p} \cdot \underline{x}$ and $p^2 = p_4^2 + \underline{p}^2$. A Wick rotation $x_4 = ix^0$ yields $\mathscr{S}(\tilde{x}, 0)$, the analytic continuation of Eq. (1.58) to imaginary "time" coordinate with $\tilde{x} = (x_4 = ix^0, \underline{x})$. At the same time we perform the change of integration variable $p_4 = ip^0$. The integral in Eq. (1.58) becomes

$$\mathscr{S}(\tilde{x}, 0) = -i \int_{+i\infty}^{-i\infty} \frac{\mathrm{d}p^0}{2\pi} \frac{\mathrm{e}^{-ip*x}}{p^2 - m^2} = i \int_{-\infty}^{\infty} \frac{\mathrm{d}p^0}{2\pi} \frac{\mathrm{e}^{-ip*x}}{p^2 - m^2 + i\varepsilon}. \tag{1.59}$$

In order to get the second equality we rotate the integration contour as shown by the red arcs in Fig. 1.2. The scalar products $p * x = p^0 x^0 - \underline{p} \cdot \underline{x}$ and $p^2 = (p^0)^2 - \underline{p}^2$ are now in Minkowski space. The $+i\varepsilon$ prescription in the denominator of Eq. (1.59) is such that no poles are encountered when rotating the contour. Equation (1.59) is the two point function $\langle T\varphi(x)\varphi(0)\rangle$ of time-ordered fields in Minkowski space [14].

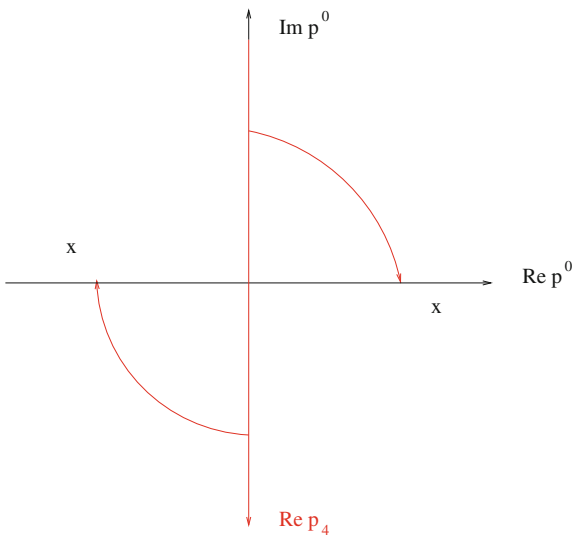


**Fig. 1.2** The change of integration contour $p_4 \to ip^0$ from Euclidean to Minkowski space. The crosses represent the poles of the propagator in Minkowski space Eq. (1.59)

### 1.4.4 Gauge Invariance on the Lattice

Non Abelian gauge theory was formulated on a Euclidean space time lattice by Wilson [12] and independently by J. Smit, see [13]. To have an exact lattice analogue of gauge invariance requires the geometrical structure of gauge symmetries to be maintained when discretising the fields. A gauge transformation on the lattice is defined by a set of independent $SU(N)$ matrices $\Omega(x)$ for each lattice point $x$. A lattice gauge field comprises elements of the gauge group $SU(N)$ denoted by $U_\mu(x)$ on each link connecting neighbouring points. Our convention is that $U_\mu(x)$ is associated to the link connecting lattice point $x + a\hat{\mu}$ to $x$. The link $U_\mu^{-1}(x)$ corresponds to the link from the lattice point $x$ to $x + a\hat{\mu}$, namely the opposite direction with respect to $U_\mu(x)$. Under a gauge transformation, the link variables become

$$U_\mu^{(g)}(x) = \Omega(x)\, U_\mu(x)\, \Omega^{-1}(x + a\hat{\mu}). \tag{1.60}$$

On a finite lattice whose points have coordinates $x_\mu = 0, a, 2a, \ldots, L - a$, $\forall \mu$, a gauge configuration is a set of $4 \times (L/a)^4$ $SU(N)$ matrices. The partition function for gauge links will involve an integral over all possible configurations of the $SU(N)$ matrices. In order to have a gauge invariant theory the integration measure $\mathrm{d}U$ must be invariant under group multiplication by matrices $V$ and $W$ in $SU(N)$ from either side so that

$$I[f] = \int_{SU(N)} \mathrm{d}U\, f(U) = \int_{SU(N)} \mathrm{d}U\, f(VUW) \tag{1.61}$$

holds for any function $f$ on $SU(N)$. The normalization is $I[1] = 1$ and the group-invariant measure $\mathrm{d}U$ is called the Haar measure. For $SU(2)$, the Haar measure has a manageable explicit form but larger values of $N$ yield cumbersome expressions. For Monte Carlo, these explicit forms do not usually need to be used. For $SU(2)$, a group element $U$ can always be written

$$U = a_0\, I + i \sum_{k=1}^{3} a_k \sigma_k, \tag{1.62}$$

with $\{a_0, a_1, a_2, a_3\}$ a set of four real parameters with the constraint $a_\mu a_\mu = 1$ and $\sigma_1, \sigma_2, \sigma_3$ are the three Pauli matrices. With this constraint these parameters are co-ordinates of a point on $S_3$, the sphere in four dimensions and the Haar measure is then the natural measure on this manifold;

$$\mathrm{d}U = \frac{1}{\pi^2}\, \delta(1 - a_\mu a_\mu) \prod_{\mu=0}^{3} da_\mu. \tag{1.63}$$

Alternatively, the constraint can be imposed by parameterising in terms of three Euler angles $\{\theta, \phi, \psi\}$;

$$\begin{aligned} a_0 &= \cos\theta & a_2 &= \sin\theta \sin\phi \cos\psi \\ a_1 &= \sin\theta \cos\phi & a_3 &= \sin\theta \sin\phi \sin\psi \end{aligned} \tag{1.64}$$

and in terms of these variables, the Haar measure is

$$\mathrm{d}U = \frac{1}{2\pi^2} \sin^2\theta \sin\phi \; d\theta d\phi d\psi. \tag{1.65}$$

### 1.4.5 The Wilson Gauge Action

We consider the product of gauge links along two paths on the lattice joining the point $x + a\hat{\mu} + a\hat{\nu}$ to the point $x$,

$$U_{\mathrm{I}} = U_\mu(x)\, U_\nu(x + a\hat{\mu}) \quad \text{and} \quad U_{\mathrm{II}} = U_\nu(x)\, U_\mu(x + a\hat{\nu}), \tag{1.66}$$

cf. Fig. 1.3. The *curvature* around the elementary square on the lattice defined by the two paths, is given by the difference $M = U_{\mathrm{I}} - U_{\mathrm{II}}$. The expression

$$M\, M^\dagger = 2 - P_{\mu,\nu}(x) - P^{-1}_{\mu,\nu}(x), \tag{1.67}$$

is positive: $\mathrm{tr}\,(M\, M^\dagger) \geq 0$, and $\mathrm{tr}\,(M\, M^\dagger) = 0$ if and only if $M = 0$. $P_{\mu,\nu}(x)$ is called the *plaquette* and is given by

$$P_{\mu,\nu}(x) = U_\mu(x)\, U_\nu(x + a\hat{\mu})\, U^{-1}_\mu(x + a\hat{\nu})\, U^{-1}_\nu(x). \tag{1.68}$$

Under a gauge transformation defined in Eq. (1.60), it transforms as

$$P^{(g)}_{\mu,\nu}(x) = \Omega(x)\; P_{\mu,\nu}(x)\; \Omega^{-1}(x). \tag{1.69}$$

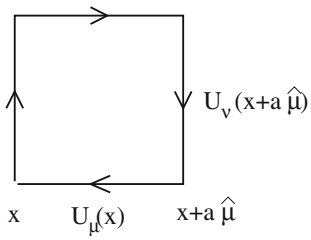


**Fig. 1.3** Oriented plaquette $P_{\mu,\nu}(x)$

Figure 1.3 shows the links and their orientation composing the plaquette $P_{\mu,\nu}(x)$ in Eq. (1.68). The plaquette satisfies the property $P^{-1}_{\mu,\nu}(x) = P_{\nu,\mu}(x)$. Motivated by Eq. (1.67), the Wilson plaquette gauge action is defined as [12]

$$S_{\rm w}[U] = \frac{\beta}{N} \sum_x \sum_{\mu<\nu} \mathrm{Re\,tr}\,[1 - P_{\mu,\nu}(x)], \tag{1.70}$$

where the trace is taken over the gauge group index. The parameter $\beta \geq 0$ will be related to the bare gauge coupling $g_0$ of the continuum theory in Eq. (1.112). $S_{\rm w}$ is positive and invariant under gauge transformations. The partition function of a $SU(N)$ gauge theory on the lattice is given by

$$Z = \int \mathscr{D}[U]\ \ \mathrm{e}^{-S_{\rm w}[U]}, \tag{1.71}$$

where $\mathscr{D}[U] = \prod_{x,\mu} \int \mathrm{d}U_\mu(x)$ and we use the Haar measure $\mathrm{d}U$ to integrate over all gauge links on the lattice, see Sect. 1.4.4. The trace in the action Eq. (1.70) is taken over gauge links in the fundamental representation of $SU(N)$. More general actions involve a sum over different representations. In the continuum limit these actions all reproduce the same continuum action Eq. (1.6). For example, the fundamental plus adjoint gauge action is

$$S[U] = \sum_x \sum_{\mu<\nu} \left\{ -\frac{\beta_f}{N} \mathrm{Re\,tr}\,[P_{\mu,\nu}(x)] - \frac{\beta_a}{N^2-1} \mathrm{tr}\,[P^{-1}_{\mu,\nu}(x)]\,\mathrm{tr}\,[P_{\mu,\nu}(x)] \right\}, \tag{1.72}$$

where all the traces are in the fundamental representation. In order to recover the continuum Yang–Mills action the couplings $\beta_f$ and $\beta_a$ have to satisfy [17]

$$\frac{1}{g_0^2} = \frac{\beta_f}{2N} + \frac{\beta_a N}{N^2-1}. \tag{1.73}$$

### 1.4.6 Strong Coupling Expansions

The lattice path integral can be computed analytically in the limit $\beta \to 0$, which corresponds to the bare coupling constant $g_0^2 \to \infty$. This limit gives the *strong coupling expansion* and as well as providing insight into the theory, it often provides useful data to test and debug Monte Carlo code. In this limit, the Boltzmann weight can be expanded as a power series in $\beta$. The integration rules of the gauge fields over the Haar measure give a simple recipe for computing expectation values. For integration over a single group-valued variable $U$, we have

$$\int \mathrm{d}U = 1, \quad \int \mathrm{d}U\ U = 0, \tag{1.74}$$

and

$$\int \mathrm{d}U \; U_{ij}[U]^{\dagger}_{kl} = \frac{1}{N}\delta_{il}\delta_{jk}. \tag{1.75}$$

Now consider evaluating the partition function for the $SU(N)$ Yang-Mills theory in this limit, keeping just the first two non-trivial terms

$$Z = \int \mathscr{D}U \; \mathrm{e}^{\beta W[U]} = \int \mathscr{D}U \; \left(1 + \beta W[U] + \frac{\beta^2}{2} W^2[U] + \mathscr{O}(\beta^3)\right), \tag{1.76}$$

with $W[U]$ related trivially to the Wilson plaquette action given in Eq. (1.70) via $S_{\mathrm{W}}[U] = \beta\,(W_0 - W[U])$. The term proportional to $\beta$ vanishes but there is a non-zero contribution at the next order. The rule for evaluating expectation values involving Wilson loops is to 'tile' the loops with plaquettes, which gives a non-zero contribution through the expression in Eq. (1.75) when two tilings with the opposite orientation sit on top of each other. The integral becomes

$$\begin{aligned} Z &= 1 + \frac{\beta^2}{2N^2} \int \mathscr{D}U \; \left( \sum_x \sum_{\mu<\nu} \mathrm{tr} \, \frac{P_{\mu,\nu}(x) + P^{\dagger}_{\mu,\nu}(x)}{2} \right)^2 + \mathrm{O}(\beta^3) \\ &= \begin{cases} 1 + (3\beta^2 V)/(2N^2) + \mathrm{O}(\beta^3) & \text{for } N > 2 \\ 1 + (3\beta^2 V)/4 + \mathrm{O}(\beta^3) & \text{for } N = 2 \end{cases}. \end{aligned} \tag{1.77}$$

The different expression for $SU(2)$ is because the trace of the plaquettes is real in this case. Next consider $\langle W_{L_1,L_2} \rangle$, the expectation value of a $L_1 \times L_2$ planar Wilson loop. $W_{L_1 L_2}$ is defined as the trace of the product of links along the rectangle multiplied for convenience by the factor of $1/N$. How this expectation value varies as $L_1$, $L_2$ change tells us about the potential between two static colour charges and different functional dependence gives either confined or screened colour charges. The first non-zero term in the strong coupling expansion occurs when the loop can be tiled completely so every link inside the loop is included both forwards and backwards. The leading-order term in this expansion is illustrated in Fig. 1.4. The first term appears at $\mathscr{O}(\beta^{L_1 L_2})$ and the resulting expression for the Wilson loop expectation value is (see Ref. [18])

$$\langle W_{L_1,L_2} \rangle = \begin{cases} (\beta/(2N^2))^A & \text{for } N > 2 \\ (\beta/4)^A & \text{for } N = 2 \end{cases}, \tag{1.78}$$

with $A = L_1 L_2$ the area of the loop. We see that at leading-order in the strong coupling expansion, the Wilson loop obeys an area law $\langle W_{L_1,L_2} \rangle = \exp(-K A)$, where the string tension $K$ can be read from Eq. (1.78); the expectation value falls exponentially in proportion to the area of the loop, which is the behaviour expected of a confining theory. These results, while remarkable in their simplicity should be interpreted with caution since strong coupling data is far from the critical point in the limit $g_0 \to 0$ where the continuum theory resides.

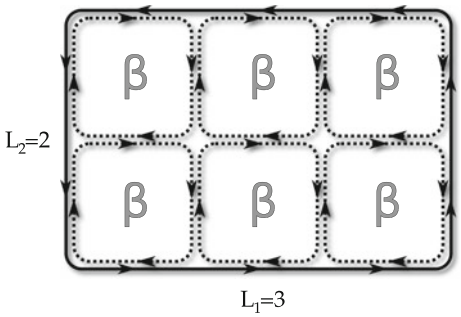


**Fig. 1.4** Strong coupling expansion of the Wilson loop: the tiling needed to give the lowest-order non-zero term in the expansion. All links in the measured Wilson loop (*solid lines*) are paired with links in the plaquette action (*dashed lines*)

### *1.4.7 The Wilson Fermion Action*

As we saw in Sect. 1.2 quarks are described by spin-$\frac{1}{2}$ fermion fields. On the lattice quark and antiquark fields are defined on the lattice points. Their gauge transformation is the same as continuum fields in Eq. (1.10). The Wilson fermion action [12] is

$$S_{\rm F} = a^4 \sum_x \bar{\psi}_i^\alpha(x)[D_{\rm w} + m_0]_{ij}^{\alpha\beta}\psi_j^\beta(x), \tag{1.79}$$

where the Wilson–Dirac operator is given by

$$[D_{\rm w}]_{ij}^{\alpha\beta} = \frac{1}{2}\sum_\mu \left\{[\gamma_\mu]^{\alpha\beta}(\nabla_\mu^* + \nabla_\mu)_{ij} - a[\delta]^{\alpha\beta}(\nabla_\mu^*\nabla_\mu)_{ij}\right\}. \tag{1.80}$$

The reason for the form Eq. (1.80) of the Wilson–Dirac operator will be explained in the next subsection. Fields acted on by covariant difference operators

$$(\nabla_\mu\psi)_i^\alpha(x) = \{[U_\mu(x)]_{ij}\psi_j^\alpha(x+a\hat{\mu}) - \psi_i^\alpha(x)\}/a \tag{1.81}$$

$$(\nabla_\mu^*\psi)_i^\alpha(x) = \{\psi_i^\alpha(x) - [U_\mu^{-1}(x-a\hat{\mu})]_{ij}\psi_j^\alpha(x-a\hat{\mu})\}/a. \tag{1.82}$$

transform under gauge transformations as $[(\nabla_\mu\psi)^{(g)}]_i^\alpha(x) = [\Omega(x)]_{ij}[\nabla_\mu\psi]_j^\alpha(x)$ and $[(\nabla_\mu^*\psi)^{(g)}]_i^\alpha(x) = [\Omega(x)]_{ij}[\nabla_\mu^*\psi]_j^\alpha(x)$. As a consequence the action Eq. (1.79) is invariant under gauge transformations. In the following the Dirac spinor indices $\alpha$, $\beta$ and the group indices $i$, $j$ will be omitted unless specified. Rescaling the field $\psi$ in Eq. (1.79) by $\psi' = a^2\sqrt{4/a + m_0}\psi$ (and similarly for $\bar{\psi}'$) yields $S_{\rm F} = \sum_x \bar{\psi}'(x)D'_{\rm w}\psi'(x)$ where

$$D'_{\rm w}\psi(x) = \psi(x) - \kappa\sum_\mu \left\{(1-\gamma_\mu)U_\mu(x)\psi(x+a\hat{\mu}) + (1+\gamma_\mu)U_\mu^{-1}(x-a\hat{\mu})\psi(x-a\hat{\mu})\right\}. \tag{1.83}$$

$\kappa = 1/(2am_0 + 8)$ is the *hopping parameter*. The fermion field is massless at

$$\kappa_c = \begin{cases} 1/8 & \text{for free fermions } (U \equiv I) \\ >1/8 & \text{for fermions coupled to the gauge field} \end{cases}. \tag{1.84}$$

At this point we have all the ingredients to write the partition function of Wilson's lattice QCD in terms of the gauge field $U$ and a number $N_\mathrm{f}$ of quark fields $\psi_f$, $f = 1, \ldots, N_\mathrm{f}$ whose bare masses are $m_{0f}$. It is

$$Z = \int \mathscr{D}[U] \prod_{f=1}^{N_\mathrm{f}} \mathscr{D}[\bar{\psi}_f]\, \mathscr{D}[\psi_f]\, \mathrm{e}^{-S_\mathrm{w}[U] + \sum_{f=1}^{N_\mathrm{f}} \bar{\psi}_f (D_\mathrm{w} + m_{0f})\psi_f}, \tag{1.85}$$

where $\mathscr{D}[\psi_f] = \prod_{x,i,\alpha} \mathrm{d}(\psi_f)_i^\alpha(x)$ (and similarly for $\mathscr{D}[\bar{\psi}_f]$). The quark fields in the partition function of lattice QCD Eq. (1.85) take values in the Grassmann algebra and a direct simulation of this type of variables would require a prohibitively large amount of storage. Using the Matthews-Salam formula Eq. (A.10) the integrals over the quark fields can be performed analytically and yield

$$Z = \int \mathscr{D}[U]\, \mathrm{e}^{-S_\mathrm{w}[U]} \prod_{f=1}^{N_\mathrm{f}} \det(D_\mathrm{w} + m_{0f}). \tag{1.86}$$

The Wilson–Dirac operator Eq. (1.80) obeys the relation

$$\gamma_5 D_\mathrm{w} \gamma_5 = D_\mathrm{w}^\dagger \tag{1.87}$$

which is usually termed "$\gamma_5$-hermiticity". The matrix $\gamma_5$ is defined in Sect. A.2. Equation (1.87) in combination with $\det(\gamma_5) = 1$ implies $\det(D_\mathrm{w} + m_{0f})^\dagger = \det(D_\mathrm{w} + m_{0f})$ which means that the quark determinant $\det(D_\mathrm{w} + m_{0f})$ is real.

### 1.4.8 Chiral Symmetry and the Nielsen–Ninomiya No-Go Theorem

The mass of Wilson fermions on the lattice receives an additive renormalisation due to quantum corrections originating from the interaction with the gauge field. Setting the bare mass parameter $m_0$ in Eq. (1.79) equal to zero does not imply that the physical (renormalized) fermion mass is zero. Equivalently, the critical value $\kappa_c$ of the hopping parameter deviates from its classical value $1/8$, see Eq. (1.84). In the following we explain this is due to the breaking of chiral symmetry on the lattice with Wilson fermions [19, 20]. A chiral transformation is defined by

$$\psi(x) \longrightarrow \psi'(x) = \mathrm{e}^{i\alpha\gamma_5}\psi(x), \qquad \bar{\psi}(x) \longrightarrow \bar{\psi}'(x) = \bar{\psi}(x)\mathrm{e}^{i\alpha\gamma_5}, \tag{1.88}$$

where $\alpha$ is a real parameter. Let us define

$$\not{\partial}\psi(x) = \frac{1}{2}\sum_{\mu}\gamma_{\mu}(\nabla_{\mu}^{*} + \nabla_{\mu})\psi(x). \tag{1.89}$$

This operator is anti-hermitian with respect to the scalar product of two fermion fields $\psi$ and $\chi$ defined as $(\psi, \chi) = a^4 \sum_x \psi(x)^* \chi(x)$. This means $(\psi, \not{\partial}\chi) = -(\not{\partial}\psi, \chi)$. Moreover since $\{\not{\partial}, \gamma_5\} = 0$, the action

$$S = a^4 \sum_{x} \bar{\psi}(x)(\not{\partial} + m_0)\psi(x) \tag{1.90}$$

is invariant under the chiral transformation Eq. (1.88) when $m_0 = 0$. The action Eq. (1.90) for free fermions (i.e. the gauge field is set to unity) can be equivalently written in momentum space as (see Sect. A.2)

$$S = \int \frac{\mathrm{d}^4 p}{(2\pi)^4} \tilde{\bar{\psi}}(p) S(p)^{-1} \tilde{\psi}(p), \tag{1.91}$$

with the propagator $S(p)$ given by

$$S(p) = \left[\frac{i}{a}\sum_{\mu}\gamma_{\mu}\sin(ap_{\mu}) + m_0\right]^{-1}. \tag{1.92}$$

We define $\bar{p}_{\mu} = \frac{1}{a}\sin(ap_{\mu})$. In the classical continuum limit, when $ap_{\mu} \ll 1$, we have $\bar{p}_{\mu} \approx p_{\mu}$ and the propagator Eq. (1.92) reduces to its continuum form. But also if $ap_{\mu} = \pi - aq_{\mu}$ with $aq_{\mu} \ll 1$, then $\bar{p}_{\mu} \approx q_{\mu}$. This means that there are $2^4 = 16$ regions in the Brillouin zone which exhibit continuum behavior. The continuum limit has 16 degenerate "flavours" of the fermion. This fact is called *species doubling* on the lattice. Even if the copies can be forbidden as asymptotic states, they contribute in loops, for example to the renormalisation group $\beta$ function.

This problem is expressed by the Nielsen–Ninomiya theorem [21–24]. A simple form of this theorem holds for free fermions on a Euclidean lattice. It is assumed that the massless Dirac operator $D$ is invariant under translations, such that

$$D\mathrm{e}^{ipx}u = \tilde{D}(p)\mathrm{e}^{ipx}u, \tag{1.93}$$

where $u$ is a constant Dirac spinor and $\tilde{D}(p)$ is a complex $4 \times 4$ complex matrix. The Nielsen–Ninomiya theorem states that the following properties cannot hold simultaneously:

1. *locality*: $\tilde{D}(p)$ is an analytic periodic function of $p_{\mu}$ with period $2\pi/a$;
2. *continuum limit*: for $ap_{\mu} \ll \pi$, $\tilde{D}(p) = i\sum_{\mu}\gamma_{\mu}p_{\mu} + \mathrm{O}(ap^2)$;

3. *no species doubling*: $\tilde{D}(p)$ is invertible for all non-zero momenta $p$ (mod $2\pi/a$);
4. *continuum chiral symmetry*: $\{D, \gamma_5\} = 0$.

Properties 1 and 2 have to hold for a sensible continuum limit. If one insists on having chiral symmetry in its continuum form (Property 4), then species doubling cannot be avoided. Possible cures for non-chiral gauge theories like QCD are

(a) add a Wilson term to $\not{\partial}$;
(b) staggered fermions, which have a $U(1)$ chiral symmetry but come in four copies;
(c) Ginsparg–Wilson fermions, which are undoubled and fulfill a lattice-form of chiral symmetry [25].

The solution of adding a Wilson term is the replacement

$$\not{\partial} \longrightarrow d_W = \frac{1}{2} \sum_\mu \left\{ \gamma_\mu (\nabla_\mu^* + \nabla_\mu) - ar \nabla_\mu^* \nabla_\mu \right\}, \tag{1.94}$$

which for $r = 1$ is the operator in Eq. (1.80). The propagator is

$$S_W(p) = \left[ \frac{i}{a} \sum_\mu \gamma_\mu \bar{p}_\mu + m_0 + \frac{ar}{2} \sum_\mu \hat{p}_\mu^2 \right]^{-1}, \tag{1.95}$$

where $\hat{p}_\mu = \frac{2}{a} \sin(a p_\mu / 2)$. The extra term is

$$a \sum_\mu \hat{p}_\mu^2 \approx \begin{cases} a \sum_\mu p_\mu^2 = \mathrm{O}(a) & \text{if } a p_\mu \ll 1 \\ a \sum_\mu \left( \frac{2}{a} \cos(a q_\mu / 2) \right)^2 \simeq \frac{16}{a} & \text{if } p_\mu = \frac{\pi}{a} - q_\mu \text{ and } a q_\mu \ll 1. \end{cases} \tag{1.96}$$

This has the effect of making the doublers as heavy as the cut-off. Since

$$\{d_W + m_0, \gamma_5\} = \big( - ar \sum_\mu \nabla_\mu^* \nabla_\mu + 2 m_0 \big) \gamma_5, \tag{1.97}$$

chiral symmetry is broken even if $m_0 = 0$ by $\{d_w, \gamma_5\} \sim a \sum_\mu p_\mu^2$. It can be shown that the axial anomaly emerges correctly in the continuum limit, see Ref. [14] and references therein. The parameter $r$ is usually set to unity [26] since the existence of a positive transfer matrix can be shown in this case.

#### 1.4.8.1 Locality

We show that Property 1 of the Nielsen–Ninomiya theorem, namely analyticity and periodicity of $\tilde{D}(p)$, implies locality in $x$-space. For simplicity we consider one dimension with coordinates $x = na$, $n \in \mathbb{Z}$. The integral of $\tilde{D}$ in the complex plane along the contour sketched in Fig. 1.5 is zero due to analyticity

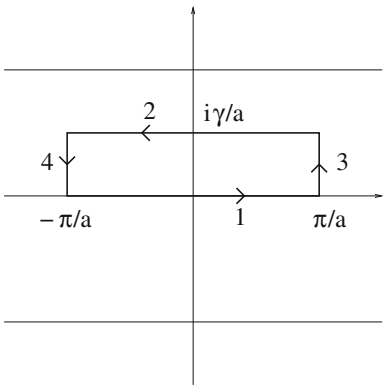


**Fig. 1.5** Contour in the complex plane for the integration of the Dirac operator $\tilde{D}(p)$. $\gamma < \pi$ is a positive number

$$0 = \oint \frac{\mathrm{d}p}{2\pi} \tilde{D}(p) \mathrm{e}^{ipx} = \Big( \underbrace{\int_1}_{D(x)} + \int_2 + \underbrace{\int_3 + \int_4}_{\text{periodicity} \Rightarrow 0} \Big) \frac{\mathrm{d}p}{2\pi} \tilde{D}(p) \mathrm{e}^{ipx}$$

$$\Rightarrow |D(x)| = \left| \int_2 \frac{\mathrm{d}p}{2\pi} \tilde{D}(p) \mathrm{e}^{ipx} \right| \leq C \mathrm{e}^{-\gamma |n|}, \quad \gamma > 0. \tag{1.98}$$

It follows that the elements of the Dirac operator $D(x)$ fall off exponentially with the distance $|x|$ at a rate proportional to $1/a$.

### *1.4.9 Other Fermion Formulations*

Wilson's solution to formulate lattice fermions in compliance with the Nielsen–Ninomiya theorem is not the only possibility. Staggered fermions retain a remnant chiral symmetry at the price of coming in multiple species. Ginsparg–Wilson fermions are invariant under a lattice version of chiral symmetry which in the continuum limit becomes equivalent to full chiral symmetry. In the following we describe briefly these alternative formulations.

The construction of staggered fermions [27, 28] starts with the naive free fermion operator defined in Eq. (1.89), where the gauge links are set to unity. The propagator Eq. (1.92) has poles at momenta $p$ for $g = 1, \ldots, 16$

$$p \in \{\pi_g\} \text{ with } (\pi_g)_\mu = 0 \quad \text{or} \quad (\pi_g)_\mu = \pi/a. \tag{1.99}$$

These poles correspond to 16 fermion doublers. The naive action Eq. (1.90) is invariant under the set $\mathscr{G}$ of 16 discrete doubling transformations

$$\tilde{\psi}(p) \to M_g \tilde{\psi}(p + \pi_g), \quad \tilde{\bar{\psi}}(p) \to \tilde{\bar{\psi}}(p + \pi_g) M_g^\dagger \tag{1.100}$$

with

$$M_g = M_g^{(0)} M_g^{(1)} M_g^{(2)} M_g^{(3)}, \quad M_g^{(\mu)} = \begin{cases} i\gamma_5\gamma_\mu & \text{for } (\pi_g)_\mu = \pi/a \\ I & \text{for } (\pi_g)_\mu = 0 \end{cases}. \tag{1.101}$$

The maximal diagonalization of $\mathscr{G}$ constrains $\psi$ to have only one independent pair of Grassmann variables $\chi(x)$ and $\bar{\chi}(x)$ per site

$$\psi_\alpha = e_\alpha(x)\chi(x), \quad \bar{\psi}_\alpha = e_\alpha^\dagger(x)\bar{\chi}(x), \tag{1.102}$$

where $e(x)$ is a complex-valued spinor field projected on a one-dimensional subspace and $e(x + 2a\hat{\mu}) = e(x)$, $e^\dagger(x)e(x) = 1$, see [29]. After the transformation Eq. (1.102) the action becomes

$$S = a^4 \sum_x \bar{\chi}(x) \left[ m_0 + \sum_\mu \frac{1}{2}\eta_\mu(x)(\nabla_\mu^\star + \nabla_\mu) \right] \chi(x) \tag{1.103}$$

with

$$\eta_\mu(x) = e^\dagger(x)\gamma_\mu e(x + a\hat{\mu}). \tag{1.104}$$

An explicit choice of the staggered phases is $\eta_\mu(x) = (-1)^{\sum_{\nu<\mu} n_\nu}$. Equation (1.103) is the action for a single staggered fermion $\chi$. One can combine its components in a $2^4$ hypercube to construct four Dirac fields which are called tastes, see [15]. In the continuum a staggered fermion is equivalent to four degenerate tastes of Dirac fermions. The introduction of a gauge field is straightforward in the derivatives $\nabla_\mu$ and $\nabla_\mu^*$, see Eqs. (1.81) and (1.82) and the constraint $\psi_\alpha = e_\alpha(x)\chi(x)$ is unchanged. For $m_0 = 0$, staggered fermions have an axial taste non-singlet (i.e. non-anomalous) $U(1)$ chiral symmetry given by

$$\chi(x) \to \mathrm{e}^{i\beta\varepsilon(x)}\chi(x), \quad \bar{\chi}(x) \to \mathrm{e}^{i\beta\varepsilon(x)}\bar{\chi}(x), \quad \varepsilon(x) = (-1)^{\sum_\mu n_\mu}. \tag{1.105}$$

As a consequence, staggered fermions have no additive quark mass renormalization. The symmetry Eq. (1.105) is dynamically broken giving one Goldstone pion. The full $SU(4)$ symmetry of the four tastes is recovered in the continuum limit.

Staggered fermions are computationally cheaper than Wilson fermions. Moreover their discretisation effects are proportional to $a^2$. A disadvantage is that the construction of quark fields and hadron operators is more complicated due to the $\mathrm{O}(a^2)$ mixing of the tastes. As we mentioned above the staggered action describes four tastes of quark fields in the continuum. In practical computations one resorts to the so called "fourth-root" trick to reduce the number of tastes from four to one. This trick amounts to replacing the determinant of the staggered fermion operator (cf. Eq. (1.86)) by its fourth root. But at present no local action which is equivalent to this procedure is known, see [30].

Consider a Dirac operator $D$ which fulfills the Ginsparg–Wilson relation [31]

$$\{D, \gamma_5\} = aD\gamma_5 D \Leftrightarrow D^{-1}(x, y)\gamma_5 + \gamma_5 D^{-1}(x, y) = a\gamma_5\delta(x - y). \quad (1.106)$$

The fermion action for such an operator $D$ is invariant under an exact continuous symmetry [25] with infinitesimal form for a small parameter $\varepsilon$ given by

$$\delta\psi = \varepsilon\gamma_5(1 - aD/2)\psi, \quad \delta\bar{\psi} = \varepsilon\bar{\psi}(1 - aD/2)\gamma_5. \quad (1.107)$$

The axial anomaly emerges from the Jacobian of the measure [25]. Operators satisfying the relation Eq. (1.106) obey the index theorem on the lattice [32]. An explicit solution for such an operator $D$ is the *overlap Dirac operator* [33]

$$D = \frac{1}{a}\{1 - A(A^\dagger A)^{-1/2}\}, \quad A = 1 + s - aD_{\mathrm{w}}, \quad (1.108)$$

where $D_{\mathrm{w}}$ is the Wilson operator defined in Eq. (1.80) and $s$ is a real parameter in the range $|s| < 1$. The locality of the operator in Eq. (1.108) has been shown in Ref. [34]. Exact symmetry comes at a price; the overlap operator is numerically a factor O(100) more expensive to evaluate than the Wilson–Dirac operator. Recent progress on the numerical evaluation of the operator is discussed in [35].

## 1.5 Recovering Continuum QCD

Once QCD is formulated on the lattice, physical quantities can be computed from path integral expectation values. In this section we show that Wilson's lattice gauge action reproduce its continuum form when the lattice spacing $a$ is extrapolated to zero.[2] The *continuum limit* of lattice QCD is reached at zero bare coupling $g_0 = 0$ or, equivalently, at infinite lattice coupling $\beta = \infty$. This result is derived from the renormalisation group equation which we will present.

The limit $a \to 0$ generally requires a *renormalisation* of the quantities computed on the lattice [37] to be performed. An exception is the spectrum of energies of states, which can be directly extracted from lattice correlators without renormalisation. For other quantities, like the currents associated with chiral transformations, renormalisation can be performed by requiring Ward identities of the continuum theory to be fufilled at finite lattice spacing. We will present the Ward identities associated with chiral transformations, which lead to a definition of the quark mass.

[2] It is not necessary for the lattice action to reproduce the continuum action at the classical level. There may be a larger class of actions which share the same quantum continuum limit despite they do not reproduce the classical continuum form, see e.g. the so called topological actions for the non-linear sigma model [36].

The approach of the lattice theory to the continuum can be systematically discussed in the framework of Symanzik's theory of lattice artifacts. At the same time this analysis allows the design of actions which reduce the size of the lattice corrections. This is called *improvement*. We discuss improvement for the pure gauge theory and for lattice QCD including fermions. We close the section by presenting the twisted mass formulation of Wilson fermions, which has the property of "automatic O($a$) improvement".

### *1.5.1 Classical Continuum Limit*

The parameter $\beta$ in Eq. (1.70) is related to the bare gauge coupling $g_0$ in the continuum. We can find this relation by expressing the lattice gauge fields $U_\mu(x)$ in terms of the continuum gauge field $A_\mu(x)$ through

$$U_\mu(x) = \exp(aA_\mu(x)). \tag{1.109}$$

This relation does not preserve gauge-invariance and in fact could be replaced by a gauge-invariant relation, see [38]. But for our purpose here we can use Eq. (1.109), insert it in Eq. (1.70) and expand in powers of $a$. The leading term in an asymptotic expansion of $S_\mathrm{w}$ is (see for example [14])

$$S_\mathrm{W} = -\frac{\beta}{4N}\sum_x\sum_{\mu,\nu} a^4 \mathrm{tr}\,\{F_{\mu\nu}(x)F_{\mu\nu}(x)\} + O(a^5), \tag{1.110}$$

where the field strength tensor is here defined by

$$F_{\mu\nu} = \nabla_\mu A_\nu - \nabla_\nu A_\mu + [A_\mu, A_\nu], \tag{1.111}$$

with the forward lattice derivative $\nabla_\mu A_\nu = \{A_\nu(x + a\hat{\mu}) - A_\nu(x)\}/a$. Therefore, the expression in Eq. (1.111) reduces to its continuum form Eq. (1.8) as $a \to 0$. A comparison of Eq. (1.110) with the continuum Yang-Mills action Eq. (1.6) yields the relation

$$\beta = \begin{cases} 2N/g_0^2 & \text{for gauge group } SU(N) \\ 1/g_0^2 & \text{for gauge group } U(1) \end{cases}. \tag{1.112}$$

Another useful relation is a lattice definition of the field strength tensor

$$P_{\mu,\nu}(x) - 1 = a^2 F_{\mu\nu}(x) + O(a^3). \tag{1.113}$$

It should be noted that the $O(a^5)$ terms in Eq. (1.110) vanish by gauge invariance and the lattice symmetries. Therefore the leading lattice corrections are actually $O(a^6)$. We will return to this point in Sect. 1.5.4.

### 1.5.2 Renormalisation Group Equation

Consider the pure gauge theory, which has a single bare parameter, the gauge coupling $g_0$. We denote by $\bar{g}(\mu)$ a renormalised running coupling with renormalisation scale $\mu$. In the continuum a physical quantity $F = F(\mu, \bar{g})$ is defined to be independent of the scale $\mu$, i.e. $\mu \frac{\mathrm{d}F}{\mathrm{d}\mu} = 0$. On the lattice, the quantity $F = F(\bar{g}, a)$ depends on the lattice spacing $a$. A line of constant physics (LCP) is defined by taking the continuum limit $a \to 0$ at fixed value of $\bar{g}$. Physical quantities depend on the lattice spacing $a$ as

$$a \frac{\mathrm{d}}{\mathrm{d}a} F(\bar{g}, a) = 0 + O(a^2), \tag{1.114}$$

where $O(a^2)$ corrections are called scaling violations. Actually $O(a^2)$ stands here also for terms $O(a^2 \ln a)$. The renormalisation group equation is

$$\left( a \frac{\partial}{\partial a} - \beta_{\mathrm{LAT}} \frac{\partial}{\partial g_0} \right) F(\bar{g}, a) = O(a^2), \tag{1.115}$$

in terms of the lattice $\beta$ function

$$\beta_{\mathrm{LAT}}(g_0, a) = -a \frac{\partial g_0}{\partial a}\bigg|_{\bar{g}}. \tag{1.116}$$

$\beta_{\mathrm{LAT}}$ can be computed in perturbation theory; $\beta_{\mathrm{LAT}}(g_0, a) = \beta(g_0)[1 + O(a^2)]$ with

$$\beta(g_0) = -(b_0 g_0^3 + b_1 g_0^5 + \ldots), \quad b_0 = \frac{1}{(4\pi)^2} \frac{11N}{3}, \quad b_1 = \frac{1}{(4\pi)^4} \frac{34N^2}{3}. \tag{1.117}$$

The coefficients $b_0$ and $b_1$ are universal, i.e. they do not depend on the choice of the coupling $\bar{g}$ in Eq. (1.116) provided $\bar{g} = g_0 + F_1(t) g_0^3 + F_2(t) g_0^5 + \ldots$ where $F_1$, $F_2$ are functions of $t = \ln(a\mu)$, see [17]. Neglecting the $O(a^2)$ terms, Eq. (1.116) becomes $-a\{\partial g_0/\partial a\}|_{\bar{g}} = \beta(g_0)$ and has the solution

$$a(g_0) = \Lambda_{\mathrm{LAT}}^{-1} \, \mathrm{e}^{-1/(2b_0 g_0^2)} \, (b_0 g_0^2)^{-b_1/(2b_0^2)} \, [1 + O(g_0^2)], \tag{1.118}$$

with an energy scale $\Lambda_{\mathrm{LAT}}$, see Sect. 1.5.2.1. The relation Eq. (1.118) can be inverted and yields

$$b_0 g_0^2 \approx \frac{1}{\left| \ln(a^2 \Lambda_{\mathrm{LAT}}{}^2) \right|}. \tag{1.119}$$

This shows that the continuum limit $a \to 0$ is reached when $g_0 \to 0$. Note that in the classical pure-gauge action there are no parameters with the dimension of an energy. The energy scale $\Lambda_{\mathrm{LAT}}$ is generated by the renormalisation of the theory, a property known as *dimensional transmutation*. Moreover, it follows from Eq. (1.114) that a

physical quantity such as the mass $M$ of a glueball state calculated on the lattice approaches the continuum limit like

$$M = c\Lambda_{\rm LAT}[1 + O(a^2\Lambda_{\rm LAT}^2)] \tag{1.120}$$

for some dimensionless constant $c$. The same arguments hold for a gauge theory with massless O($a$) improved Wilson fermions, see Sect. 1.5.4. The universal coefficients of the $\beta$ function for $N_{\rm f}$ massless quarks are

$$b_0 = \frac{1}{(4\pi)^2}\left(\frac{11N}{3} - \frac{2N_{\rm f}}{3}\right), \quad b_1 = \frac{1}{(4\pi)^4}\left(\frac{34N^2}{3} - \frac{10NN_{\rm f}}{3} - 2C_{\rm F}N_{\rm f}\right), \tag{1.121}$$

where $C_{\rm F} = (N^2 - 1)/(2N)$.

#### 1.5.2.1 Solution of the Renormalisation Group Equation

We derive here the result Eq. (1.118). The starting point is the renormalisation group equation

$$-\frac{\partial g_0}{\partial \ln a} = \beta(g_0) = -[b_0 g_0^3 + b_1 g_0^5 + O(g_0^7)]. \tag{1.122}$$

Integration gives

$$\begin{aligned} -\ln a(g_0) &= -\ln a(x_0) + \int_{x_0}^{g_0} \frac{{\rm d}x}{\beta(x)} \\ &= -\ln a(x_0) + \int_{x_0}^{g_0} {\rm d}x \left[\frac{-1}{b_0 x^3} + \frac{b_1}{b_0^2 x} + O(x)\right] \\ &= \frac{1}{2b_0 g_0^2} + \frac{b_1}{b_0^2}\ln g_0 + k + O(g_0^2). \end{aligned} \tag{1.123}$$

The integration constant $k$ is independent of $g_0$. It can be partially combined with $\ln a$ to form a dimensionless quantity $\ln(a\Lambda_{\rm LAT})$ in a way that has become standard

$$-\ln(a^2 {\Lambda_{\rm LAT}}^2) = \frac{1}{b_0 g_0^2} + \frac{b_1}{b_0^2}\ln(b_0 g_0^2) + O(g_0^2). \tag{1.124}$$

This is called the "ln $b_0$ convention" [17]. We emphasize that the Lambda parameter $\Lambda_{\rm LAT}$ can only be defined precisely if the $b_1$ term is taken into account.

### 1.5.3 Isospin Symmetry and Ward Identities

Consider a doublet of quarks $\psi(x) = (\psi_1(x)\ \psi_2(x))^T$ with equal mass $m$. Its components $\psi_f$ are labelled by a flavour index $f$. An example in nature are the up and down quarks in the approximation where their masses are the same, called the *isospin limit*. In the continuum, the action of the doublet is

$$S = \sum_f \int \mathrm{d}^4x\ \bar{\psi}_f(x)(\gamma_\mu D_\mu + m_0)\psi_f(x), \tag{1.125}$$

where we make the flavour index explicit. This action is invariant under $SU(2)$ isospin rotations of the flavour components. Following Ref. [39], consider infinitesimal local isovector axial rotations, parameterised by $\omega^a(x)$, $a = 1, 2, 3$. The functions $\omega^a$ are assumed to vanish outside a bounded region $R$ in space. The quark fields change as $\psi' = \psi + \delta\psi$ and $\bar{\psi}' = \bar{\psi} + \delta\bar{\psi}$ with

$$\delta\psi_f(x) = \frac{1}{2}\omega^a(x)\sigma^a_{ff'}\gamma_5\psi_{f'}(x), \quad \delta\bar{\psi}_f(x) = \frac{1}{2}\omega^a(x)\bar{\psi}_{f'}(x)\gamma_5\sigma^a_{f'f}. \tag{1.126}$$

These rotations are called axial because of the presence of the matrix $\gamma_5$ acting on the spinor indices and isovector because of the Pauli matrices $\sigma^a$ acting on the flavour indices. The expectation value of a function $\mathcal{O}$ of the quark and gauge fields is

$$\langle\mathcal{O}\rangle = \frac{1}{Z}\int \mathcal{D}\psi'\mathcal{D}\bar{\psi}'\mathcal{D}U\,\mathcal{O}(\psi', \bar{\psi}', U)\mathrm{e}^{-S[\psi',\bar{\psi}',U]}. \tag{1.127}$$

The finite form of the infinitesimal transformations Eq. (1.126) is $\psi' = A\psi$ and $\bar{\psi}' = \bar{\psi}A$ with $A = \exp(\frac{1}{2}\omega^a(x)\delta_{x,y}\sigma^a\gamma_5)$. The Jacobian is $\det(A)^{-2} = \exp(-2\mathrm{tr}_{x,\sigma,c}\ \ln A) = 1$, see Sect. A.2. The trace is over coordinate, spin and colour indices and the Jacobian is unity since $\mathrm{tr}\,\sigma^a = 0$. Under Eq. (1.126) we have $\mathcal{O}(\psi', \bar{\psi}', U) = \mathcal{O}(\psi, \bar{\psi}, U) + \delta\mathcal{O}(\psi, \bar{\psi}, U)$ and similarly $S(\psi', \bar{\psi}', U) = S(\psi, \bar{\psi}, U) + \delta S(\psi, \bar{\psi}, U)$. Inserting into Eq. (1.127) we obtain

$$\langle\mathcal{O}\delta S\rangle = \langle\delta\mathcal{O}\rangle\,. \tag{1.128}$$

The change of the action is given by

$$\delta S = \int_R \mathrm{d}^4x\omega^a(x)\left[-\partial_\mu A^a_\mu(x) + 2mP^a(x)\right] \tag{1.129}$$

where the isovector axial current $A^a_\mu$ and isovector axial density $P^a$ are defined as

$$A^a_\mu(x) = \frac{1}{2}\bar{\psi}_f(x)\gamma_\mu\gamma_5\sigma^a_{ff'}\psi_{f'}(x) \quad \text{and} \quad P^a(x) = \frac{1}{2}\bar{\psi}_f(x)\gamma_5\sigma^a_{ff'}\psi_{f'}(x). \tag{1.130}$$

If the fields in the function $\mathscr{O}$ are localised outside the region $R$, then $\delta\mathscr{O} = 0$ and from Eqs. (1.128) and (1.129) it follows

$$\left\langle \partial_\mu A^a_\mu(x)\mathscr{O}\right\rangle = 2m\left\langle P^a(x)\mathscr{O}\right\rangle, \quad \forall a. \tag{1.131}$$

Since for zero mass Eq. (1.131) expresses the conservation of the axial current, Eq. (1.131) is called the partially conserved axial current (PCAC) relation. It is an example of a chiral Ward identity. The importance of Eq. (1.131) is that it can be used to define the (current) quark mass $m$. At finite lattice spacing the PCAC relation Eq. (1.131) does not hold. One needs to renormalise the axial current and the axial density in Eq. (1.130). Then Eq. (1.131) can be used to define a renormalised quark mass up to lattice spacing corrections of $\mathrm{O}(a)$ which vanish as the continuum limit is taken. We refer to [39] for more details. In the continuum a infinitesimal chiral transformation is given by (cf. Eq. (1.88))

$$\delta\psi_f(x) = i\omega(x)\gamma_5\psi_f(x), \quad \delta\bar{\psi}_f(x) = i\omega(x)\bar{\psi}_f(x)\gamma_5, \tag{1.132}$$

The corresponding Noether current is the $U(1)$ axial current defined as

$$A^0_\mu = \bar{\psi}_f(x)\gamma_\mu\gamma_5\psi_f(x). \tag{1.133}$$

According to Noether's theorem this current is conserved $\partial_\mu A^0_\mu(x) = 0$. Quantum effects break this relation and lead to an *anomaly*. The renormalised current $A^0_{\mathrm{R}\mu}$ is not conserved in the limit of massless quarks. The anomaly is responsible for example for the electromagnetic decay of the pion into two photons. When QCD is fomulated on the lattice, the correct anomaly has to emerge in the continuum limit. For a derivation of the anomalous chiral Ward identity for Wilson fermions we refer to [14]. A review on the chiral anomaly is given in [40].

### *1.5.4 Improvement of the Continuum Limit*

Symanzik conjectured that when the continuum limit $a \to 0$ is approached, the lattice theory can be described by an effective continuum theory with the lattice spacing $a$ as an expansion parameter [41]. In the effective continuum theory only operators which respect the symmetry of the lattice theory can appear. By "operator" we mean a Euclidean complex-valued field constructed from the fundamental fields. In the case of the pure gauge theory on the lattice, the action of the effective continuum theory is [38, 42]

$$S = \int \mathrm{d}^4x\, \mathscr{L}_{\mathrm{eff}}(x), \tag{1.134}$$

with the local effective Lagrangian

$$\begin{aligned}\mathscr{L}_{\text{eff}} &= Z_0(g_0^2)\sum_{\mu,\nu}\text{tr}\,\{F_{\mu\nu}F_{\mu\nu}\}\\ &+a^2Z_1(g_0^2)\sum_{\mu,\nu}\text{tr}\,\{D_\mu F_{\mu\nu}D_\mu F_{\mu\nu}\}\\ &+a^2Z_2(g_0^2)\sum_{\mu,\nu,\rho}\text{tr}\,\{D_\mu F_{\nu\rho}D_\mu F_{\nu\rho}\}\\ &+a^2Z_3(g_0^2)\sum_{\mu,\nu,\rho}\text{tr}\,\{D_\mu F_{\mu\rho}D_\nu F_{\nu\rho}\}+O(a^4)\end{aligned}\tag{1.135}$$

where

$$D_\mu F_{\nu\rho}=\partial_\mu F_{\nu\rho}+[A_\mu,F_{\nu\rho}].\tag{1.136}$$

The coefficients $Z_i(g_0^2)$ of the effective Lagrangian can be computed in perturbation theory in the gauge coupling $g_0$. The three operators in Eq. (1.135) which are multiplied by $a^2$ are a complete set of gauge-invariant operators of dimension equal to 6 which are invariant under parity und $\pi/2$ rotations. Any such operator of dimension 6 can be represented as a linear combination of the three operators in Eq. (1.135) plus a total derivative. Due to these symmetries no operators with odd powers of the lattice spacing can appear in Eq. (1.135). Notice that in Eq. (1.135) the term multiplied by $Z_1$ breaks the continuum rotational symmetry but the other terms multiplied by $Z_2$ and $Z_3$ don't.

The argument of the Symanzik effective theory can be turned around. The Symanzik improvement programme [43–45] applied to the pure gauge theory is a systematic design of a lattice action which reduces the $O(a^2)$ dependence in Eq. (1.120). In principle it is possible to reduce the lattice corrections to $O(a^4)$. To achieve this it is necessary to introduce loops up to length $6a$ in the action. This class of action was first considered in [46]. The coefficients of the action can be determined in order to eliminate the $O(a^2)$ corrections arising in the energy spectrum and scattering amplitudes ("on-shell improvement") at tree level [38] and at one-loop level in perturbation theory [47]. In particular the tree-level Symanzik-improved action has the form

$$S=\frac{2}{g_0^2}\sum_{i=0}^{1}c_i\sum_{\mathscr{C}\in\mathscr{S}_i}\text{Re}\,\text{Tr}\,[1-U(\mathscr{C})]\tag{1.137}$$

where $\mathscr{S}_0$ denotes the set of $1\times1$ plaquettes and $\mathscr{S}_1$ the set of $1\times2$ rectangles. Loops $\mathscr{C}$ that differ by orientation only are considered equivalent. The values of the coefficients are [38, 47]

$$c_0=\frac{5}{3},\quad c_1=-\frac{1}{12}.\tag{1.138}$$

These values can be derived by a simple geometric argument. Consider a rectangular $a \times b$ Wilson loop $W_{a,b}$. Keeping the shape of the loop fixed, i.e. $b = \gamma a$ and $\gamma$ fixed, its Symanzik expansion is

$$W_{a,b} = a^2 b^2 G_{2,2} + a^2 b^4 G_{2,4} + a^4 b^2 G_{4,2} + \mathrm{O}(a^8), \tag{1.139}$$

where $G_{2,2} = \int \mathrm{d}^4 x \, \mathrm{tr}\,\{F_{\mu\nu} F_{\mu\nu}\}$. The plaquette can be written

$$W_{a,a} = a^4 G_{2,2} + a^6 (G_{2,4} + G_{4,2}) + \mathrm{O}(a^8), \tag{1.140}$$

and the sum of the two orientations of the $2 \times 1$ rectangle becomes

$$W_{2a,a} + W_{a,2a} = 8a^4 G_{2,2} + 20a^6 (G_{2,4} + G_{4,2}) + \mathrm{O}(a^8). \tag{1.141}$$

The dimension-six operators can be cancelled by taking the linear combination

$$\frac{5}{3} W_{a,a} - \frac{1}{12} \left\{ W_{2a,a} + W_{a,2a} \right\} = a^4 G_{2,2} + \mathrm{O}(a^8), \tag{1.142}$$

which reproduces Eq. (1.138).

### 1.5.5 *Improvement of Wilson Fermions*

Starting from the fermion action in the continuum Eq. (1.12), perform the local field rotations [48, 49]

$$\psi = \left(1 - \frac{a}{4}(\not{D} - m_0)\right) \psi' + \mathrm{O}(a^2) \tag{1.143}$$

$$\bar{\psi} = \bar{\psi}' \left(1 + \frac{a}{4}(\overleftarrow{\not{D}} + m_0)\right) + \mathrm{O}(a^2). \tag{1.144}$$

Here $a$ is treated in the abstract as a small parameter and the derivatives in $\overleftarrow{\not{D}}$ act on the fields on their left. The Jacobian of the rotations is given to leading order in $a$ by $\det\left(1 + \frac{a}{2} m_0\right)$ and is therefore constant. After the transformations Eqs. (1.143) and (1.144) the action Eq. (1.12) becomes

$$S'_{\mathrm{F}} = \int \mathrm{d}^4 x \, \bar{\psi}'(x) \left\{ \not{D} + m_0 \left(1 + \frac{a}{2} m_0\right) - \frac{a}{2} D^2 + i \frac{a}{4} \sigma_{\mu\nu} F_{\mu\nu}(x) \right\} \psi'(x) + \mathrm{O}(a^2), \tag{1.145}$$

where we used integration by parts in the form $\bar{\psi} \overleftarrow{\not{D}} = -\bar{\psi} \overrightarrow{\not{D}}$ and the identity

$$\not{D}^2 = D^2 - \frac{i}{2} \sum_{\mu,\nu} \sigma_{\mu\nu} F_{\mu\nu}, \quad D^2 = D_\mu D_\mu, \quad \sigma_{\mu\nu} = \frac{i}{2} [\gamma_\mu, \gamma_\nu]. \tag{1.146}$$

Let us now discretise the action Eq. (1.145) and set $a$ equal to the lattice spacing. The rotations Eqs. (1.143) and (1.144) have generated the Wilson term $(-a/2)\nabla^*_\mu\nabla_\mu$ and the Sheikholeslami–Wohlert term $(ia/4)\sigma_{\mu\nu}\hat{F}_{\mu\nu}$ [48]. Here $\hat{F}_{\mu\nu}$ a lattice discretisation of the field strength tensor. This means that, up to a redefinition of the mass term, keeping the Wilson term and the Sheikholeslami–Wohlert term in the action has the effect of cancelling the O($a$) lattice corrections at the classical level. The O($a$) improved Wilson–Dirac operator is

$$D = D_{\mathrm{w}} + c_{\mathrm{sw}} \sum_{\mu,\nu=0}^{3} \frac{i}{4}\sigma_{\mu\nu}\hat{F}_{\mu\nu} + m_0. \tag{1.147}$$

The Sheikholeslami–Wohlert coefficient $c_{\mathrm{sw}}$ is one at the classical (tree) level. A symmetric definition of $\hat{F}_{\mu\nu}$ is given in Ref. [39]

$$\hat{F}_{\mu\nu}(x) = \frac{1}{8a^2}\left[Q_{\mu,\nu}(x) - Q^\dagger_{\mu,\nu}(x)\right], \tag{1.148}$$

where

$$\begin{aligned} Q_{\mu,\nu}(x) = {} & U_\mu(x)\, U_\nu(x+a\hat{\mu})\, U_\mu^{-1}(x+a\hat{\nu})\, U_\nu^{-1}(x) + \\ & U_\nu(x)\, U_\mu^{-1}(x-a\hat{\mu}+a\hat{\nu})\, U_\nu^{-1}(x-a\hat{\mu})\, U_\mu(x-a\hat{\mu}) + \\ & U_\mu^{-1}(x-a\hat{\mu})\, U_\nu^{-1}(x-a\hat{\mu}-a\hat{\nu})\, U_\mu(x-a\hat{\mu}-a\hat{\nu})\, U_\nu(x-a\hat{\nu}) + \\ & U_\nu^{-1}(x-a\hat{\nu})\, U_\mu(x-a\hat{\nu})\, U_\nu(x+a\hat{\mu}-a\hat{\nu})\, U_\mu^{-1}(x). \end{aligned} \tag{1.149}$$

The implementation of Eq. (1.147) is discussed in the documentation of the openQCD package.[3]

### 1.5.6 Twisted Mass Fermions

The breaking of chiral symmetry by the Wilson term leads to an additive renormalisation of the quark mass. Light quarks typically have negative values of bare mass. On a given gauge background field, the Wilson–Dirac operator $D_{\mathrm{w}} + m_0$ Eq. (1.80) is not protected from having zero eigenvalues unless $m_0 > 0$. This affects the simulations of light Wilson quarks; during the Hybrid Monte Carlo evolution, evaluation of the fermionic force requires the inversion of the Dirac operator and accidental zero eigenvalues lead to infinite forces which destabilise the molecular dynamics integration.

In the continuum limit these "exceptional" configurations disappear due to the restoration of chiral symmetry. At finite lattice spacing a cure is provided by adding

[3] http://luscher.web.cern.ch/luscher/openQCD/.

a twisted-mass term to the Wilson–Dirac operator [50]. The lattice action for $N_f = 2$ twisted-mass Wilson fermions is given by

$$S = a^4 \sum_x \bar{\psi}(x)(D_w + m_0 + i\mu\gamma_5\sigma_3)\psi(x), \tag{1.150}$$

where $\mu$ is the bare twisted-mass parameter and $\sigma_3$ is the Pauli matrix acting on the two flavours of the fermion field $\psi$. The operator in Eq. (1.150) has a manifestly positive determinant given by $\det(Q^2 + \mu^2)$, where $Q = \gamma_5(D_w + m_0)$ is the Hermitian Wilson-Dirac operator. Twisted mass and the standard Wilson fermion are equivalent in the continuum limit, where they are related by a chiral field rotation [51]

$$\psi' = R(\alpha)\psi, \quad \bar{\psi}' = \bar{\psi}R(\alpha), \quad R(\alpha) = \exp\left(i\alpha\gamma_5\frac{\sigma_3}{2}\right), \tag{1.151}$$

where $\alpha$ is called the twist angle and the rotated fields $\psi'$ and $\bar{\psi}'$ are those of the standard physical basis of QCD. At finite lattice spacing the choice $\alpha = \pi/2$ (maximal twist) corresponds to tuning the standard quark mass $m_0$ to its critical value $m_c$, cf. Eq. (1.84). Lattice spacing effects are reduced to $O(a^2)$ when using twisted mass fermions at maximal twist [52], a property called "automatic $O(a)$ improvement" and no extra terms are required in contrast to Wilson fermions, as we saw in Sect. 1.5.5. For a proof of automatic $O(a)$ improvement based on Symanzik's analysis we refer to Ref. [51]. Unlike Wilson fermions, parity and isospin symmetry are broken at finite lattice spacing for twisted-mass fermions. A consequence is for example a splitting between the masses of the neutral and charged pions at finite lattice spacing.

## 1.6 Further Reading

This chapter motivates the construction of the path integral formulation of quantum field theory on a Euclidean lattice. It focuses on the fields which are needed for QCD, the spin-$\frac{1}{2}$ quarks and the gluons. This book mainly uses Wilson's formulation of lattice QCD and so this chapter explains this description of QCD on a lattice in more detail. Other formulations, such as staggered, overlap and twisted-mass fermions, are briefly introduced. The relation of the lattice theory to its continuum limit is discussed, in particular Symanzik's theory of lattice artifacts.

We have not covered all the topics pertaining to an introduction to lattice QCD. We mention e.g. the general importance of understanding the phase diagram of the theory, i.e. the existence of critical points where the continuum limit can be taken. We also point out the unfortunate lack of rigorous results, e.g. the proof of the mass gap of pure Yang–Mills theory and of asymptotic freedom of the continuum limit of lattice QCD. In this book we will concentrate on techniques used for Monte Carlo simulations of lattice QCD. An important complementary tool is lattice perturbation theory

which we did not cover. In particular we mention the results obtained in perturbation theory concerning renormalisability, see [37], and the numerical techniques used in perturbative calculations like automatisation and stochastic perturbation theory, see [53] for a review.

There are a number of textbooks on the lattice formulation of quantum field theory [14, 15, 17, 18, 54, 55]. In the text we refer to the books where one can find more details and references.

There are also a number of review articles and lectures available. A compact introduction to lattice field theory which discusses its connection to statistical mechanics is given in an article by G. Münster in scholarpedia.[4] More advanced lecture notes on lattice QCD by M. Lüscher can be found in Ref. [39]. A comprehensive review of the renormalisation of lattice theories and on the study of lattice artifacts by P. Weisz can be found in Ref. [37].

## References


1. M. Gell-Mann, Phys. Lett. **8**, 214 (1964)
2. G. Zweig, Preprints CERN-TH 401 and 412 (1964)
3. J.D. Bjorken, E.A. Paschos, Phys. Rev. **185**, 1975 (1969)
4. R.P. Feynman, Gordon and Breach, p. 237 (1970)
5. R.P. Feynman, Phys. Rev. Lett. **23**, 1415 (1969)
6. H. Fritzsch, M. Gell-Mann, H. Leutwyler, Phys. Lett. **47B**, 365 (1973)
7. H. Weyl, Z. Phys. **56**, 330 (1929)
8. G.'t Hooft, unpublished. See, however, *Proceedings of Colloquium on Renormalization of Yang-Mills Fields and Applications to Particle Physics*, Marseilles, 1972, ed. by C.P. Korthals-Altes. See also Nucl. Phys. **B254**, 11 (1985)
9. D.J. Gross, F. Wilczek, Phys. Rev. Lett. **30**, 1343 (1973)
10. H.D. Politzer, Phys. Rev. Lett. **30**, 1346 (1973)
11. P. Söding, Eur. Phys. J. **H35**, 3 (2010). doi:10.1140/epjh/e2010-00002-5
12. K.G. Wilson, Phys. Rev. D **10**, 2445 (1974). doi:10.1103/PhysRevD.10.2445
13. K.G. Wilson, Nucl. Phys. Proc. Suppl. **140**, 3 (2005). doi:10.1016/j.nuclphysbps.2004.11.271. [,3(2004)]
14. I. Montvay, G. Münster, *Quantum Fields on a Lattice* (Univ. Pr., Cambridge, UK, 1994), p. 491 (Cambridge monographs on mathematical physics), http://www.slac.stanford.edu/spires/find/hep/www?key=3030474
15. T. DeGrand, C. DeTar, *Lattice Methods for Quantum Chromodynamics* (World Scientific, Singapure, 2006)
16. U. Wolff, *Quantum Field Theory*, lecture note, HU Berlin, unpublished (2010)
17. J. Smit, Cambridge. Lect. Notes Phys. **15**, 1 (2002)
18. M. Creutz, in *Quarks, Gluons and Lattices*. Cambridge Monographs on Mathematical Physics (Cambridge Univ. Press, Cambridge, UK, 1985), http://www-spires.fnal.gov/spires/find/books/www?cl=QC793.3.F5C73::1983
19. M. Bochicchio, L. Maiani, G. Martinelli, G.C. Rossi, M. Testa, Nucl. Phys. B **262**, 331 (1985). doi:10.1016/0550-3213(85)90290-1
20. M. Lüscher, S. Sint, R. Sommer, P. Weisz, Nucl. Phys. B **478**, 365 (1996). doi:10.1016/0550-3213(96)00378-1


[4] http://www.scholarpedia.org/article/Lattice_quantum_field_theory.

21. H.B. Nielsen, M. Ninomiya, Phys. Lett. B **105**, 219 (1981). doi:10.1016/0370-2693(81)91026-1
22. H.B. Nielsen, M. Ninomiya, Nucl. Phys. B **185**(20), 1981 (1982). doi:10.1016/0550-3213(81)90361-8.[Erratum:Nucl.Phys.B195541]
23. H.B. Nielsen, M. Ninomiya, Nucl. Phys. B **193**, 173 (1981). doi:10.1016/0550-3213(81)90524-1
24. D. Friedan, Commun. Math. Phys. **85**, 481 (1982). doi:10.1007/BF01403500
25. M. Lüscher, Phys. Lett. B **428**, 342 (1998). doi:10.1016/S0370-2693(98)00423-7
26. M. Lüscher, Commun. Math. Phys. **54**, 283 (1977). doi:10.1007/BF01614090
27. J.B. Kogut, L. Susskind, Phys. Rev. D **11**, 395 (1975). doi:10.1103/PhysRevD.11.395
28. L. Susskind, Phys. Rev. D **16**, 3031 (1977). doi:10.1103/PhysRevD.16.3031
29. H.S. Sharatchandra, H.J. Thun, P. Weisz, Nucl. Phys. B **192**, 205 (1981). doi:10.1016/0550-3213(81)90200-5
30. B. Bunk, M. Della Morte, K. Jansen, F. Knechtli. Nucl. Phys. **B697**, 343 (2004). doi:10.1016/j.nuclphysb.2004.07.023
31. P.H. Ginsparg, K.G. Wilson, Phys. Rev. D **25**, 2649 (1982). doi:10.1103/PhysRevD.25.2649
32. P. Hasenfratz, V. Laliena, F. Niedermayer, Phys. Lett. B **427**, 125 (1998). doi:10.1016/S0370-2693(98)00315-3
33. H. Neuberger, Phys. Lett. B **417**, 141 (1998). doi:10.1016/S0370-2693(97)01368-3
34. P. Hernandez, K. Jansen, M. Luscher, Nucl. Phys. B **552**, 363 (1999). doi:10.1016/S0550-3213(99)00213-8
35. J. Brannick, A. Frommer, K. Kahl, B. Leder, M. Rottmann, A. Strebel, Numer. Math. (2015). doi:10.1007/s00211-015-0725-6
36. W. Bietenholz, U. Gerber, M. Pepe, U.J. Wiese, JHEP **12**, 020 (2010). doi:10.1007/JHEP12(2010)020
37. P. Weisz, in *Modern Perspectives in Lattice QCD: Quantum Field Theory and High Performance Computing. Proceedings, International School, 93rd Session, Les Houches, France, August 3–28, 2009* (2010), pp. 93–160, https://inspirehep.net/record/852286/files/arXiv:1004.3462.pdf
38. M. Lüscher, P. Weisz, Commun. Math. Phys. **97**, 59 (1985). doi:10.1007/BF01206178
39. M. Lüscher, in *Probing the Standard Model of Particle Interactions. Proceedings, Summer School in Theoretical Physics, NATO Advanced Study Institute, 68th Session, Les Houches, France, July 28-September 5, 1997. Pt. 1, 2* (1998), pp. 229–280, http://alice.cern.ch/format/showfull?sysnb=0270921
40. J. Zinn-Justin, Lect. Notes Phys. **659**, 167 (2005)
41. K. Symanzik, in *Recent Developments in Gauge Theories* (Cargèse 1979), ed. by G. 't Hooft et al. (Plenum, New York, 1980)
42. P. Weisz, Nucl. Phys. B **212**, 1 (1983). doi:10.1016/0550-3213(83)90595-3
43. K. Symanzik, in *Mathematical Problems in Theoretical Physics*, ed. by R. Schrader et al. Lecture Notes in Physics, vol. 153 (Springer, New York, 1982)
44. K. Symanzik, Nucl. Phys. B **226**, 187 (1983). doi:10.1016/0550-3213(83)90468-6
45. K. Symanzik, Nucl. Phys. B **226**, 205 (1983). doi:10.1016/0550-3213(83)90469-8
46. K. Wilson, in *Recent Developments in Gauge Theories* (Cargèse 1979), ed. by G. 't Hooft et al. (Plenum, New York, 1980)
47. M. Lüscher, P. Weisz, Phys. Lett. B **158**, 250 (1985). doi:10.1016/0370-2693(85)90966-9
48. B. Sheikholeslami, R. Wohlert, Nucl. Phys. B **259**, 572 (1985). doi:10.1016/0550-3213(85)90002-1
49. G. Heatlie, G. Martinelli, C. Pittori, G.C. Rossi, C.T. Sachrajda, Nucl. Phys. B **352**, 266 (1991). doi:10.1016/0550-3213(91)90137-M
50. R. Frezzotti, P.A. Grassi, S. Sint, P. Weisz, JHEP **0108**, 058 (2001)
51. S. Sint, in *Workshop on Perspectives in Lattice QCD Nara, Japan, October 31–November 11, 2005* (2007)
52. R. Frezzotti, G.C. Rossi, JHEP **08**, 007 (2004). doi:10.1088/1126-6708/2004/08/007
53. S. Capitani, Phys. Rep. **382**, 113 (2003). doi:10.1016/S0370-1573(03)00211-4
54. H.J. Rothe, World Sci. Lect. Notes Phys. **43**, 1 (1992). [World Sci. Lect. Notes Phys.82,1(2012)]
55. C. Gattringer, C.B. Lang, Lect. Notes Phys. **788**, 1 (2010). doi:10.1007/978-3-642-01850-3

# Chapter 2
# Monte Carlo Methods

No way to compute the path integral of lattice QCD analytically is known. Even on a finite lattice it amounts of solving the very-high-dimensional integral of Eq. (1.85). The integral receives large contributions only from a miniscule fraction of the space of integration variables, which suggests one way to estimate the path integral is through importance sampling using Markov chain Monte Carlo. In this chapter we introduce the basic concepts of a Markov chain. We then focus on the simulations of the path integral for gauge fields only. The fermions fields cannot be directly simulated due their anti-commuting nature and require special treatment, which is the subject of Chap. 3.

## 2.1 Markov Chain Monte Carlo

In general, a probability space $(\Omega, \sigma(\Omega), F_\Pi)$ is given by a non-empty space $\Omega$, a sigma-algebra $\sigma(\Omega)$ of $\Omega$ a probability measure $F_\Pi$, which might be given by a probability density $\mathrm{d}F_\Pi = \Pi(x)\mathrm{d}x$ (see Sect. A.3). In QCD, we set the non-empty space $\Omega$ as $\Omega = (SU(N))^n$ (with $n$ defining the dimension of the system), and consider the probability density $\Pi$ given by

$$\Pi(U) = \frac{e^{-S(U)}}{Z} \quad \text{with} \quad Z = \int_\Omega e^{-S(U)}\,\mathrm{d}U\,, \tag{2.1}$$

defined via an action $S$ acting on $U \in \Omega$. We require $S$ to be real. The task will be to compute the expectation of an operator $\hat{O}$ acting on $U$:

$$E(\hat{O}) = \int_\Omega O(U)\Pi(U)\mathrm{d}U\,. \tag{2.2}$$

The basic idea of Markov chain Monte Carlo schemes in QCD is to approximate such expectation values $E(\hat{O})$ by Monte Carlo integration: $E(\hat{O}) \approx \frac{1}{n}\sum_{i=1}^{n} O(U_i)$, where the sequence of $U$-field configurations $\{U_1, U_2, \ldots, U_n\}$ has been drawn at



F. Knechtli et al., *Lattice Quantum Chromodynamics*,
SpringerBriefs in Physics, DOI 10.1007/978-94-024-0999-4_2

random from $\Pi(U)$. If this sequence is generated by a Markov chain that is ergodic and satisfies the detailed balance condition it will converge to the unique fixed point distribution given by the density $\Pi(U)$.

To proceed, we have to recall three concepts from stochastic analysis, for simplicity here in discrete setting: (a) Markov chain, (b) detailed balance condition and (c) ergodicity:

(a) A *Markov chain* is given by a sequence of random variables $X_1, X_2, \ldots$ with the Markov property

$$P(X_{n+1} = y | X_n = x, X_i = x_i, i = 1, \ldots, n-1) = P(X_{n+1} = y | X_n = x)$$

for conditional probabilities $P(A|B) = P(A \cap B)/P(B)$, *i.e.*, the probability of moving to the next state $X_{n+1} = y$ depends only on the present state $X_n = x$, but not on previous states.
Hence the transition probability from $x$ to $y$ can be described by a transition function $T(y, z)$, which fulfills the property

$$\sum_y T(x, y) = 1 \,. \tag{2.3}$$

(b) The detailed balance condition links the transition function and the fixed point distribution:

$$\Pi(x)T(x, y) = \Pi(y)T(y, x) \,. \tag{2.4}$$

In the non-discrete setting, as given in Sect. 2.3 for the Hybrid Monte Carlo scheme, the transition function has to be generalised to a transition kernel.

(c) The Markov process is ergodic, if for any pair of states $x$ and $y$ there is a finite number $n$ of applications of the transition function such that $T^n(x, y) > 0$. Moreover the property $T(x, x) > 0$ called aperiodicity has to hold in order to avoid that the Markov chain gets trapped in cycles.

In order to give insight into the behaviour of a Markov process, let us examine the simplest possible example acting on a system with just two allowed states, $\{\chi_1, \chi_2\}$. The system evolves in a discrete time variable $t$ and is in state $\psi_t$ at time $t$. The dynamics of this Markov process can be encoded in a $2 \times 2$ matrix $T$, containing the transition probabilities $T_{ij} = P(\psi_{t+1} = \chi_i | \psi_t = \chi_j)$ and it is easy to see that the Markov property tells us

$$P(\psi_{t+k} = \chi_i | \psi_t = \chi_j) = [T^k]_{ij}. \tag{2.5}$$

Suppose the Markov matrix can be expressed as

$$T = \begin{pmatrix} 1-p & q \\ p & 1-q \end{pmatrix} \text{ with } 0 \le p, q \le 1\,, \tag{2.6}$$

then the detailed balance condition gives us the fixed-point probability $\underline{\pi}$ as

$$T\underline{\pi} = \underline{\pi} \quad \text{with} \quad \underline{\pi} = \frac{1}{p+q}\begin{pmatrix} q \\ p \end{pmatrix}. \tag{2.7}$$

The other eigenvalue of $T$ is $\lambda = 1 - p - q$ with $|\lambda| < 1$. So we can write a general expression for $T^k$ using the decomposition $T = SDS^{-1}$ which gives

$$T^k = \frac{1}{p+q}\begin{pmatrix} p & q \\ p & q \end{pmatrix} + \frac{\lambda^k}{p+q}\begin{pmatrix} q & -q \\ -p & p \end{pmatrix}. \tag{2.8}$$

The first term in this expression is the projection operator onto the fixed point and the second gives the rate of approach to this steady state, since $\lim_{k\to\infty} \lambda^k = 0$. We see that the memory of the chain falls exponentially as the Markov time-separation grows; states along the chain are correlated exponentially. Writing $\lambda^k = \exp(-k \ln \lambda)$, defines the *exponential autocorrelation time* $\tau = -1/\ln(1-p-q)$ for this system. The difference between Markov chain algorithms lie in the value of the second largest eigenvalue $\lambda$, $|\lambda| < 1$ which determines the rate of approach to the steady state. The better algorithm has the smaller $\lambda$.

## 2.2 Sampling Yang–Mills Gauge Fields

We will consider in this section local Monte Carlo updates of the gauge links. The terms of the gauge action in Eq. (1.70) which contain a particular link $U_\mu(x)$ are

$$S[U_\mu(x)] = -\frac{\beta}{N}\mathrm{Re\,tr}\,\left(U_\mu(x)\,\Sigma_\mu^\dagger(x)\right)\,, \tag{2.9}$$

where

$$\begin{aligned}\Sigma_\mu(x) = \sum_{\nu\neq\mu} \big[&U_\nu(x)\,U_\mu(x+a\hat{\nu})\,U_\nu(x+a\hat{\mu})^{-1} + \\ &U_\nu(x-a\hat{\nu})^{-1}\,U_\mu(x-a\hat{\nu})\,U_\nu(x-a\hat{\nu}+a\hat{\mu})\big]\end{aligned} \tag{2.10}$$

is the sum of the $2(d-1)$ so-called "staples". The lattice can be divided into a checkerboard ordering of even and odd points. A point is even (odd) if the sum of its integer coordinates is even (odd). Since the staples contain links of the same direction $\mu$ as the link $U_\mu(x)$ we want to update located at nearest-neighbour points

of $x$, we can update the links of a given direction $\mu$ on all the even (or odd) sites independently. From here on we drop the argument $(x, \mu)$ of the gauge link to be updated.

We remark that Eq. (2.9) holds also for improved gauge actions like Eq. (1.137). The staples $\Sigma$ contains more terms than in Eq. (2.10) originating from the $1 \times 2$ rectangles. Even/odd ordering of the lattice points is not enough to parallelize the update in this case.

### 2.2.1 Random Numbers and the Rejection Method

We assume that the reader is familiar with the generation of samples $W_1, W_2, \ldots$ for a pseudorandom variable $W$ which is uniformly distributed in the interval $[0, 1]$. For the algorithms which we will describe below it is crucial to have excellent random number generators, e.g. we mention the program RANLUX [1]. The density function for this variable is $f_W(w) = 1$. Typically one needs to generate samples $X_1, X_2, \ldots$ of a variable $x \in [a, b]$ with a given density $f_X(x)$. The conservation of probability yields the relation

$$W = \int_0^W \mathrm{d}w f_W(w) = \int_a^X \mathrm{d}x f_X(x) = y(X) \tag{2.11}$$

By inverting the function $y$ one finds the desired sample sample $X = y^{-1}(W)$. One example is the generation of a random variable $X \geq 0$ with an exponential density $f_X(x) = \exp(-x)$. A sample is obtained by setting $X_1 = -\ln(1 - W_1)$. Another example are normal (or Gaussian) distributed variables with density $f_X(x) = \exp(-x^2)/\sqrt{\pi}$. In the Box–Muller algorithm, two independent samples $X_1$ and $X_2$ are generated simultaneously according to

$$X_1 = \sqrt{-\ln(1 - W_2)}\cos(2\pi W_1)\,, \quad X_2 = \sqrt{-\ln(1 - W_2)}\sin(2\pi W_1)\,. \tag{2.12}$$

This result can be derived by setting in Eq. (2.11) $x_1 = \rho\cos(\phi)$, $x_2 = \rho\sin(\phi)$.

If the function $y(X)$ in Eq. (2.11) cannot be analytically inverted, an alternative is provided by the rejection method. One generates a trial sample $X_1$ from a trial density $h_{\mathrm{trial}}(x)$. Then a uniform random number $W_1$ is drawn and the trial $X_1$ is accepted if

$$W_1 \leq \rho(X_1) = A\,\frac{f_X(X_1)}{h_{\mathrm{trial}}(X_1)}\,, \tag{2.13}$$

where the factor $A$ ensures $\rho(x) \leq 1$. Otherwise the trial $X_1$ is rejected and this step is repeated until a new trial is accepted. The average acceptance is given by $\int dx\, h_{\mathrm{trial}}(x)\rho(x) = A$. One can show, by summing a geometric series which represents all possibilities to generate $X$, that the desired density function $f_X$ is obtained.

### 2.2.2 Heatbath Algorithms

Heatbath algorithms visit each gauge link $U = U_\mu(x)$ on the lattice in turn and draw a new, independent value for the link from the distribution

$$\mathrm{d}P(U) \propto \exp(-S[U])\,\mathrm{d}U\,, \tag{2.14}$$

where $\mathrm{d}P/\mathrm{d}U$ is the density $\exp(-S[U])$ and $S[U]$ is defined in Eq. (2.9). We discuss in detail how this can be implemented for the gauge groups $U(1)$, $SU(2)$ and $SU(3)$.

*Gauge group* $U(1)$. We parameterise a $U(1)$ link variable by $U = \exp(i\phi)$ with an angle $\phi \in [-\pi, \pi]$. If we write the sum of staples in Eq. (2.10) as $\Sigma = s\exp(i\psi)$, Eq. (2.9) becomes

$$S[U] = -\beta\, s\, \cos(\phi - \psi)\,. \tag{2.15}$$

The heatbath algorithm produces a new link variable $U = \exp(i\phi)$ by generating an angle $\Phi$ whose density function is (cf. Eq. (2.15))

$$f_\Phi(\varphi) = N_q^{-1}\, \mathrm{e}^{b\,\cos(\varphi)}\,, \tag{2.16}$$

where the normalisation factor is

$$N_q = 2\pi I_0(b)\,. \tag{2.17}$$

$I_0$ is the modified Bessel function. Then for the new link we set

$$\phi = \Phi + \psi\,. \tag{2.18}$$

Equation (2.16) is called the von Mises distribution. The procedure is described in [2, 3] and consists of a trial density with the rejection method described above,

$$h_{\mathrm{trial}}(\varphi) = \frac{N_t^{-1}}{1 - \alpha\cos(\varphi)}\,, \quad N_t = 2\pi(1-\alpha^2)^{-1/2}\,, \tag{2.19}$$

which has a free parameter $\alpha$.

1. draw a uniform random number $W_1 \in [0, 1]$ and compute a trial $\Phi(W_1)$ from

$$\tan(\Phi/2) = \left(\frac{1-\alpha}{1+\alpha}\right)^{1/2} \tan(\pi(W_1 - \frac{1}{2})) \tag{2.20}$$

2. draw a second uniform random number $W_2 \in [0, 1]$ and accept the trial if

$$W_2 \;\le\; \rho(\Phi) = A\,\frac{f_\Phi(\Phi)}{h_{\mathrm{trial}}(\Phi)}\,. \tag{2.21}$$

If rejected go back to step 1. and repeat until the trial is accepted. The acceptance $A$ can be computed analytically through $A = \min_{-\pi \le \varphi \le \pi} \frac{h_{\text{trial}}(\varphi)}{f_\Phi(\varphi)}$. The optimal value $\alpha_{\text{opt}}$ for the parameter $\alpha$, which maximizes the acceptance $A$ is

$$\alpha_{\text{opt}} = \frac{2b}{1 + \sqrt{1 + 4b^2}} \tag{2.22}$$

and results in

$$\rho(\varphi) = \mu(\varphi) \mathrm{e}^{1-\mu(\varphi)} \tag{2.23}$$

with $\mu(\varphi) = \frac{1}{2}\left(1 + \sqrt{1 + 4b^2}\right) - b\cos(\varphi)$. The maximal acceptance is

$$A(\alpha_{\text{opt}}) = I_0(b)\cosh(\beta)\mathrm{e}^{-\sinh^2\beta}\,, \tag{2.24}$$

where we introduced $2b = \sinh 2\beta$ in terms of which $\alpha_{\text{opt}} = \tanh\beta$. We remark that this procedure works both for positive and negative $b$.

*Gauge group SU(2).* We represent a $SU(2)$ matrix using Eq. (1.62). This representation is also valid for any complex $2 \times 2$ matrix $W$ which can be written as $W = w_0 + iw_j\sigma_j$, where now $w_\mu$ are complex numbers. For any two such matrices $W$ and $W'$ we have $\mathrm{tr}\,(WW') = 2(w_0 w_0' - w_j w_j')$. We define a new SU(2) variable $V = U\hat{\Sigma}^\dagger$ with $\hat{\Sigma} = \Sigma/\sqrt{\det(\Sigma)} \in \mathrm{SU}(2)$. Then Eq. (2.14) becomes

$$\mathrm{d}P(V) = \mathrm{d}P(U) \propto \exp[\frac{\rho}{2}\,\mathrm{tr}\,(V)]\,\mathrm{d}V\,, \tag{2.25}$$

where $\rho = \beta\sqrt{\det(\Sigma)}$ and we used the invariance property of the Haar measure. The algorithm we describe here is based on Refs. [4, 5]. Using Eq. (1.62) for $V$, Eq. (2.25) becomes

$$\mathrm{d}P(V) \propto \sqrt{1 - a_0^2}\,\exp(\rho a_0)\,\mathrm{d}a_0\,\mathrm{d}^3 n\,\delta(n^2 - 1)\,, \tag{2.26}$$

where $a_j = n_j\sqrt{1 - a_0^2}, j = 1, 2, 3$. Once $a_\mu$ have been generated from the distribution Eq. (2.26), the new link variable is

$$U' = V\hat{\Sigma}\,. \tag{2.27}$$

In order to generate $a_0 \in [-1, 1]$, we perform a change of variable

$$y = \rho\,(1 - a_0)\,. \tag{2.28}$$

The probability density of $y$ follows from Eq. (2.26) and is given by

$$f_Y(y) \propto \sqrt{2 - \frac{y}{\rho}}\sqrt{y}\,\exp(-y)\,. \tag{2.29}$$

It is realised by first generating a number $Y$ with the trial density

$$h_{\text{trial}}(y) = \frac{2}{\sqrt{\pi}}\sqrt{y}\,\exp(-y)\,, \tag{2.30}$$

and then correcting for the omitted factor $\sqrt{2 - \frac{y}{\rho}}$ by the rejection method. A random number $W_3$ is generated and $Y$ is accepted if $2W_3^2 \le 2 - \frac{Y}{\rho}$. The rejection rate is small in the limit when $\beta$ is large (because $\rho$ is large), which improves the original method in Ref. [6]. For the generation of $Y$ we present the method of Ref. [7], which is a slight variation of that of Ref. [4]. First we generate a pseudorandom variable $A \ge 0$ with density

$$f_A(a) = \frac{2}{\sqrt{\pi}}\,\exp(-a^2) \tag{2.31}$$

and a second variable $B \ge 0$ with density

$$f_B(b) = \exp(-b)\,. \tag{2.32}$$

Then

$$Y = A^2 + B \tag{2.33}$$

has the desired density Eq. (2.30). The generation of $A$ and $B$ can be done as described in Sect. 2.2.1. Notice that in Eq. (2.12) the angle $2\pi$ has to be replaced by $\pi/2$ so $A \ge 0$. Four uniform random numbers give two values of the trial $Y$. The last step is the generation of points $n$ uniformly distributed on the unit sphere $S^2$ in three dimensions. This can be done by setting

$$n_1 = 1 - 2W_4\,, \quad n_2 = \sqrt{1 - n_1^2}\,\cos(2\pi W_5)\,, \quad n_3 = \sqrt{1 - n_1^2}\,\sin(2\pi W_5)\,, \tag{2.34}$$

with the help of two uniform random numbers $W_4$ and $W_5$.

*Gauge group $SU(3)$.* $SU(N)$ gauge links can be updated [8] by applying sequential updates in $SU(2)$ subgroups embedded in $SU(N)$. Here this is described for $SU(3)$ following [9]. Consider three $SU(2)$ subgroups of $SU(3)$ parameterised by the matrices

$$A_{1,2} = \begin{pmatrix} a_{11} & a_{12} & 0 \\ a_{21} & a_{22} & 0 \\ 0 & 0 & 1 \end{pmatrix}\,, \quad A_{2,3} = \begin{pmatrix} 1 & 0 & 0 \\ 0 & a_{11} & a_{12} \\ 0 & a_{21} & a_{22} \end{pmatrix}\,, \quad A_{1,3} = \begin{pmatrix} a_{11} & 0 & a_{12} \\ 0 & 1 & 0 \\ a_{21} & 0 & a_{22} \end{pmatrix}\,, \tag{2.35}$$

where $a \in SU(2)$. The Cabibbo–Marinari heatbath algorithm is a sequence of updates in the subgroups defined in Eq. (2.35). A minimal set consists of two of the

subgroups but all three subgroups can be taken. In each step the current gauge link $U$ is multiplied by a matrix $A = A_{i,j}$ from Eq. (2.35). Equation (2.9) becomes $S[AU] = s[a] +$ terms independent of $a$, where

$$s[a] = -\frac{\beta}{3}\mathrm{Re\,tr}\,(AW)\,, \quad W = U\Sigma^{\dagger}\,. \tag{2.36}$$

We denote by $w$ the complex $2 \times 2$ submatrix of $W$, whose elements $W_{ij}$ corresponds to the $SU(2)$ subgroup of $A$ in Eq. (2.35). Using the quaternionic representations for $a$ and $w$ gives,

$$s[a] = -\frac{\beta}{3}\mathrm{Re\,tr}\,(aw) = -\frac{\beta}{6}\mathrm{tr}\,(av^{\dagger})\,, \tag{2.37}$$

where $v = 2\mathrm{Re}w_0\, I - i\sum_{k=1}^{3} 2\mathrm{Re}\, w_k\sigma_k$. From here we follow the $SU(2)$ heatbath described above to generate a matrix $a$. The $SU(3)$ link is updated according to

$$U' = A\,U\,, \tag{2.38}$$

and then the next SU(2) subgroup in the sequence is considered. In Ref [8] it is shown this procedure defines a Monte–Carlo heatbath algorithm for SU(3).

### 2.2.3 *Overrelaxation Algorithms*

The heatbath algorithms described in Sect. 2.2.2 suffer from critical slowing down, becoming less efficient as the lattice spacing is decreased. Acceleration is achieved using a different type of algorithm called overrelaxation. It proposes changing link $U$ to $U'$ such that the action in Eq. (2.9) is preserved $S[U] = S[U']$ *i.e.* the change is microcanonical, the measure is preserved $\mathrm{d}U = \mathrm{d}U'$ and the change is reversible, *i.e.* applying the update to $U'$ gives back $U$. Such a change is always accepted. Since it is not ergodic, the overrelaxation algorithm has to be used in combination with an ergodic algorithm like the heatbath. This combination is called a hybrid overrelaxation algorithm. A change of all links of the lattice is called a sweep. Usually one separates two heatbath sweeps by $L/(2a)$ overrelaxation sweeps to propagate the changes over a lattice of linear size $L$.

The $U(1)$ transformation (cf. Eq. (2.15))

$$\phi' = 2\,\psi - \phi \tag{2.39}$$

defines a overrelaxation update for gauge group $U(1)$.

The $SU(2)$ transformation (cf. Eq. (2.9))

$$U' = \hat{\Sigma}\,U^{\dagger}\,\hat{\Sigma} = -U + \mathrm{tr}\,(U\hat{\Sigma}^{\dagger})\,\hat{\Sigma} \tag{2.40}$$

defines an overrelaxation update for gauge group $SU(2)$.

For gauge group $SU(3)$ it is possible to make overrelaxation updates with respect to the various SU(2) subgroups of the form $U \to U' = A\,U$, where $A = A_{i,j}$ is one of the matrices in Eq. (2.35) [10, 11]. The action Eq. (2.37) is preserved, i.e. the property $\mathrm{tr}\, v^\dagger = \mathrm{tr}\,(av^\dagger)$ holds if

$$a = \frac{2}{\mathrm{tr}\,(vv^\dagger)} v^2 = -I + 2\frac{2v_0}{\mathrm{tr}\,(vv^\dagger)} v \quad \text{with} \quad v_0 = \frac{1}{2}\mathrm{tr}\, v\,. \tag{2.41}$$

Since $av^\dagger = v$, performing the same update on $U'$ one has $a' = a^\dagger$ and the link changes to $U'' = A^\dagger U' = U$, i.e. the update is a involution. As a consequence the Jacobian of the update has unit modulus and the integration measure is preserved.

## 2.3 Hybrid Monte Carlo

Hybrid Monte Carlo (HMC) uses an augmented Markov chain that constructs samples of pairs of links $U \in \Omega = SU(N)$ and momenta $P \in \hat{\Omega} = \mathfrak{su}(N)$ according to the probability distribution $F_\nu$ with probability density $\nu(U, P)$ given by

$$\nu(U,P) = \underbrace{\frac{(2\pi)^{N/2}}{Z_H}\exp(-S(U))}_{\Pi(U)} \underbrace{\frac{1}{(2\pi)^{N/2}}\exp(-\langle P,P\rangle/2)}_{\varphi(P)} = \frac{1}{Z_H}\exp(-H(U,P))\,, \tag{2.42}$$

with $Z_H = \int_{\Omega\times\hat{\Omega}} \nu(U,P)d(U,P)$ and $H(U,P) = \langle P,P\rangle/2 + S(U)$ where $\langle P,P\rangle = \sum_{x,\mu}\langle P_{x,\mu}, P_{x,\mu}\rangle$, cf. Eq. (A.4). The transition from one configuration $(U_0, P_0)$ to the next consists of a proposal step

$$(U_0, P_0) \to g(U_0, P_0)\,, \tag{2.43}$$

with a mapping $g : \Omega \times \hat{\Omega} \to \Omega \times \hat{\Omega}$ which is for the moment arbitrary, followed by an acceptance step: $g(U_0, P_0)$ is accepted with probability

$$\alpha((U_0,P_0), g(U_0,P_0)) = \min\left(1, \frac{\nu(g(U_0,P_0))}{\nu(U_0,P_0)}\right) = \min\left(1, \mathrm{e}^{-(H(g(U_0,P_0))-H(U_0,P_0))}\right), \tag{2.44}$$

otherwise the old configuration $(U_0, P_0)$ is kept as the next entry in the chain. In the following we show that the detailed balance equation holds, iff this mapping $g$ is both time-reversible, i.e.,

$$P \cdot g(P \cdot g(U_0,P_0)^\top) = (U_0,P_0)^\top \qquad \text{for } P = \begin{pmatrix} 1 & 0 \\ 0 & -1 \end{pmatrix}, \tag{2.45}$$

and volume preserving:

$$\left|\det\left(\frac{\partial g(U_0, P_0)}{\partial(U_0, P_0)}\right)\right| = 1\,. \tag{2.46}$$

### 2.3.1 Detailed Balance Condition

The transition kernel $K((U_0, P_0), (\Omega' \times \hat{\Omega}'))$ describes the probability of drawing the sample following $(U_0, P_0)$ from the subset $(\Omega' \times \hat{\Omega}') \subset (\Omega \times \hat{\Omega})$, i.e.,

$$K((U_0, P_0), (\Omega' \times \hat{\Omega}')) = P((U^*, P^*) \in (\Omega' \times \hat{\Omega}')|(U_0, P_0)), \tag{2.47}$$

where $(U^*, P^*)$ is the next element in the Markov chain defined by the proposal and acceptance step. The transition kernel for HMC is given by

$$\begin{aligned} K((U_0, P_0), (\Omega' \times \hat{\Omega}')) = \alpha((U_0, P_0), g(U_0, P_0))\delta_{g(U_0,P_0)}(\Omega' \times \hat{\Omega}') + \\ (1 - \alpha((U_0, P_0), g(U_0, P_0)))\delta_{(U_0,P_0)}(\Omega' \times \hat{\Omega}'). \end{aligned} \tag{2.48}$$

As we are only interested in the transition of the links, we can define a restricted transition kernel

$$K_L(U_0, \Omega') = P(U_0^* \in \Omega'|U_0) = \int_{\hat{\Omega}} K((U_0, P), (\Omega' \times \hat{\Omega}))\varphi(P)\mathrm{d}P\,. \tag{2.49}$$

Now we have to check whether the detailed balance condition holds for $K_L$ with respect to the static distribution $\Pi(U)$, *i.e.*,

$$\int_A K_L(U, B)\Pi(U)\mathrm{d}U = \int_B K_L(U, A)\Pi(U)\mathrm{d}U \tag{2.50}$$

holds for all $A, B \in \sigma(\Omega)$. With $\delta_{(U,P)}(B \times \hat{\Omega}) = \delta_U(B)$, the left-hand side of (2.50) becomes

$$\begin{aligned} &\int_A \int_{\hat{\Omega}} \min\left(1, \frac{\nu(g(U, P))}{\nu(U, P)}\right) \delta_{g(U,P)}(B \times \hat{\Omega})\varphi(P)\Pi(U)\mathrm{d}P\mathrm{d}U \\ &+ \int_{A\cap B} \int_{\hat{\Omega}} \left(1 - \min\left(1, \frac{\nu(g(U, P))}{\nu(U, P)}\right)\right) \varphi(P)\Pi(U)\mathrm{d}P\mathrm{d}U. \end{aligned}$$

Correspondingly, the right-hand side reads

$$\int_B \int_{\hat{\Omega}} \min\left(1, \frac{\nu(g(U,P))}{\nu(U,P)}\right) \delta_{g(U,P)}(A \times \hat{\Omega}) \varphi(P) \Pi(U) \mathrm{d}P \mathrm{d}U + \int_{B \cap A} \int_{\hat{\Omega}} \left(1 - \min\left(1, \frac{\nu(g(U,P))}{\nu(U,P)}\right)\right) \varphi(P) \Pi(U) \mathrm{d}P \mathrm{d}U.$$

As the last terms on both sides coincide, it remains to show

$$\int_A \int_{\hat{\Omega}} \min\left(\nu(U,P), \nu(g(U,P))\right) \delta_{g(U,P)}(B \times \hat{\Omega}) \mathrm{d}(P,U) = \int_B \int_{\hat{\Omega}} \min\left(\nu(U,P), \nu(g(U,P))\right) \delta_{g(U,P)}(A \times \hat{\Omega}) \mathrm{d}(P,U).$$

With $\delta_{g(U,P)}(B \times \hat{\Omega}) = \delta_{(U,P)}(g^{-1})(B \times \hat{\Omega}))$ this is equivalent to

$$\underbrace{\int_{(A \times \hat{\Omega}) \cap g^{-1}(B \times \hat{\Omega})} \min\left(\nu(U,P), \nu(g(U,P))\right) \mathrm{d}(P,U)}_{F_1} = \underbrace{\int_{(B \times \hat{\Omega}) \cap g^{-1}(A \times \hat{\Omega})} \min\left(\nu(U,P), \nu(g(U,P))\right) \mathrm{d}(P,U)}_{F_2}$$

As $\varphi(P) = \varphi(-P)$, $\nu(U,P) = \nu(U,-P)$, and the time reversibility of $g$ leads to

$$\nu(g(U,P)) = \nu(g^{-1}(U,-P)). \tag{2.51}$$

Integration by substitution now yields

$$\begin{aligned} F_1 &= \int_{g^{-1}(B \times \hat{\Omega})} \min\left(\nu(U,P), \nu(g(U,P))\right) \delta_{(U,P)}(A \times \hat{\Omega}) d(P,U) \\ &= \int_{B \times \hat{\Omega}} \min\left(\nu(g^{-1}(U,P)), \nu(U,P)\right) \delta_{g^{-1}(U,P)}(A \times \hat{\Omega}) \cdot \left|\det \frac{dg^{-1}(U,P)}{d(U,P)}\right| d(P,U) \\ &= \int_{B \times \hat{\Omega}} \min\left(\nu(g(U,-P)), \nu(U,-P)\right) \delta_{g^{-1}(U,P)}(A \times \hat{\Omega}) \cdot \left|\det \frac{dg^{-1}(U,P)}{d(U,P)}\right| d(P,U) \\ &= \int_{B \times \hat{\Omega}} \min\left(\nu(g(U,-P)), \nu(U,-P)\right) \delta_{g(U,-P)}(A \times \hat{\Omega}) \cdot \left|\det \frac{dg^{-1}(U,P)}{d(U,P)}\right| d(P,U), \end{aligned}$$

where we have used in the last step that $\delta_{g^{-1}(U,P)}(A \times \hat{\Omega}) = \delta_{g(U,-P)}(A \times \hat{\Omega})$. With $\delta_{g(U,P)}(A \times \hat{\Omega}) = \delta_{(U,P)}(g^{-1}(A \times \hat{\Omega}))$, we finally have

$$F_1 = \int_{(B \times \hat{\Omega}) \cap g^{-1}(A \times \hat{\Omega})} \min\left(\nu(g(U,P)), \nu(U,P)\right) \left|\det \frac{dg^{-1}(U,P)}{d(U,P)}\right| d(P,U) = F_2.$$

Hence $F_1 = F_2$, iff the mapping $g$ is time-reversible and volume-preserving.

As a conclusion we can state that the kernel $K_L$ fulfills the detailed balance condition, iff the mapping $g : \Omega \times \hat{\Omega} \to \Omega \times \hat{\Omega}$ is time-reversible and volume preserving. This can be achieved if we define $g$ to be the Hamiltonian flow $(U(T), P(T)) = g(U_0, P_0)$ at some arbitrary time point $T$ according to the Hamiltonian $H(U, P) = \langle P, P \rangle / 2 + S(U)$, if started from the initial value $(U_0, P_0)$. Note that we do not have to compute the flow exactly, any numerical approximation is feasible, provided it is both time-reversible and volume preserving. We will come back to this point in Sect. 2.5.

### 2.3.2 Hamilton's Equation of Motion

There are several ways to derive Hamilton's equation of motion. A first, physically intuitive way can be found in many textbooks. The time derivative of $U_\mu(x)$ is derived via an infinitesimal rotation on the group manifold:

$$\dot{U}_\mu(x) = P_\mu(x)\, U_\mu(x)\,. \tag{2.52}$$

The remaining equation for $\dot{P}_\mu(x)$ is then obtained from the fact that the total time derivate of the Hamiltonian is zero, and $\dot{H}(U, P)$ is solved for $\dot{P}_\mu(x)$. For details we refer to Chap. 7.2.3 in [12]. Alternatively, $\dot{P}_\mu(x)$ can be computed via

$$\dot{P}_\mu(x) = -\partial_{x,\mu} H(U, P) = -\partial_{x,\mu} S(U)\,, \tag{2.53}$$

where the link differential operator acting on $S(U)$ and is defined in Eq. (A.6). We will use the Wilson action defined in Eq. (1.70),

$$S(U) = S_{\mathrm{w}}(U) = \frac{\beta}{2N} \sum_x \sum_{\mu,\nu} \mathrm{Re\ tr}\,[1 - P_{\mu,\nu}(x)], \tag{2.54}$$

for $U \in SU(N)$, as an example for this approach, where the sum runs over all oriented plaquettes $P_{\mu,\nu}(x)$. In the following we will need to collect all the terms in the action that depends on a specific link variable $U_\mu(x)$:

$$S(U) = -\frac{\beta}{N} \mathrm{Re\ tr}\,(U_\mu(x)\, \Sigma_\mu^\dagger(x)) + \text{terms independent of } U_\mu(x)\,,$$

where $\Sigma_\mu(x)$ is the sum of staples defined in Eq. (2.10). Computing now the link derivative of the Wilson action, one gets its Lie-algebra components

$$\partial^i_{x,\mu} S(U) = -\frac{\beta}{N} \mathrm{Re\ tr} \left\{ T^i U_\mu(x) \Sigma^\dagger_\mu(x) \right\} + \sum_{(y,\nu)\neq(x,\mu)} 0$$
$$= -\frac{\beta}{N} \mathrm{Re\ tr} \left\{ T^i U_\mu(x) \Sigma^\dagger_\mu(x) \right\}. \tag{2.55}$$

Finally we obtain

$$\partial_{x,\mu} S(U) = -\frac{\beta}{2N} Z_\mu(x)\,, \tag{2.56}$$

in terms of the Lie-algebra-valued field

$$Z_\mu(x) = -\{U_\mu(x) \Sigma^\dagger_\mu(x)\}_{TA}\,. \tag{2.57}$$

Here we have used the notation

$$W_{TA} = \frac{W - W^\dagger}{2} - \frac{\mathrm{tr}\,(W - W^\dagger)}{2N},$$

for the traceless, antihermitian part of a matrix $W$. Equation (2.56) follows from the identity

$$-2T^i \mathrm{Re\ tr} \left\{ T^i U_\mu(x) \Sigma^\dagger_\mu(x) \right\} = \left\{ U_\mu(x) \Sigma^\dagger_\mu(x) \right\}_{TA}, \tag{2.58}$$

which can be proved by computing the components of $W_{TA}$ in the Lie algebra. These components are given by $-2\mathrm{tr}\,(W_{TA} T^i)$.

A second approach generalizes the case of classical Hamiltonian mechanics to Lattice QCD. In classical Hamiltonian mechanics, the symplectic structure of the phase space $(q, p)$ is defined by the closed 2-form $\omega = dq \wedge dp$. Correspondingly, the equations of motion for a Hamiltonian function $H(p, q) = T(p) + U(q)$ are

$$\dot{q} = \{H, q\} = \hat{H} q, \tag{2.59}$$
$$\dot{p} = \{H, p\} = \hat{H} p, \quad (i = 1, \ldots, n) \tag{2.60}$$

where the Poisson brackets are defined via the closed 2-form by

$$\{A, B\} = -\omega(\hat{A}, \hat{B}) = \begin{pmatrix} \frac{\partial A}{\partial q} & \frac{\partial A}{\partial p} \end{pmatrix} J \begin{pmatrix} \frac{\partial B}{\partial q} \\ \frac{\partial B}{\partial p} \end{pmatrix} = \frac{\partial A}{\partial p}\frac{\partial B}{\partial q} - \frac{\partial A}{\partial q}\frac{\partial B}{\partial p}, \tag{2.61}$$

with

$$J = \begin{pmatrix} 0 & -I \\ I & 0 \end{pmatrix} \tag{2.62}$$

and the Hamiltonian vector field $\hat{A}$ for the 0-form $A$ is given by

$$\frac{\partial A}{\partial p}\frac{\partial}{\partial q} - \frac{\partial A}{\partial q}\frac{\partial}{\partial p}. \tag{2.63}$$

This gives the well-known equations of motion

$$\begin{pmatrix}\dot{q}\\ \dot{p}\end{pmatrix} = J\begin{pmatrix}\frac{\partial H}{\partial q}\\ \frac{\partial H}{\partial p}\end{pmatrix} = \begin{pmatrix}\frac{\partial H}{\partial p}\\ -\frac{\partial H}{\partial q}\end{pmatrix}. \tag{2.64}$$

As $\Omega$ is a Lie group and $\hat{\Omega}$ the corresponding Lie-algebra, we can write $P \in \hat{\Omega}$ as $P = p^i T_i$ with $T_i$ generators of the representation of $P$ in $\hat{\Omega}$. These generators are linked to the group variables $U$ via the right-hand invariant vector field defined by $e_i$: $e_i U = -T_i U$. We can now define Hamilton's equations governing the Hamiltonian flow $(U, P)$:

$$\begin{aligned}\dot{U} &= \{H, U\} = \hat{H}U,\\ \dot{P} &= \{H, P\} = \hat{H}P,\end{aligned} \tag{2.65}$$

where now the Lie brackets are defined via the closed 2-form $\omega = -dp$ defining the symplectic structure of the phase space $(U, P)$. For this 2-form, the vector field $\hat{H}$ associated to the Hamiltonian 0-form $H = p^i p_i/2 + S(U)$ turns out to be

$$\hat{H} = p_i e_i - e_i(S)\frac{\partial}{\partial p_i}, \tag{2.66}$$

which gives

$$\begin{aligned}\dot{U} &= \hat{H}U = p^i e_i(U) = -p_i T_i U = -PU,\\ \dot{P} &= \hat{H}P = -e_i(S)\frac{\partial P}{\partial p_i} = -e_i(S)T_i.\end{aligned} \tag{2.67}$$

Depending on the action $S$, the force $e_i(S)T_i$ can be computed further: for the pure gauge part $S = -(\beta/N)S_G$ with $S_G = \mathrm{Re}\,\mathrm{tr}(\Sigma^\dagger U)$ see Eq. (2.9), we get

$$e_i(S_G)T_i = \mathrm{Re}\,\mathrm{tr}(\Sigma^\dagger e_i(U))T^i = -\mathrm{Re}\,\mathrm{tr}(\Sigma^\dagger T_i U)T^i = -\mathrm{Re}\,\mathrm{tr}(U\Sigma^\dagger T_i)T^i,$$

which is equivalent to the result already obtained in (2.56).

## 2.4 Symplectic Integration Schemes

As seen in Sect. 2.3, any time-reversible and volume-preserving numerical approximation scheme is suitable to establish the detailed balance condition. Before discussing the non-Abelian case of Lattice QCD, we will briefly recapitulate the

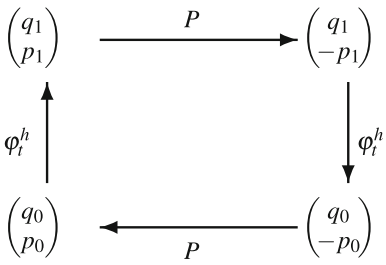


**Fig. 2.1** Time-reversibility of a numerical flow $\varphi_t^h$: applying the transformations $\varphi_t^h$, $P$, $\varphi_t^h$ and finally $P$ to the initial value $(q_0, p_0)$ yields the initial value again

concepts of time-reversibility and symplecticity of numerical schemes applied to Hamiltonian initial-value problems (ODE-IVP)

$$\dot{y} = J^{-1}\nabla H(y), \quad y(t_0) = y_0, \tag{2.68}$$

with $y = (q, p)^\top, f : \mathbb{R}^n \times \mathbb{R}^n \to \mathbb{R}^{2n}$ at least continuously differentiable.

Consider a numerical scheme defined by $\varphi_t^h(y_0)$ applied to the ODE-IVP, which constructs a numerical approximation at time $t_0 + h$, starting at the exact solution $y_0$ at time $t_0$. $\varphi_t^h(y_0)$ is said to be

- *symplectic*, if the numerical scheme defines a symplectic transformation, i.e. if

$$\left(\frac{\partial \varphi_t^h}{\partial y_0}\right)^\top J \left(\frac{\partial \varphi_t^h}{\partial y_0}\right) = J \tag{2.69}$$

  with the matrix $J$ defined in (2.62).
- *time reversible*, if (see Fig. 2.1)

$$P \cdot \varphi_t^h(P \cdot \varphi_t^h(y_0)) = y_0 \qquad \text{for } P = \begin{pmatrix} I_n & 0 \\ 0 & -I_n \end{pmatrix}, \tag{2.70}$$

  which is equivalent to $P\varphi_t^h = \varphi_t^{-h} P$ for symmetric schemes $\varphi_t^h \varphi_t^{-h} = I$.

A consequence of symplecticity is volume preservation:

$$\left|\det\left(\frac{\partial \varphi_t^h}{\partial y_0}\right)\right| = 1\,, \tag{2.71}$$

which implies that symplecticity is a sufficient condition for volume-preservation.

Due to the symmetry of the scheme, the most simple symplectic and symmetric numerical method has at least order two, i.e., the difference between exact solution and numerical approximation at time $T$ after $n$ steps of step size $h$ ($T = nh$) is of order $\mathcal{O}(h^2)$ when $h$ is sufficiently small. It is given by the Störmer-Verlet method (or Leap-Frog scheme), which can be written as an explicit scheme for separable

Hamiltonians $H(q,p) = V(p) + U(q)$. One step, starting from initial values $(q_0, p_0)$, to obtain numerical approximations $(q_1, p_1)$ at time $t_0 + h$ reads

$$\begin{aligned} p_{1/2} &= p_0 - \frac{h}{2} U_q(q_0)\,, \\ q_1 &= q_0 + h V_p(p_{1/2})\,, \\ p_1 &= p_{1/2} - \frac{h}{2} U_q(q_1)\,, \end{aligned} \tag{2.72}$$

with short-hands $U_q$ and $V_p$ for $\partial U/\partial q$ and $\partial V/\partial p$, respectively. Symplecticity of the scheme follows directly from the fact that is defined by the composition of three symplectic mappings

$$\begin{aligned} (q_0, p_0) &\to p_{h/2}(q_0, p_0) = (q_0, p_{1/2})\,, \\ (q_0, p_{1/2}) &\to q_h(q_0, p_{1/2}) = (q_1, p_{1/2})\,, \\ (q_1, p_{1/2}) &\to p_{h/2}(q_1, p_{1/2}) = (q_1, p_1)\,, \end{aligned} \tag{2.73}$$

so-called $p$- and $q$-updates with step sizes $h/2$, $h$ and $h/2$, resp., which enables us to rewrite the leap-frog scheme as

$$p_{h/2} \circ q_h \circ p_{h/2}(q_0, p_0)\,. \tag{2.74}$$

Symmetry follows directly by changing the sign of $h$ and replacing $(q_0, p_0)$ by $(q_1, p_1)$. Time reversibility is then given for symmetrical Jacobians $V_p$ which fulfill $V_p(p) = -V_p(-p)$.

An easy way to derive symplectic and time-reversible higher-order schemes $\widetilde{\varphi}_t^h$ is based on the composition of $m$ symplectic and time-reversible basic schemes $\varphi_t^h$:

$$\widetilde{\varphi}_t^h = \varphi_t^{\gamma_1 h} \circ \varphi_t^{\gamma_2 h} \circ \cdots \circ \varphi_t^{\gamma_m h}\,. \tag{2.75}$$

Besides the time-reversibility of the underlying basic schemes $\varphi_t^h$, the coefficients have to be symmetric too to get an overall time-reversible system:

$$\gamma_{m-k+1} = \gamma_k \quad \text{for} \quad k = 1, 2, \ldots, m\,. \tag{2.76}$$

It can easily be shown that the composition scheme has order $p + 1$ (with the underlying scheme having order $p$), if the following two conditions hold for the free parameters $\gamma_1, \ldots, \gamma_m$:

$$\sum_{j=1}^{m} \gamma_j = 1, \qquad \sum_{j=1}^{m} \gamma_j^p = 0. \tag{2.77}$$

Symplecticity and time-revesibility of the composition scheme follow directly from symplecticity and time-revesibility of the underlying scheme.

This approach allows us to construct symplectic and time-reversible schemes of any arbitrary (even) high order. We start with the Störmer-Verlet scheme $\varphi_t^h$ and define

$$\widetilde{\varphi}_t^h = \varphi_t^{\gamma_1 h} \circ \varphi_t^{\gamma_2 h} \circ \varphi_t^{\gamma_3 h} \tag{2.78}$$

with

$$\gamma_1 = \gamma_3 = \frac{1}{2 - 2^{\frac{1}{3}}}, \gamma_2 = 1 - 2\gamma_1. \tag{2.79}$$

These coefficients fulfill both conditions above, which gives at least order 3 for the composition scheme $\widetilde{\varphi}_t^h$. As the order of symmetric methods is even, we get order 4 for $\widetilde{\varphi}_t^h$. We can now repeat this process by just replacing $\varphi_t^h$ by $\widetilde{\varphi}_t^h$, and we get schemes of order 6, 8, etc.

Another idea is to use splitting schemes to treat different parts of the right-hand side independently, i.e., the different parts of the right-hand side are updated one after the other, while freezing the remaining part. In other words: for the momenta, we solve

$$\dot{q} = 0\,, \qquad \dot{p} = -\nabla_q U(q)\,,$$

and for the coordinates

$$\dot{q} = \nabla_p V(p)\,, \qquad \dot{p} = 0\,.$$

In general, this approach yields schemes of order one. If the splitting is symmetric, one gets methods of at least order two. An important class of splitting schemes is given by Omelyan et al. [13] and force-gradient schemes [14]. Omelyan schemes are based on a symmetric five-stage scheme (updating the sequence $U, P, U, P$ and $U$), introducing a free parameter $\lambda$ in the step size of the $P$-updates. Though the scheme is only of second order, the parameter $\lambda$ can be used to minimize the leading error term. This gives, for example, the optimal five stage method

$$\begin{aligned} &p_{\lambda h} \circ q_{h/2} \circ p_{(1-2\lambda)h} \circ q_{h/2} \circ p_{\lambda h}(q_0, p_0) \quad \text{with} \\ &\lambda = \frac{1}{2} - \frac{(2\sqrt{326} + 36)^{1/3}}{12} + \frac{1}{6(2\sqrt{326} + 36)^{1/3}} \end{aligned} \tag{2.80}$$

with the $p$- and $q$-updates defined above, cf. Eq. (2.74). The idea of force-gradient schemes is to add an additional update of a higher-order term, the so-called force-gradient term, which introduces additional parameters $\xi$ and $\chi$, and to use the freedom in the additional parameters to increase the accuracy. To obtain order four, only five stages are needed, yielding the family of force-gradient schemes

$$\widetilde{p}_{\lambda h, \xi h^3} \circ q_{h/2} \circ \widetilde{p}_{(1-2\lambda)h, \chi h^3} \circ q_{h/2} \circ \widetilde{p}_{\lambda h, \xi h^3}(q_0, p_0) \tag{2.81}$$

with the force gradient updates $\widetilde{p}_{\alpha h, \beta h^3}$ being defined by the mapping

$$\begin{pmatrix} q_0 \\ p_0 \end{pmatrix} \to \begin{pmatrix} q_0 \\ p_0 - \alpha h U_q(q_0) + \beta h^3 \nabla_q |V_q(q_0)|^2. \end{pmatrix} \tag{2.82}$$

One possible choice of parameters to obtain fourth order is $\lambda = 1/6, \xi = 0, \chi = 1/72$. Both schemes can be linked to the idea of nested integration (or multirate integration in the mathematical literature) described in Sect. 3.4.2.

In Lattice QCD, where the links $U \in \Omega = SU(N)$ and momenta $P \in \hat{\Omega} = \mathfrak{su}(N)$ we have to deal with more structure compared to the Abelian case where both $q$ and $p \in \mathbb{R}^n$. To preserve the non-Abelian structure, the leap-frog scheme for one step with step size $h$ from $(U^0, P^0)$ to $(U^1, P^1)$, defined by a sequence of $P$, $U$ and $P$ updates with step sizes $h/2$, $h$ and $h/2$, has to be rewritten as

$$\begin{aligned} P^{1/2} &= P^0 - \frac{h}{2} \partial_{x,\mu} S(U^0)\,, \\ U^1 &= \mathrm{e}^{hP^{1/2}} \cdot U^0, \\ P^1 &= P^{1/2} - \frac{h}{2} \partial_{x,\mu} S(U^1)\,. \end{aligned} \tag{2.83}$$

This follows from defining an $U$-update $U^0 \to U_1$ with step size $h$ and initial values $(U^0, P^0)$ by $U_h(U^0, P^0) = \mathrm{e}^{hP^0} \cdot U^0$ to preserve the multiplicative structure of the Lie group $SU(N)$ according to the Lie-group differential equation (2.52). The $P$-update $P^0 \to P_1$ with step size $h$ and initial values $(U^0, P^0)$ can be defined in the usual way as $P_h(U^0, P^0) = P^0 - h\partial_{x,\mu} S(U^0)$ due to the additive structure of the Lie algebra $\mathfrak{su}(N)$. This defines completely the non-Abelian setting, as all schemes can be described as a sequence of $U$ and $P$ updates with different step sizes and coefficients. An alternative approach to preserve the non-Abelian structure of links and momenta based on Runge-Kutta schemes is discussed in [15].

## 2.5 Summary and Further Reading

In this chapter the conditions for a Markov chain Monte Carlo algorithm are formulated. The focus is on algorithms to simulate the path integral of a pure gauge theory. Heatbath and overrelaxation algorithms for gauge groups $U(1)$, $SU(2)$ and $SU(3)$ are described in detail. An alternative algorithm is the Hybrid Monte Carlo based on Hamilton's equations of motion. The detailed balance condition is proved and two derivations of the equations of motion are presented. These equations are solved by numerical integration schemes. Detailed balance requires that the integration schemes are time-reversible and volume preserving. The construction of such schemes is discussed in detail, first for the Abelian and then for the case of non Abelian Lie groups.

The theory of Markov chains is reviewed by M. Lüscher in Ref. [16]. The formulation of Hamilton's equations of motion on Lie groups is discussed in detail by A. D. Kennedy at al. in Ref. [17]. We mention that the search for other algorithms for gauge theories to improve critical slowing down is an active field, see e.g. [18–20].

## References


1. M. Lüscher, Comput. Phys. Commun. **79**, 100 (1994). doi:10.1016/0010-4655(94)90232-1
2. D. Best, N. Fisher, Appl. Statist. **28**, 152 (1979)
3. B. Bunk, *Heatbath Update for U(1)*, Internal notes (1995)
4. K. Fabricius, O. Haan, Phys. Lett. B **143**, 459 (1984). doi:10.1016/0370-2693(84)91502-8
5. A. Kennedy, B. Pendleton, Phys. Lett. B **156**, 393 (1985). doi:10.1016/0370-2693(85)91632-6
6. M. Creutz, Phys. Rev. D **21**, 2308 (1980). doi:10.1103/PhysRevD.21.2308
7. P. Weisz, *A Haan-Fabricius Updating Program for the APE-100 Parallel Computer*, Internal report of the ALPHA collaboration (1993)
8. N. Cabibbo, E. Marinari, Phys. Lett. B **119**, 387 (1982). doi:10.1016/0370-2693(82)90696-7
9. P. Weisz, *A Cabibbo-Marinari SU(3) Updating Program for the Quadrics Parallel Computer*, Internal report of the ALPHA collaboration (1995)
10. M. Creutz, Phys. Rev. D **36**, 515 (1987). doi:10.1103/PhysRevD.36.515
11. F.R. Brown, T.J. Woch, Phys. Rev. Lett. **58**, 2394 (1987). doi:10.1103/PhysRevLett.58.2394
12. T. DeGrand, C. DeTar, *Lattice Methods for Quantum Chromodynamics* (World Scientific, Singapure, 2006)
13. I.P. Omelyan, I.M. Mryglod, R. Folk, Phys. Rev. E **65**, 056706 (2002). doi:10.1103/PhysRevE.65.056706
14. I.P. Omelyan, I.M. Mryglod, R. Folk, Phys. Rev. E **66**, 026701 (2002). doi:10.1103/PhysRevE.66.026701
15. M. Wandelt, M. Günther, F. Knechtli, M. Striebel, Appl. Numer. Math. **62**(12), 1740 (2012)
16. M. Lüscher, in *Modern Perspectives in Lattice QCD: Quantum Field Theory and High Performance Computing. Proceedings, International School, 93rd Session, Les Houches, France, August 3–28, 2009* (2010), pp. 331–399. https://inspirehep.net/record/846344/files/arXiv:1002.4232.pdf
17. A. Kennedy, P. Silva, M. Clark, Phys. Rev. D **87**(3), 034511 (2013). doi:10.1103/PhysRevD.87.034511
18. T. Korzec, U. Wolff, Nucl. Phys. B **871**, 145 (2013). doi:10.1016/j.nuclphysb.2013.02.012
19. T. Korzec, U. Wolff, PoS **LATTICE2010**, 029 (2010)
20. Y. Delgado Mercado, C. Gattringer, A. Schmidt, Comput. Phys. Commun. **184**, 1535 (2013). doi:10.1016/j.cpc.2013.02.001

# Chapter 3
# Handling Fermions on the Lattice

In Chap. 2, the ideas of Monte Carlo estimation of the path integral of a bosonic field were introduced. Consider now the problem of evaluating path integrals of fermions, remembering that defining the fermion path integral means introducing Grassmann integrals, see Sect. 1.3.2. These can not be evaluated easily by Monte Carlo in the same direct way presented in Chap. 2, so we need to include some extra steps which will re-write the path integral of a quantum field theory with bosons and fermions in terms of path integrals of bosons only. Physical intuition tells us the action of this effective theory will be non-local.

## 3.1 Wick Contractions

The algebra and the rules of integration of Grassmann numbers are reviewed in Section A.2. In a path integral, observables are computed by inserting an appropriate function of the integration variables, weighted by the Boltzmann factor. Let us review a toy example before writing the most general expression, which gives us the lattice version of Wick's theorem. Consider a system with just eight integration variables (not fields), collected into two sets of four; $(\{\eta_1, \ldots \eta_4\}, \{\bar{\eta}_1, \ldots \bar{\eta}_4\})$. We have chosen this form for our toy model since it resembles the path integral for a Dirac fermion; later we will also consider Majorana fermions, where the two sets of integration variables are no longer independent. Now choose an observable to evaluate, such as

$$\langle \bar{\eta}_1 \eta_1 \bar{\eta}_2 \eta_2 \rangle = \frac{1}{\det M} \int \mathscr{D}[\eta] \mathscr{D}[\bar{\eta}] \;\; \bar{\eta}_1 \eta_1 \bar{\eta}_2 \eta_2 \;\; \exp\{\bar{\eta} M \eta\} \;,$$

where $M$ is a non-singular matrix. To begin, note that the exponential function, like all functions on a finite set of grassmannians must be a finite polynomial. The Taylor series, which stops after the fifth term, can be used to find an exact expression:

$$\exp\{\bar{\eta} M \eta\} = 1 + (\bar{\eta} M \eta) + \frac{1}{2!} (\bar{\eta} M \eta)^2 + \frac{1}{3!} (\bar{\eta} M \eta)^3 + \frac{1}{4!} (\bar{\eta} M \eta)^4 \,.$$



F. Knechtli et al., *Lattice Quantum Chromodynamics*,
SpringerBriefs in Physics, DOI 10.1007/978-94-024-0999-4_3

Now when multiplied by the operator insertion, the only terms that remain in the integrand are truncated by two more powers;

$$\bar{\eta}_1\eta_1\bar{\eta}_2\eta_2 \ \exp\{\bar{\eta}M\eta\} = \bar{\eta}_1\eta_1\bar{\eta}_2\eta_2\left\{1 + (\bar{\eta}M\eta) + \frac{1}{2!}(\bar{\eta}M\eta)^2\right\}.$$

Finally, the path integral can be evaluated. The only terms that survive the integration rule are those in the last part in the Taylor sequence, which contain the four integration variables $\eta_3$, $\eta_4$, $\bar{\eta}_3$ and $\bar{\eta}_4$, since every variable must occur once only. These terms are $(\bar{\eta}_3 M_{33}\eta_3)(\bar{\eta}_4 M_{44}\eta_4) + (\bar{\eta}_3 M_{34}\eta_4)(\bar{\eta}_4 M_{43}\eta_3)$. Integrating now gives our result. Note that a minus sign appears as we need to re-order the integration variables to match the integrand in Eq. (A.9), giving

$$\langle\bar{\eta}_1\eta_1\bar{\eta}_2\eta_2\rangle = \frac{M_{33}M_{44} - M_{34}M_{43}}{\det M}.$$

For this simple case, the expression is very neat but rapidly becomes more cumbersome as more variables are introduced. A little algebra relates this expression to a form that will be more familiar and more useful for quantum field theory;

$$\langle\bar{\eta}_1\eta_1\bar{\eta}_2\eta_2\rangle = \frac{M_{33}M_{44} - M_{34}M_{43}}{\det M} = [M^{-1}]_{12}[M^{-1}]_{21} - [M^{-1}]_{11}[M^{-1}]_{22}$$

which we will see will become the method needed to express a two-point function for a meson (used to evaluate its mass) in terms of the quark propagator on a gauge background.

More complicated expressions with realistic quantum field theories with many degrees of freedom can be evaluated most easily by using Wick's theorem, which generalises and simplifies the manipulations we have just seen in our toy. The simplest non-zero contraction in a quantum field theory is the fermion two-point correlation function $\Delta_{ij}$;

$$\Delta_{ij} = \langle\eta_i\bar{\eta}_j\rangle = \frac{1}{\det M}\int\mathscr{D}[\eta]\mathscr{D}[\bar{\eta}] \ \ \eta_i\bar{\eta}_j \ e^{\bar{\eta}M\eta}. \tag{3.1}$$

On a finite lattice, the integration is over the large-but-finite set of $D$ Grassmann variables. If $M$ is non-singular, a change of one of the sets of integration variables $\psi = M\eta$ gives

$$\Delta_{ij} = \int\mathscr{D}[\psi]\mathscr{D}[\bar{\eta}] \ \ [M^{-1}]_{ik}\psi_k\bar{\eta}_j \ e^{\bar{\eta}\psi} = [M^{-1}]_{ik}\int\mathscr{D}[\psi]\mathscr{D}[\bar{\eta}] \ \ \psi_k\bar{\eta}_j \ e^{\bar{\eta}\psi}.$$

As with ordinary integration, a change of variable brings a factor of the Jacobian along with the measure. Here the Jacobian is simply $\det M$, which cancels the factor introduced in the definition of Eq. 3.1. The Berezin integral needed is

$$I_{kj} = \int \mathscr{D}[\psi]\mathscr{D}[\bar{\eta}] \;\; \psi_k \bar{\eta}_j \; e^{\bar{\eta}\psi} = \frac{1}{(D-1)!} \int \mathscr{D}[\psi]\mathscr{D}[\bar{\eta}] \;\; \psi_k \bar{\eta}_j \;\; (\bar{\eta}_a \psi_a)^{D-1} \, .$$

We have again made use of the integration rules, noting the only way to get a non-zero value for the integral is for all Grassmann variables to appear in the integrand and there is only one term in the expansion of the exponential that fulfils this requirement. Next, we see immediately the only non-zero value for $I_{kj}$ occurs when $k = j$ since all terms in $\bar{\eta}_a \psi_a$ come in pairs with matching indices. When $k = j$, there are $(D-1)!$ terms in the sum that survive integration, giving simply $I_{kj} = \delta_{kj}$. Finally we arrive at the expression for the lattice two-point quark correlation function, commonly called the *propagator*:

$$\Delta_{ij} = \langle \eta_i \bar{\eta}_j \rangle = [M^{-1}]_{ij}. \tag{3.2}$$

Computing more interesting physics will require the evaluation of a $2N$-point function and the same analysis can be used to write a general result. The path integral is

$$\langle \eta_{i_1} \eta_{i_2} \ldots \eta_{i_N} \bar{\eta}_{j_1} \bar{\eta}_{j_2} \ldots \bar{\eta}_{j_N} \rangle = \frac{1}{\det M} \int \mathscr{D}[\eta]\mathscr{D}[\bar{\eta}] \;\; \eta_{i_1} \eta_{i_2} \ldots \eta_{i_N} \bar{\eta}_{j_1} \bar{\eta}_{j_2} \ldots \bar{\eta}_{j_N} \; e^{\bar{\psi} M \psi}, \tag{3.3}$$

and after integration, the result in terms of the quark propagator is

$$\langle \eta_{i_1} \eta_{i_2} \ldots \eta_{i_N} \bar{\eta}_{j_1} \bar{\eta}_{j_2} \ldots \bar{\eta}_{j_N} \rangle = \sum_{\{k_1,k_2,\ldots k_N\} \in \mathscr{P}_n} \sum_{\{l_1,l_2,\ldots l_N\} \in \mathscr{P}_n} \varepsilon_{k_1 k_2 \ldots k_N} \; \varepsilon_{l_1 l_2 \ldots l_N} \;\; [M^{-1}]_{k_1,l_1} [M^{-1}]_{k_2,l_2} \ldots [M^{-1}]_{k_N,l_N}. \tag{3.4}$$

The first sum is over all possible permutations of the $N$ indices labelling the $\eta$ fields and the second is correspondingly the permutations over the $\bar{\eta}$ fields. The $\varepsilon$ is the minus sign resulting from commuting the grassmann fields and takes values $\pm 1$ when the permutation is even or odd. We will use this expression later when evaluating properties of hadrons in QCD.

The expressions presented so far are suitable for Dirac fermions, where the fields $\bar{\psi}$ and $\psi$ are treated as independent integration variables. For Majorana fermions, the two fields are dependent and so different sets of expressions are generated following the same rules for integrating Grassmann variables. Before establishing the general result, let us start with another simple example; consider the four dimensional Berezin integral

$$P_4 = \int \mathscr{D}[\eta] \;\; e^{\frac{1}{2}\eta^T A \eta}, \tag{3.5}$$

with $A$ an anti-symmetric (skew-symmetric) matrix, so $A^T = -A$. This restriction is required by the commutation rules of grassmann numbers. Remember the distinction here is that the variables appearing in $\eta^T$ are the same as those in $\eta$. Now the Taylor series for $\exp \eta^T A\eta$ stops after just three terms and again the highest term is the only one that can contribute to the integral, so we have

$$\begin{aligned} P_4 &= \frac{1}{8}\int \mathscr{D}[\eta] \quad (\eta^T A\eta)^2 \\ &= \frac{1}{2}\int \mathscr{D}[\eta]\,(\eta_1 A_{12}\eta_2 + \eta_1 A_{13}\eta_3 + \eta_1 A_{14}\eta_4 + \eta_2 A_{23}\eta_3 + \eta_2 A_{24}\eta_4 + \eta_3 A_{34}\eta_4)^2 \\ &= \int \mathscr{D}[\eta] \quad \eta_1\eta_2\eta_3\eta_4\,(A_{12}A_{34} - A_{13}A_{24} + A_{14}A_{23}) \\ &= A_{12}A_{34} - A_{13}A_{24} + A_{14}A_{23} = \mathrm{pf}(A). \end{aligned} \tag{3.6}$$

where $\mathrm{pf}(A)$ is the *Pfaffian* of the anti-symmetric matrix $A$, see [1]. This result holds more generally for any number of integration variables,

$$\int \mathscr{D}[\eta] \quad e^{\frac{1}{2}\eta^T A\eta} = \mathrm{pf}(A). \tag{3.7}$$

## 3.2 Sparse Linear Algebra

Two main linear algebra tasks arise in Lattice QCD applications:

- *Solving linear systems:* the inversion of the Wilson–Dirac operator requires the solution of a huge and sparse linear system. It arises
  - in the evaluation of the *pseudo-fermionic force* within an HMC step (see Sect. 3.4);
  - in the computation of *quark propagators* (see Sects. 3.5 and 3.6).
- *Computing eigenvalues and eigenvectors:* eigenvalue problems have to be solved in many Lattice QCD applications like:
  - in the *deflation* of solvers for the lattice Dirac operator, where the eigenvectors corresponding to the lowest eigenvalues are separated from the rest of the eigenmodes, see e.g. [2];
  - in the computation of *disconnected diagrams*, where the eigenvectors corresponding to the lowest eigenvalues of the Hermitian Wilson–Dirac operator can be used factorize the inverse of the operator into an exact leading part and the rest, which can be approximated (see Sect. 3.6);
  - in the construction of smeared quark fields based on *distillation*, where the eigenvectors with smallest eigenvalues of the gauge-covariant Laplace operator are used (see Sect. 4.4.1);

– in the calculation of the *topological charge* of a gauge field configuration (see Sect. 4.3.4) using the index theorem, where the zero eigenvalues of the overlap operator have to be computed [3, 4];
– in the determination of the *spectral range* of the Dirac operator needed in the RHMC algorithm (see Sect. 3.4.3.2);
– in the computation of the *sign function* for the evaluation of the overlap operator, where deflation of the lowest eigenmodes is used, see e.g. [3, 5, 6].

For both tasks, direct methods are not feasible due to the huge dimension of the involved matrix. Hence one aims at iterative schemes which are only based on matrix-vector multiplications and are computationally cheap thanks to the sparseness of the matrix. Krylov subspaces define the setting for this task.

### 3.2.1 Krylov Subspace Techniques

The idea behind Krylov subspaces is to define a linear space spanned by $k$ vectors, which are constructed from a vector $b \in \mathbb{C}$ and multiple matrix-vector products $Ab, A^2b, \ldots, A^{k-1}b$ based on $A \in \mathbb{C}^{n\times n}$. The $k$-th Krylov subspace $\mathscr{K}_k(A, b)$ of the matrix $A$ with respect to the vector $b$ is then given by

$$\mathscr{K}_k(A, b) = \text{span}\left\{b, Ab, A^2b, \ldots, A^{k-1}b\right\},$$

which by definition is equivalent to the set of vectors, given by a matrix-vector product of all polynomials $p_{k-1} \in \Pi_{k-1}$ in $A$ of degree $k-1$ and $b$:

$$\mathscr{K}_k(A, b) = \{p_{k-1}(A)b : p_{k-1} \in \Pi_{k-1}\}.$$

The solution of a linear system $Ax = b$ (with $A$ assumed to be regular) is now linked to Krylov subspaces as follows:

- The exact solution $x$ lies in $\mathscr{K}_m(A, b)$, where $m \leq n$ is the degree of the minimal polynomial $q$ of $A$, $q(A) = \sum_{l=0}^{m} \gamma_l A^l = 0$ with $\gamma_0 \neq 0$:

$$0 = q(A) \Rightarrow x = A^{-1}b = -\frac{1}{\gamma_0}\sum_{l=0}^{m-1} \gamma_{l+1} A^l b \in \mathscr{K}_m(A, b).$$

- For Hermitian matrices $A$, $m$ is equal to the number of distinct eigenvalues $d$. If $d$ is small, then $x$ lies in a Krylov subspace of small dimension. From a numerical perspective this leads to the following conjecture: if all eigenvalues of $A$ fall into a few clusters, we can approximate $x$ well in a Krylov subspace of small dimension.

How to compute a stable basis of $\mathscr{K}_k(A, b)$ for $k \leq m$? This can be done by the Arnoldi and Lanczos process, which in addition also enable cheap approximations of the spectrum of $A$.

**The Arnoldi process**. For an arbitrary regular matrix $A \in \mathbb{C}^{n\times n}$, the Arnoldi process [7] solves the matrix equation

$$AV_k = V_k H_k + h_{k+1,k} v_{k+1} e_k^\top, \qquad k = 1, \ldots, m-1, \tag{3.8}$$

subsequently with $e_k$ denoting the $k$-th unit vector in $\mathbb{C}^k$, yielding in each step an orthonormal basis $V_{k+1} = (v_1, \ldots, v_{k+1})$ of $\mathscr{K}_{k+1}(A, b)$ and an upper Hessenberg matrix $H_k \in \mathbb{C}^{k\times k}$ with entries $(h_{i,j})_{1\le i,j\le k}$. One starts with $v_1 = b/\|b\|_2$ and subsequently gets

$$v_{k+1} = q_{k+1}/\|q_{k+1}\|_2 \quad \text{with} \quad q_{k+1} = (I - V_k V_k^\dagger) A v_k, \quad \text{and}$$

$$h_{i,j} = \begin{cases} v_i^\dagger A v_j, & i \le j \\ \|q_i\|_2, & i = j+1 \\ 0, & i > j+1 \end{cases}. \tag{3.9}$$

For stability, the new basis vector $v_{k+1}$ is orthonormalized with respect to the previous basis vectors $v_1, \ldots, v_k$ using the modified Gram-Schmidt scheme. In contrast to the classical Gram-Schmidt method, which orthogonalizes $v_{k+1}$ with respect to $v_i$, $i = 1, \ldots, k$, by subtracting all projections of $v_{k+1}$ on $v_i$ at once from $v_{k+1}$, the modified Gram-Schmidt scheme is subsequently orthogonalizing $v_{k+1}$: one computes the projection of $v_{k+1}$ to $v_1$, and subtracts this projection to get a vector which is orthogonal to $v_1$. Now the projection of this new vector with respect to $v_2$ is computed and subtracted to give a new vector being orthogonal to $v_1$ and $v_2$. Continuing this procedure leads to the orthonomalization of $v_{k+1}$ with respect to $v_1, \ldots, v_k$. In exact arithmetic, both versions are identical. In floating-point arithmetics, however, the original Gram-Schmidt method might suffer from instabilities, whereas the modified Gram-Schmidt method is proven to be stable.

By construction, $h_{m+1,m} = 0$, as $v_{m+1} \in \mathscr{K}_m(A, b)$, and $V_m^\dagger A V_m = H_m$ holds. The spectrum of $H$ coincides with all distinct eigenvalues of $A$. For $k < m-1$, we have $AV_k = V_k H_k + h_{k+1,k} v_{k+1} e_k^\top$, and we get a good approximation of the first $k$ modes of $A$ due to $h_{k+1,k} = \|q_k\|_2 = \|(I - V_{k-1}V_{k-1}^\dagger) A v_{k-1}\|$ small.

**The Lanczos process**. For Hermitian matrices $A$ this approach reduces to a Hermitian tridiagonal matrix $H_k$ with entries

$$h_{i,j} = \begin{cases} v_i^\dagger A v_j, & i = j \\ \|q_i\|_2, & i = j \pm 1 \\ 0, & \text{otherwise} \end{cases}. \tag{3.10}$$

Note that the matrix is symmetrical in addition, as the off-diagonal elements are real. The orthonormal basis $V_k$ can be efficiently computed by the three-term recursion

$$q_{k+1} = (A - \alpha_k I) v_k - \beta_{k-1} v_{k-1}, \qquad v_{k+1} = q_{k+1}/\beta_k \qquad (k = 1, \ldots, m-1)$$

with the abbreviations $\alpha_k = v_k^\dagger A v_k$ and $\beta_k = \|q_{i+1}\|_2$. This defines the Lanczos process [8].

### 3.2.2 Iterative Solvers for Linear Systems

The idea of Krylov subspace methods for solving linear systems

$$Ax = b \qquad \text{with } A \in \mathbb{C}^{n\times n} \text{ regular}, \quad x, b \in \mathbb{C}^n$$

is to seek the best approximation $x_k \in \mathscr{K}_k(A, b)$, i.e.,

$$x_k = \operatorname{argmin}_{x\in\mathscr{K}_k(A,b)} \|b - Ax\|. \tag{3.11}$$

An immediate consequence of the best approximation property of $x_k$ is the orthogonality condition of the residual $r(x) = b - Ax$, i.e., the residual $r(x_k)$ is orthogonal to the subspace $A\mathscr{K}_k(A, b)$. This can be seen as follows: if the minimization is done over the whole space $\mathbb{C}^n$, the best approximation property of the least squares methods implies that the residual will be orthogonal to all vectors spanned by $Ax$ with $x \in \mathbb{C}^n$, i.e., the residual is orthogonal to the image of $A$. Now we minimize only on the subset $\mathscr{K}_k(A, b)$, and the residual will be only orthogonal to all vectors spanned by $Ax$ with $x \in \mathscr{K}_k(A, b)$—in other words, the residual will be orthogonal to the image of $A\mathscr{K}_k(A, b)$.

#### 3.2.2.1 Generalized Minimal Residual (GMRES) Method

Let us assume that we have already computed the orthonormal basis $V_k$ of $\mathscr{K}_k(A, b)$ using the Arnoldi process. Rewritting the Arnoldi process (3.8) as

$$AV_k = V_{k+1}\widetilde{H}_k, \qquad \widetilde{H}_k = \begin{pmatrix} H_k \\ h_{k+1,k}e_k^\top \end{pmatrix},$$

we can transform both $b$ and $Ax$ as follows

$$Ax = AV_k y = V_{k+1}\widetilde{H}_k y, \quad b = \|b\|_2 v_1 = \|b\|_2 V_{k+1}e_1$$

by setting $x = V_k y$ with some $y \in \mathbb{C}^k$. This allows to reformulate the best approximation (3.11)

$$x_k = V_k y_k \quad \text{with } y_k = \operatorname{argmin}_{y\in\mathbb{C}^k} \|\|b\|_2 e_1 - \widetilde{H}_k y\|_2, \tag{3.12}$$

as $V_{k+1}$ is preserving the Euclidian norm of a vector $x \in \mathbb{C}^k$:

$$\|V_{k+1}x\|_2 = x^\dagger V_{k+1}^\dagger V_{k+1}x = x^\dagger x = \|x\|_2.$$

Hence one has to couple the Arnoldi process to compute the orthonormal basis of $\mathscr{K}_k(A, b)$ with the least squares problem defined by (3.12): in each step, $H_k$ is updated

to $H_{k+1}$. Using QR-factorization, this matrix is transformed into an upper triangle matrix by applying Givens rotations or Householder transformations, for example. This defines a linear system of dimension $k$ to uniquely define the minimizer $y$. If the residual error is small enough, the iteration will be stopped. This approach defines the GMRES algorithm [9], a shortcut for *Generalized minimal residual method*, which subsequentially produces a sequence of approximations $x_k, k = 1, \ldots, m-1$.

*Implementational details*. In principle, the iteration will stop at $k = m-1$, as the exact solution lies in $\mathscr{K}_m(A, b)$. However, this will be not feasible for large $m$, and one will stop if an error estimate, possibly based on the residual, shows that a given tolerance is reached.

If an inital approximation $x_0$ is available, GMRES may seek approximations in the affine Krylov subspace $x_0 + \mathscr{K}_k(A, b - Ax_0)$. The approach discussed above is then the special case for $x_0 = 0$, i.e., one uses the zero vector as a first guess for the solution. This approach is used in the GMRES(l) version (with $l \in \mathbb{N}$, usually $20 \leq l \leq 40$), which is based on restarting the process: one does $l$ steps, and starts GMRES again with setting $x_0 = x_l$. This reduces computational and memory costs, as both increase linearly with the dimension of the Krylov subspace. However, convergence will not be guaranteed any longer for arbitrary matrices.

*Convergence results*. From the best approximation property of $x_k$ we see that the residual $r_k = r(x_k)$ is decreasing, not necessarily monotonically. Also the worst case can arise, as shown by Greenbaum, Ptak und Strakos [10]: the residual $r(x_k) = r(x_0)$ is constant for all $k = 1, \ldots, m-1$, and drops to zero in the last step: $r(x_m) = 0$. For special matrices one gets stronger convergence results, showing the importance of the condition of the matrix. For example, for SPD matrices $A$ (symmetric and positive definite) one gets the estimate

$$\|r_k\|_2 \leq \left( \frac{\kappa_2^2(A) - 1}{\kappa_2^2(A)} \right)^{k/2} \|r_0\|_2,$$

showing that the speed of convergence is given by the condition $\kappa_2(A) = \|A\|_2 \|A^{-1}\|_2$ of $A$, which is equivalent to the ratio of maximum and minimum eigenvalue of $A$. The convergence is extremely fast, if the spectrum is strongly clustered, and extremely slow, if the opposite holds.

The derivation of error estimates for the residuals is a direct consequence of the best approximation property of the residual. However, one is more interested in error estimates of the approximation error directly. However, no convergence results are known so far that yield estimates for the approximation error $x_k - x$ directly.

#### 3.2.2.2 Conjugate Gradient (CG) Method

Instead of GMRES, one uses the Conjugate gradient method [11] for SPD matrices, which exploits the structure of $A$ to minimize computational costs.

Again one seeks a best approximation $x_k \in \mathbb{C}^{n\times n}$, but now in the energy norm $\|x_k\|_A = \sqrt{x_k^\dagger A x_k}$ given by $A$, and not for the residual, but for the approximation error directly:

$$x_k = \text{argmin}_{y\in V_k} \|y - x\|_A \tag{3.13}$$

with $x$ being the exact solution to $Ax = b$ and $V_k$ the affine Krylov subspace $x_0 + \mathscr{K}_k(A, r_0)$ introduced for GMRES. As we are looking for the best approximation in the energy norm, the approximation error $x - x_k$ will be orthognal to $A\mathscr{K}_k(A, r_0)$. However, this is equivalent to $r_k$ being orthogonal to $\mathscr{K}_k(A, r_0)$, but not to $A\mathscr{K}_k(A, r_0)$ as in the GMRES case:

$$0 = (x - x_k)^\dagger A\mathscr{K}_k(A, r_0) = (A(x - x_k))^\dagger \mathscr{K}_k(A, r_0) = r_k^\dagger \mathscr{K}_k(A, r_0). \tag{3.14}$$

This orthogonality condition allows to compute $x_k$, if an $A$-orthogonal basis $\{d_0, \ldots, d_{k-1}\}$ of $\mathscr{K}_k(A, r_0)$ is given, defined by $d_i^\dagger A d_j = \delta_{i,j} d_i^\dagger A d_i$. An A-orthogonal projection of the unknown exact solution $x$ onto the affine Krylov subspace $x_0 + \mathscr{K}_k(A, r_0)$ then yields

$$x_k = x_0 + \sum_{l=0}^{k-1} \frac{d_l^\dagger A(x - x_0)}{d_l^\dagger A d_l} d_l = x_0 + \sum_{l=0}^{k-1} \frac{d_l^\dagger r_0}{d_l^\dagger A d_l} d_l,$$

which defines the two-term recursions

$$\alpha_{k-1} = \frac{d_k^\dagger r_0}{d_{k-1}^\dagger A d_{k-1}}, \quad x_k = x_{k-1} + \alpha_{k-1} d_{k-1}, \quad r_k = r_{k-1} - \alpha_{k-1} z \tag{3.15}$$

with $z = Ad_{k-1}$. It remains to compute the $A$-orthogonal basis $\{d_0, \ldots, d_{k-1}\}$. The orthogonality condition (3.14) together with the recursion (3.15) for $r_{k+1}$ show that also $\{r_0, \ldots, r_{k-1}\}$ defines an orthogonal basis of $\mathscr{K}_k(A, r_0)$. Hence, if $r_{k+1} \neq 0$, the vectors $d_0, \ldots, d_k$ and $r_{k+1}$ define a basis of $\mathscr{K}_{k+1}(A, r_0)$. By setting

$$d_{k+1} = r_{k+1} - \sum_{l=0}^{k+1} \frac{r_{k+1}^\dagger A d_l}{d_l^\dagger A d_l} d_l = r_{k+1} - \frac{r_{k+1}^\dagger A d_k}{d_k^\dagger A d_k} d_k$$

one gets the desired $A$-orthogonal basis and two additional two-term recursions:

$$\beta_k = -\frac{r_{k+1}^\dagger A d_k}{d_k^\dagger A d_k}, \quad d_{k+1} = r_{k+1} + \beta_k d_k. \tag{3.16}$$

The recursions for both $\alpha_k$ and $\beta_k$ can be simplified: by using

$$r_0^\dagger d_k = (x - x_0)^\dagger A d_k = (x - x_{k-1})^\dagger A d_k = r_{k-1}^\dagger d_k = r_{k-1}^\dagger r_{k-1},$$

one gets

$$\alpha_{k-1} = \frac{d_k^\dagger r_0}{d_{k-1}^\dagger A d_{k-1}} = \frac{r_{k-1}^\dagger r_{k-1}}{d_{k-1}^\dagger A d_{k-1}}, \tag{3.17}$$

and with

$$-\alpha_k r_{k+1}^\dagger A d_k = (-\alpha_k A d_k)^\dagger r_{k+1} = (r_{k+1} - r_k)^\dagger r_{k+1} = r_{k+1}^\dagger r_{k+1}$$

one gets

$$\beta_k = \frac{r_{k+1}^\dagger r_{k+1}}{r_k^\dagger r_k}. \tag{3.18}$$

*Implementation details*. Summing up, five two-term recursions defined in (3.15)–(3.18) have to be solved to get the approximative solution $x_k$ for the linear system $Ax = b$ with A being SPD: starting with $r_0 = b - Ax_0$ and $d_0 = r_0$, the iteration for $k = 1, 2, \ldots$ has to save the matrix-vector product $z = Ad_{k-1}$ first, followed by the five two-term recursions

$$\begin{aligned}
\alpha_{k-1} &= \frac{r_{k-1}^\dagger r_{k-1}}{d_{k-1}^\dagger z}, \\
x_k &= x_{k-1} + \alpha_{k-1} d_{k-1}, \\
r_k &= r_{k-1} - \alpha_{k-1} z, \\
\beta_{k-1} &= \frac{r_k^\dagger r_k}{r_{k-1}^\dagger r_{k-1}}, \\
d_k &= r_k + \beta_{k-1} d_{k-1}.
\end{aligned}$$

One step of the CG method is quite cheap, as it demands for only one matrix-vector multiplication $Ad_{k-1}$ and two scalar products $r_k^\dagger r_k$ and $d_{k-1}^\dagger z$. One can show that the CG method is a clever implementation of the Lanczos process, avoiding the three-term recursions of the Lanczos process and the large storage costs involved.

*Convergence results*. One can obtain a result similar to the SPD case of GMRES: the speed of convergence of the CG method is given by

$$\|x_k - x\|_A \leq 2 \left( \frac{\sqrt{\kappa_2(A)} - 1}{\sqrt{\kappa_2(A)} + 1} \right)^k \|x_0 - x\|_A,$$

showing that the speed of convergence is given by the ratio of maximum and minimum eigenvalue of $A$. Again, the convergence is extremely fast, if the spectrum is strongly clustered, and extremely slow, if the opposite holds.

#### 3.2.2.3 Preconditioning

When applied to linear systems, the convergence of the Krylov subspace methods described above strongly depends on the spectrum of $A$. If the spectrum of $A$ consists only of one eigenvalue, these schemes will converge in only one step—the degree of the minimal polynomial of $A$ is one. The smaller the number of eigenvalues, the smaller the degree of the minimal polynomial, the less the number of necessary iterations. Numerically, this translates into having eigenvalues located in a few clusters. From the convergence results above we see in addition that the lower the condition of $A$, the higher the speed of convergence.

If $A$ does not have these desired properties, the idea of preconditioning will transform $A$ into a matrix $M^{-1}A$ of this type. Instead of $Ax = b$ one has to solve $\widetilde{A}x = \widetilde{b}$ with $\widetilde{A} = M^{-1}A$ and $\widetilde{b} = M^{-1}b$. But how to choose $M$? The following properties are needed:

- $M^{-1}$ should be "near" to $A^{-1}$ such that the eigenvalues of $M^{-1}A$ are clustered around 1, i.e., approximate well the identity matrix.
- One has to balance the trade-off between $M^{-1}$ approximating $A^{-1}$ well and minimizing the computational costs involved in computing the preconditioner; the best way is to choose something between the extreme choices $M^{-1} = A^{-1}$ and $M^{-1} = I$.
- If $A$ has some properties that are exploited by the respective Krylov subspace scheme, $M^{-1}A$ must preserve these properties. For example, the preconditioner used for CG methods must be SPD, too.

In the following we will briefly sketch three basic ideas of preconditioning arising in Lattice QCD applications: even-odd reduction, domain decomposition and multigrid.

#### 3.2.2.4 Even-Odd Reduction

A standard preconditioning for Wilson quarks is the so called even-odd (or red-black) scheme. It is based on indexing the lattice points such that the even points (whose integer coordinates $n_\mu = x_\mu/a$ fulfill $\sum_\mu n_\mu \mod 2 = 0$) are ordered first in the index, followed by the odd points ($\sum_\mu n_\mu \mod 2 = 1$). The Wilson fermion matrix $D = D_\mathrm{w} + m_0$, which is defined in Eq. (1.80) or in Eq. (1.147) for the O($a$) improved operator, can then be written as

$$D = \begin{pmatrix} D_{ee} & D_{eo} \\ D_{oe} & D_{oo} \end{pmatrix} . \tag{3.19}$$

The matrices $D_{ee}$ and $D_{oo}$ are invertible. For the operator in Eq. (1.80), $D_{ee}$ and $D_{oo}$ are proportional to the unit matrix. For the O($a$) improved operator in Eq. (1.147), $D_{ee}$ and $D_{oo}$ are block-diagonal matrices which are defined on the even- and odd-sites of the lattice respectively with $12 \times 12$ blocks on the diagonal. The Schur decomposition is given by

$$D = \begin{pmatrix} I_{ee} & D_{eo}D_{oo}^{-1} \\ 0 & I_{oo} \end{pmatrix} \begin{pmatrix} D_{ee} - D_{eo}D_{oo}^{-1}D_{oe} & 0 \\ 0 & D_{oo} \end{pmatrix} \begin{pmatrix} I_{ee} & 0 \\ D_{oo}^{-1}D_{oe} & I_{oo} \end{pmatrix}, \tag{3.20}$$

where the operator $\hat{D} = D_{ee} - D_{eo}D_{oo}^{-1}D_{oe}$, which is defined only on the even points of the lattice, is the Schur complement and is called the even-odd preconditioned Dirac operator. The Dirac equation $D\psi = \eta$, where $\psi = \begin{pmatrix} \psi_e \\ \psi_o \end{pmatrix}$ and $\eta = \begin{pmatrix} \eta_e \\ \eta_o \end{pmatrix}$ can be solved by first solving

$$\hat{D}\psi_e = \eta_e - D_{eo}D_{oo}^{-1}\eta_o \tag{3.21}$$

for $\psi_e$ and then computing $\psi_o = D_{oo}^{-1}(\eta_o - D_{oe}\psi_e)$. This can be easily seen by using the decomposition of $D$ given in Eq. (3.20).

#### 3.2.2.5 Domain Decomposition

Domain decomposition preconditioners split the problem into subproblems. Among them, the Schwarz Alternating Procedure (SAP) was introduced by Lüscher [12] to precondition the Wilson-Dirac operator. In the following, we will sketch the main idea behind the SAP.

The starting point is a decomposition of the lattice into two blocks, denoted by $\Omega$ and $\Omega^*$, which yields the partitioned Wilson-Dirac operator

$$D = \begin{pmatrix} D_{\Omega} & D_{\partial\Omega} \\ D_{\partial\Omega^*} & \mathrm{d}_{\Omega^*} \end{pmatrix}$$

and the associated partitioned linear system

$$\begin{pmatrix} D_{\Omega} & D_{\partial\Omega} \\ D_{\partial\Omega^*} & \mathrm{d}_{\Omega^*} \end{pmatrix} \begin{pmatrix} x_1 \\ x_2 \end{pmatrix} = \begin{pmatrix} b_{\Omega} \\ b_{\Omega^*} \end{pmatrix}. \tag{3.22}$$

Solving the linear system for all lattice points in $\Omega$ and leaving the other unchanged, followed by the alternating step of solving the linear system for all lattice points in $\Omega^*$ and leaving the other unchanged, yields the following iteration process (the so-called multiplicative Schwarz procedure) for $x^{(k)} \rightsquigarrow x^{(k+1)}$:

$$\begin{aligned} D_{\Omega}\tilde{x}_1 + D_{\partial\Omega}x_2^{(k)} &= b_{\Omega}, \\ \tilde{x}_2 &= x_2^{(k)}, \\ x_1^{(k+1)} &= \tilde{x}_1, \\ D_{\partial\Omega^*}x_1^{(k+1)} + D_{\Omega^*}x_2^{(k+1)} &= b_{\Omega^*}, \end{aligned}$$

which leads to

$$\tilde{x} = \begin{pmatrix} x_1^{(k)} + {D_\Omega}^{-1} r_\Omega(x^{(k)}) \\ x_2^{(k)} \end{pmatrix}, \quad x^{(k+1)} = \begin{pmatrix} \tilde{x}_1 \\ \tilde{x}_2 + D_{\Omega^*}^{-1} r_{\Omega^*}(\tilde{x}) \end{pmatrix}$$

with $r_\Omega(y) = b_\Omega - D_\Omega y_1 - D_{\partial\Omega} y_2$ and $r_{\Omega^*}(y) = b_{\Omega^*} - D_{\partial\Omega^*} y_1 - D_{\Omega^*} y_2$. Eliminating the intermediate step one gets the two-term recursion

$$x^{(k+1)} = (I - KD)x^{(k)} + Kb \quad \text{with} \quad K = \begin{pmatrix} D_\Omega^{-1} & 0 \\ D_{\Omega^*}^{-1} D_{\partial\Omega^*} D_\Omega^{-1} & D_{\Omega^*}^{-1} \end{pmatrix}, \tag{3.23}$$

which can be rewritten as a von-Neumann series in the right-hand side only:

$$x^{(k+1)} = Mb, \quad \text{with} \quad M = K \sum_{l=0}^{k} (I - DK)^l.$$

One can show that the spectral radius of $I - DK$ is bounded by one, if the condition number of $D$ is not too large. Instead of using the domain decomposition procedure as an iteration scheme for solving the linear system $Dx = b$, the recursion matrix $M$ defined above can be now used as preconditioner of $D$, i.e. one solves $DMy = b$, which gives the desired solution $x$ by matrix-vector multiplication: $x = My$. Note that if the number of cycles $k$ is big enough, $M$ will be a good approximation of $D^{-1}$. The preconditioned system can then be solved by GMRES, for example.

Of course, $M$ is never built directly. As Krylov subspace schemes are based on matrix-vector multiplications, we only have to evaluate matrix-vector multiplications involving $M$. For doing so, one uses the multiplicative Schwarz procedure defined above, that runs through all blocks of the lattice, alternately updating $x$ on each block, with the right-hand side $b$ now replaced by $y$.

### 3.2.3 Algebraic Multigrid Methods

The idea behind multigrid schemes can be easily explained for the case of two grids, which can be recursively extended to multigrid. Assume we have to solve a linear system

$$A_h u_h = b_h \quad \text{with} \quad A_h \in \mathbb{C}^{n \times n},\ u_h, b_h \in \mathbb{C}^n. \tag{3.24}$$

To start with, we define two sets of indices $C_h \subset \{1, \ldots n\}$ and $F_h = \{1, \ldots n\} \backslash C_h$ with $m$ and $n - m$ elements, resp. These sets are called coarse and fine grid, as they are associated to choosing different geometric grids, if the linear system arises from discretizing a PDE system. In the algebraic setting such a connection is missing to properly define both sets. Here one has to use information given by $A_h$ itself. One

aims at minimizing $m$ and having a strong connection of all fine grid variables to coarse grid ones at the same time.

We can now define a second linear system on the coarse grid

$$A_H u_H = b_H \quad \text{with} \quad A_H \in \mathbb{C}^{m \times m},\ u_H, b_H \in \mathbb{C}^m \tag{3.25}$$

by setting $A_H = I_h^H A_h I_H^h$, $b_H = I_h^H b_h$ with interpolation operators $I_H^h$, interpolating from the coarse to the fine grid, and $I_h^H$, restricting the fine to the coarse grid.

Starting with an approximate solution $u_h^{(0)}$ to the fine grid problem (3.24), we compute a new approximate $u_h^{(1)}$, which only demands for solving the coarse grid problem:

- *Compute the residual at the fine grid:* $r_h^{(0)} = b_h - A_h u_h^{(0)}$.
- *Restrict the residual to the coarse grid:* $r_H^{(0)} = I_h^H r_h^{(0)}$.
- *Solve the coarse grid problem to get the defect on the coarse grid:* $A_H d_H = r_H^{(0)}$
- *Interpolate the defect to the fine grid:* $d_h = I_H^h d_H$.
- *Update the approximation:* $u_h^{(1)} = u_h^{(0)} + d_h$

This defines the following error recursion for $e_h^{(k)} = u_h^{(k)} - u_h$:

$$e_h^{(k+1)} = M_{h,H} e_h^{(k)} \quad \text{with} \quad M_{h,H} = I - I_H^h A_H^{-1} I_h^H A_h.$$

In addition, $l_1$ and $l_2$ smoothing steps with smoother $S_h$ are incorporated at the beginning and the end of the procedure, in order to damp the high-frequency error part on the fine grid. This turns the recursion matrix $M_{h,H}$ into $S_h^{l_2} M_{h,H} S_h^{l_1}$. One classical choice of $S_h$ is Gauss-Seidel smoothing: $S_h = I - L_h^{-1} A_h$, with $L_h$ being the lower triangular part of $A_h$. This two-grid scheme can be easily generalized recursively to a multigrid approach, where the residual equation is solved only at the coarsest grid.

Algebraic multigrid has proven to be an efficient tool in Lattice QCD quite recently. Frommer et al. [13] have derived an algebraic multigrid preconditioner for the Wilson–Dirac operator, which make use of SAP as smoother in the algebraic multigrid scheme. In Brannick et al. [14] it is shown that the Wilson-Dirac operator can be used efficiently as a preconditioner for the overlap operator, assuming that the Wilson-Dirac operator is nearly normal, which is the case if smearing techniques are used.

### 3.2.4 Other Uses of Krylov Subspaces

Besides solving linear systems, Krylov subspace techniques play an important role in two other fields: computing eigenpairs and evaluating matrix functions.

#### 3.2.4.1 Eigenvalues and Eigenvectors

As we have already stated, one may use the Arnoldi and Lanczos process to compute eigenvalues of a matrix $A$.

**Ritz values**. Can we approximate eigenpairs of $A$ in the Krylov subspace $\mathscr{K}_k(A, b)$ in general? For doing so, we seek for the best approximation of the eigenvalue equation

$$y(\mu) = \text{argmin}_{y \in \mathscr{K}_k(A,b)} \|Ay - \mu y\|$$

for $\mu$ given, which is equivalent to

$$x(\mu) = \text{argmin}_{x \in \mathbb{C}^{k \times k}} \|AV_k x - \mu V_k x\|$$

with $V_k$ being an unitary matrix describing the orthogonal basis of $\mathscr{K}_k(A, b)$. As the residual of the eigenvalue equation has to be orthogonal to $\mathscr{K}_k(A, b)$ in this case, $V_k^\dagger A V_k x(\mu) = \mu x(\mu)$ has to hold. Thus the eigenpairs $(x(\mu), \mu)$ of $V_k^\dagger A V_k$, the so-called Ritz pairs, define best approximations $(V_k x(\mu), \mu)$ of eigenpairs of $A$. The eigenvalues $\mu$ are called Ritz values.

The Arnoldi and Lanczos process define important special cases:

- *Arnoldi process:* $V_k^\dagger A V_k$ is given by the Hessenberg matrix $H_k$ defined in (3.9). In this case, the (harmonic) Ritz pairs and values are called (harmonic) Arnoldi-Ritz pairs and values.
- *Lanczos process:* $V_k^\dagger A V_k$ is given by the SPD tridiagonal matrix $H_k$ defined in (3.10). In this case, the (harmonic) Ritz pairs and values are called (harmonic) Lanczos-Ritz pairs and values.

Are Arnoldi-Ritz and Lanczos-Ritz pairs good approximations of eigenpairs of $A$? The residual for a Ritz pair $(y, \mu)$ with $y = V_k x$ is given by

$$Ay - \mu y = h_{k+1} v_{k+1} e_k^\top \Rightarrow (A + E)y - \mu y = 0 \quad \text{with } E = -h_{k+1,k} v_{k+1} e_k^\top.$$

Hence the Arnoldi-Ritz value turns out to be in the $\varepsilon$-pseudospectrum $\sigma_\varepsilon(A)$ of $A$ for all $\varepsilon > |h_{k+1,k}|$, with the $\varepsilon$-pseudospectrum defined by

$$\sigma_\varepsilon(A) = \{\lambda \in \mathbb{C} : \exists E \text{ with } \|E\| < \varepsilon \text{ and } \lambda \in \sigma(A + E)\}.$$

For normal matrices the eigenvalues are well-conditioned, i.e., small perturbations to $A$ produce small changes to the eigenvalues, and the pseudospectrum $\sigma_\varepsilon(A)$ differs only slightly from the spectrum $\sigma(A)$ of $A$. Hence $|h_{k+1,k}|$ being small guarantees that the Ritz value is a good approximation to an eigenvalue of $A$. This is the case for the Lanczos-Ritz value, as SPD matrices are normal.

In the general case, this does not necessarily hold: the eigenvalues may be ill-conditioned, and $|h_{k+1,k}|$ being small may not lead to a good approximation of $\mu$. Consequently, Arnoldi-Ritz values may not be good approximations to eigenvalues of $A$, if $A$ is not normal.

**Convergence towards extreme eigenvalues**. In general, one observes a convergence of the Ritz values towards "extreme" eigenvalues, i.e., eigenvalues which are separated from all other eigenvalues.

For diagonalizable matrices $A$ this can be seen quite easily: using the Jordan decomposition $A = X\Lambda X^{-1}$ of $A$ and expand $b$ in terms of the eigenvectors $x_i$ spanning the columns of $X$: $b = \sum_{i=1}^{n} \alpha_i x_i$ with $\alpha_1, \ldots, \alpha_n \in \mathbb{C}\backslash\{0\}$ for $b \neq 0$. Then one can show the following bound [15]

$$\begin{aligned} \|(I - V_k V_k^\dagger)x_i\| &\leq \sum_{j=1, j\neq i}^{n} \frac{|\alpha_j|}{|\alpha_i|} \cdot \min_{p\in\Pi_{k-1}, p(\lambda_i)=1} \max_{j=1,\ldots,n; j\neq i} (|p(\lambda_j)|) \\ &\leq \sum_{j=1, j\neq i}^{n} \frac{|\alpha_j|}{|\alpha_i|} \cdot \max_{j\neq i} \min_{p\in\Pi_{k-1}, p(\lambda_i)=1} |p(\lambda_j)| \end{aligned} \tag{3.26}$$

with $\lambda_j$ denoting the eigenvalues of $A$. The left hand side is the orthogonal complement of the projection of the eigenvector $x_i$ onto the space spanned by $V_k$, which vanishes, if $x_i \in \mathscr{K}_k(A, b)$. Thus it is an indicator for how good $x_i$ can be represented in the Krylov subspace. Let us have a closer look to the bound on the right-hand side, if $\lambda_i$ is well separated from all other eigenvalues:

$$|\lambda_j - c| \leq \rho \, \forall j \in \{1, \ldots, n\}\backslash\{i\}, \quad |\lambda_i - c| > \rho.$$

Then the right-hand side bound can be estimated by

$$\begin{aligned} \max_{j\neq i} \min_{p\in\Pi_{k-1}, p(\lambda_i)=1} |p(\lambda_j)| &\leq \max_{j\neq i} \left(\frac{|\lambda_j - c|}{|\lambda_i - c|}\right)^{k-1} \\ &\leq \left(\frac{\rho}{|\lambda_i - c|}\right)^{k-1}. \end{aligned}$$

The smaller the radius $\rho$ of the disc around $c$, which contains all eigenvalues but $\lambda_i$, and the larger the distance of $\lambda_i$ to the disc, the faster the convergence for $\lambda_i$. Thus the Arnoldi process will converge fast to eigenvalues which are well separated from the rest of the eigenvalues and lie in an outer part of the spectrum.

**Harmonic Ritz values.** However, if one is interested in the interior eigenvalues of $A$, harmonic Ritz values may provide good approximations. Harmonic Ritz values are the reciprocals of the Ritz values of $A^{-1}$ in $A\mathscr{K}_k(A, b)$. The orthogonality condition yields in this case

$$W_k^\dagger A^{-1} W_k x(\mu) - \mu W_k^\dagger W_k x(\mu) = 0$$

with $W_k$ being defined by $W_k = AV_k$, which is equivalent to

$$V_k^\dagger A^\dagger V_k x(\mu) = \mu(V_k^\dagger A^\dagger V_k H_k + V_k^\dagger A^\dagger h_{k+1,k} v_{k+1} e_k^T) x(\mu)$$

by replacing $AV_k$ by (3.8). Using that $v_{k+1}$ is orthogonal to $V_k$ one finally gets

$$(H_k^\dagger H_k + (e_k h_{k+1,k})(e_k h_{k+1,k})^\dagger)x(\mu) = \frac{1}{\mu} H_k^\dagger x(\mu).$$

This defines a symmetric positive-definite generalized eigenvalue problem. Alternatively, this problem can be formulated by the eigenvalue problem

$$(H_k + H_k^\dagger (e_k h_{k+1,k})(e_k h_{k+1,k})^\dagger)x(\mu) = \frac{1}{\mu} x(\mu)$$

Hence the harmonic Ritz pairs can be easily extracted from the Krylov subspace decomposition of $A$, as we only have to make a rank-1 update of $H_k$.

**Restarted Arnoldi process**. The bound (3.26) also shows that the convergence depends on the choice of $b$, as the term $\sum_{j=1, j\neq i}^{n} \frac{|\alpha_j|}{|\alpha_i|}$ enters the right-hand side. One should choose $b$ such that the wanted eigenvectors are augmented and the others are diminished. This can be done using an implicitely restarted Arnoldi process, which roughly works as follows: if one is interested at the largest $k$ eigenvalues, one does $m = k + j$ Arnoldi steps leading to

$$AV_m = V_m H_m + v_{m+1} h_{m+1,m} e_m^\top. \tag{3.27}$$

The $k$ largest Ritz values of $H_m$ are estimates for the largest eigenvalues of $A$, and the remaining $j$ eigenvalues approximate the lower eigenvalues. To get rid of the undesired part of the spectrum, one does $j$ iterations of the shifted QR-algorithm on $H_m$ with the $j$ smallest Ritz values used as shifts $\nu_i$. This results in

$$\prod_{i=1}^{j} (H_m - \nu_i I) = Q_m R_m.$$

Multiplying (3.27) with $Q_m$ from the right, one gets

$$A\widetilde{Q}_m = \widetilde{Q}_m \widetilde{H}_m + v_{m+1} h_{m+1,m} e_m^\top Q_m \tag{3.28}$$

by setting

$$\widetilde{H}_m = Q_m^{-1} H_m Q_m, \; \widetilde{Q}_m = V_m Q_m.$$

As new starting vector replacing $b$ one uses the first column of $V_m Q_m$. Dropping the last $j$ entries of (3.28), one does another $j$ steps of the Arnoldi process and may continue iteratively. For implementational details, one may refer to the ARPACK users' guide available at http://www.caam.rice.edu/software/ARPACK/.

#### 3.2.4.2 Matrix Functions

For matrices $A \in \mathbb{C}^{n\times n}$, the matrix function $f : \Omega \subset \mathbb{C} \to \mathbb{C}$ is defined as the mapping $f(A) = p(A)$ via the Hermite interpolator $p$, which interpolates $f$ on the spectrum of $A$. Matrix functions play an important role in Lattice QCD. For example, the simulation of overlap fermions requires the solution of linear systems involving the overlap Dirac operator introduced in Eq. (1.108), which can be rewritten into $\frac{1}{a}(I - \gamma_5 \mathrm{sign}(Q))$ by setting $Q = \gamma_5 A$. Remember that $Q$ denotes a very large, sparse and complex matrix describing a periodic nearest-neighbor coupling on the lattice. Therefore it is not feasible to explicitly compute $\mathrm{sign}(Q)$. The idea is to directly approximate the vector $f(A)b$, which is needed for iterative solvers of linear system such as Krylov subspace techniques discussed above.

Based on the Krylov subspace $\mathscr{K}_m(A, b)$, the Arnoldi-process (3.8) produces an upper Hessenberg matrix $H_m$ together with an orthonormal basis given by the columns of $V_m$. The idea is now to approximate $f(A)b = p(A)b$ via the $m$-th Arnoldi approximation

$$f_m = V_m f(H_m) V_m^\dagger b = \|b\| V_m f(H_m) e_1. \tag{3.29}$$

One has to face two drawbacks: first, the whole Arnoldi basis $V_m$ has to be stored; and second, the function $f(H_m)$ of a $m \times m$-matrix has to be evaluated, which becomes costly for large values of $m$. One way out is using the restarted Arnoldi method, which is based on a characterisation of the approximation via an error formula

$$f(A)b - f_m = e_m(A) v_{m+1}.$$

As the error itself is given by a matrix-vector product involving the matrix function $e_m$, one can iteratively increase the approximation by adding an approximation of the defect $e_m(A)v_{m+1}$. The latter can be computed using the approximation (3.29) obtained by the Krylov subspace $\mathscr{K}_m(A, V_{m+1})$ corresponding to the matrix-vector product $e_m(A)v_{m+1}$.

A first characterisation of $e_m$ was derived by Eiermann and Ernst [16], which demands for computing the $m$-th divided differences of $f$ with respect to the interpolation nodes. However, this procedure becomes unstable for larger $m$ due to the instabilities occurring when computing high-order divided differences. Another characterisation [17], which is based on Stieltjes functions of the form

$$f(z) = \int_{-\infty}^{0} \frac{g(t)}{t - z}\, dt, \quad z \in \mathbb{C}\backslash(-\infty, 0],$$

avoids this problem. The approximation error is then given by

$$e_m(A)v_{m+1} = \left( \prod_{i=1}^{m} h_{i+1,i} \cdot \|b\| \cdot \int_{-\infty}^{0} \frac{g(t)}{w_m(t)} (tI - A)^{-1}\, dt \right) v_{m+1}$$

with $w_m(t) = (t-\theta_1)\cdots(t-\theta_m)$ and $\mathrm{spec}(H_m) = \{\theta_1, \ldots, \theta_m\}$. It remains to approximate the integral above by numerical quadrature of the type

$$\prod_{i=1}^{m} h_{i+1,i} \cdot \|b\| \sum_{i=1}^{l} \omega_i \frac{g(t_i)}{w_m(t_i)} \frac{1}{t_i - z}$$

with quadrature nodes $t_i$ and corresponding weights $\omega_i$.

To finish this section, we show that this approach is feasible for the sign function. Using the relation

$$sign(Q)b = (Q^2)^{-1/2} Qb, \tag{3.30}$$

one can use the techniques above with $f(z) = z^{-1/2}$. Fortunately, this is a Stieltjes function, as it holds for $\alpha \in (0, 1)$:

$$z^{-\alpha} = \frac{\sin((\alpha-1)\pi)}{\pi} \int_{-\infty}^{0} \frac{(-t)^{-\alpha}}{t-z}\, dt.$$

For numerical quadrature, this infinite integral can be transformed into a finite one.

The relation (3.30) is also the starting point for an alternative, quite standard approach to treat matrix functions by rational approximations. See Sect. 3.4.3.1 for more details.

## 3.3 Fermion Determinant

### *3.3.1 Pseudofermions*

The determinant of a matrix can be evaluated using LU decomposition. In lattice QCD the matrix represents the Dirac operator and its size is (for Wilson fermions) $n = 12V$, where the number of lattice points is typically $V = L^4$ and the number of color and spin components is $12 = 3 \times 4$. If $L > 8$ it is impractical to evaluate the determinant by LU decomposition. Instead the determinant can be estimated by stochastic methods.

The starting point is the integral representation

$$\frac{1}{\det A} = \int \mathscr{D}[\eta]\, \mathrm{e}^{-\eta^\dagger A \eta}, \tag{3.31}$$

where $A \in \mathbb{C}^{n\times n}$ and $\eta \in \mathbb{C}^n$. The definition $\mathscr{D}[\eta] = \prod_i^n \frac{d\mathrm{Re}(\eta_i)\, d\mathrm{Im}(\eta_i)}{\pi}$ ensures the normalization $\int \mathscr{D}[\eta]\, \mathrm{e}^{-\eta^\dagger \eta} = 1$. The necessary and sufficient condition for the absolute convergence of the integral in Eq. (3.31) is [18]

$$\lambda(A + A^\dagger) > 0\,, \tag{3.32}$$

where $\lambda(A + A^\dagger)$ are the eigenvalues of $A + A^\dagger$.

If the condition Eq. (3.32) is satisfied, the determinant can be evaluated stochastically. Let $\{\eta_k,\ k = 1, \ldots, N_\eta\}$ be an ensemble of random complex vectors with probability distribution $p(\eta)$. The determinant can then be estimated as

$$\frac{1}{\det A} = \left\langle \frac{\mathrm{e}^{-\eta^\dagger A \eta}}{p(\eta)} \right\rangle_{p(\eta)} = \frac{1}{N_\eta} \sum_{k=1}^{N_\eta} \frac{\mathrm{e}^{-\eta_k^\dagger A \eta_k}}{p(\eta_k)} + \mathrm{O}(1/\sqrt{N_\eta})\,, \tag{3.33}$$

where $\langle \mathscr{O} \rangle_{p(\eta)} = \int \mathscr{D}[\eta]\ p(\eta)\mathscr{O}(\eta)$. It is convenient to choose a Gaussian distribution $p(\eta) = \exp(-\eta^\dagger \eta)$, which we will assume from now on. The estimator in Eq. (3.33) can be complex. In this case, the variance of the estimator is given by the sum of the variance of its real and imaginary parts, which is given by

$$\sigma_\eta^2 = \left\langle \frac{\mathrm{e}^{-\eta^\dagger (A + A^\dagger)\eta}}{p(\eta)^2} \right\rangle_{p(\eta)} - \left\langle \frac{\mathrm{e}^{-\eta^\dagger A \eta}}{p(\eta)} \right\rangle_{p(\eta)} \left\langle \frac{\mathrm{e}^{-\eta^\dagger A^\dagger \eta}}{p(\eta)} \right\rangle_{p(\eta)} \tag{3.34}$$

$$= \frac{1}{\det(A + A^\dagger - I)} - \frac{1}{\det(AA^\dagger)}\,. \tag{3.35}$$

The first integral in Eq. (3.34) exists if

$$\lambda(A + A^\dagger) > 1\,. \tag{3.36}$$

The condition $\lambda(A + A^\dagger) > 1$ automatically implies the existence of the second and third integral, cf. Eq. (3.32). Therefore, if in an implementation of the estimator in Eq. (3.33) the variance Eq. (3.34) is monitored, its convergence assures the convergence of the mean. We note that Eq. (3.36) implies the weaker condition $\mathrm{Re}(\lambda(A)) > 0.5$.

When the determinant in Eq. (3.31) is evaluated stochastically on an ensemble of gauge configurations, the variance receives two contributions [19]

$$\sigma^2 = \sigma_{\mathrm{st}}^2 + \sigma_{\mathrm{ens}}^2\,. \tag{3.37}$$

The contribution to the variance from the stochastic estimation is

$$\sigma_{\mathrm{st}}^2 = \frac{1}{N_\eta} \left( \left\langle \frac{1}{\det(A + A^\dagger - I)} \right\rangle - \left\langle \frac{1}{\det(AA^\dagger)} \right\rangle \right)\,, \tag{3.38}$$

where the expectation value $\langle \cdot \rangle$ is taken over the gauge ensemble. The other piece is

$$\sigma_{\mathrm{ens}}^2 = \left\langle \frac{1}{\det(AA^\dagger)} \right\rangle - \left\langle \frac{1}{\det A} \right\rangle \left\langle \frac{1}{\det A^\dagger} \right\rangle\,. \tag{3.39}$$

The stochastic contribution to the variance Eq. (3.38) is inversely proportional to the number $N_\eta$ of stochastic vectors and can therefore be made small. Instead the contribution to the variance Eq. (3.39) purely coming from the ensemble average is independent of $N_\eta$ (and of the ensemble size). The variance scales proportionally to the lattice volume $V$, which makes simulations on large lattices difficult. Possible ways to mitigate the volume scaling will be discussed in the next section.

### 3.3.2 *Factorisations*

In practical applications of lattice QCD, the determinant $\det(A)$ of a large matrix $A$ is estimated stochastically using the pseudofermion representation Eq. (3.31). It is likely that the matrix $A$ does not fulfill the condition Eq. (3.36), which guarantees a finite variance of the estimate. *Variance reduction techniques* based on factorisations of $\det(A)$ are very helpful, as we explain in a few examples in the following. Historically factorisations of $\det(A)$ aimed at splitting the determinant in a product of factors of equal small variance. Later factorisations into unequal pieces were considered in the context of the Hybrid Monte Carlo algorithm, see Sect. 3.4, where they reduce the forces in the molecular dynamics equations of motion.

In applications like mass-reweighting, see [18, 20, 21], the matrix $A$ can be written as a ratio

$$A = \frac{D + \varepsilon X}{D} = I + \varepsilon X D^{-1} . \tag{3.40}$$

Here $D = D_\mathrm{w} + m$ is the Wilson Dirac operator as defined in Eq. (1.80). The eigenvalues of $A$ lie in the complex plane within a circle around one. Since typically $\varepsilon ||X D^{-1}|| \gtrsim 1$, it is unlikely that $A$ fulfills the condition Eq. (3.36). A way to circumvent this problem is to factorise the matrix $A$ (and thus $1/\det(A)$) in $N$ factors as

$$A = \prod_{i=0}^{N-1} D_{i+1} D_i^{-1} \tag{3.41}$$

with $D_i = D + \delta_i X, \delta_0 = 0$ and $\delta_N = \varepsilon$. Equation (3.41) assumes that $D_i$ is invertible for all $i = 0, \ldots, N-1$. The factors are

$$D_{i+1} D_i^{-1} = I + \bar{\varepsilon}_i X D_i^{-1} \tag{3.42}$$

with $\bar{\varepsilon}_i = \delta_{i+1} - \delta_i$. The shifts $\bar{\varepsilon}_i$ can be chosen sufficiently small such that the factors satisfy Eq. (3.36). One possibility is to choose the shifts all equal to $\bar{\varepsilon}_i = \varepsilon / N$ [20]. An unbiased estimator of the determinant in Eq. (3.31) is given by

$$\frac{1}{\det A} = \prod_{i=0}^{N-1} \left( \frac{1}{N_\eta} \sum_{k=1}^{N_\eta} \frac{\mathrm{e}^{-\eta_{k,i}^\dagger D_{i+1} D_i^{-1} \eta_{k,i}}}{p(\eta_k)} \right) + \mathrm{O}(1/\sqrt{N N_\eta}) , \tag{3.43}$$

where $\eta_{k,i}$ are independent random vectors for each factor. A factorisation similar to Eq. (3.41) is [22]

$$A = \prod_{i=1}^{N} A^{1/N} . \tag{3.44}$$

At leading order in $1/N$ the effect of the $Nth$-root factorisation Eq. (3.44) is the same as that of Eq. (3.41) with equidistant shifts $\bar{\varepsilon}_i = \varepsilon/N$ in Eq. (3.42). A comparison of the two methods beyond leading order can be found in [19].

Even-odd preconditioning was discussed in Sect. 3.2.2.4. It leads to a factorisation of the determinant of the Wilson–Dirac operator. Equation (3.20) implies the relation

$$\det(D) = \det(D_{oo}) \det(\hat{D}) . \tag{3.45}$$

Both factors are real. $\det(D_{oo})$ can be computed exactly. The determinant of the Schur complement $\det(\hat{D})$ has to be evaluated stochastically, which requires inverting $\hat{D}$. Since $\hat{D}$ is defined on the even-sites of the lattice only, less numerical effort is needed to invert it. An extension of the idea of even-odd preconditioning is domain decomposition, for which we refer to [23].

The variance in Eq. (3.37) increases proportionally to the lattice volume $V$. In the context of low mode reweighting the fluctuations of the determinant of $D^{\dagger}_{\text{low}} D_{\text{low}}$, where $D_{\text{low}}$ is a restriction of $D$ to its low modes, are found to depend only mildly on the volume [24]. The explanation for this observation might be the fact that the width of the distribution of the small eigenvalues of $\sqrt{D^{\dagger} D}$ decrease like $1/V$ [24] (the fluctuations of the eigenvalue gap go instead like $1/\sqrt{V}$ [25]). Thus, given a factorisation of the determinant that separates low (infrared IR) and high (ultraviolet UV) modes

$$\det(D) = \det(D_{\text{UV}}) \cdots \det(D_{\text{IR}}) , \tag{3.46}$$

the ensemble variance of $\det(D_{\text{IR}})$ is expected to have a milder dependence on the volume. This hierarchy of modes may induce also a hierarchy of costs since it is the low modes that cause the most cost in lattice QCD. A hierarchy based on recursive domain decomposition has been studied in [26].

The factorisation introduced in [27, 28] is based on the identity

$$\det(D D^{\dagger}) = \det(\tilde{D} \tilde{D}^{\dagger}) \det((D \tilde{D}^{-1})(D \tilde{D}^{-1})^{\dagger}) , \tag{3.47}$$

which holds for any non-singular matrix $\tilde{D}$. We note that when even-odd preconditioning is used, the factorization Eq. (3.47) can be applied to the Schur complement $\hat{D}$ instead of $D$.

A special case of the factorisation Eq. (3.47) is obtained by setting $\tilde{D} = D + i\mu\gamma_5$. Equation (3.47) then becomes

$$\det(D D^{\dagger}) = \det(D D^{\dagger} + \mu^2) \det\left( \frac{D D^{\dagger}}{D D^{\dagger} + \mu^2} \right) . \tag{3.48}$$

The first determinant $\det(DD^\dagger + \mu^2) = \det\{(D + i\mu\gamma_5)(D + i\mu\gamma_5)^\dagger\}$ (the equality can be shown using Eq. (1.87)) is identical to the determinant of the Dirac operator for $N_\mathrm{f} = 2$ twisted-mass Wilson quarks in Eq. (1.150). Therefore the parameter $\mu$ is called twisted mass parameter. It separates the high modes larger than $\mu^2$ of the Dirac operator, which dominate the first determinant factor in Eq. (3.48), from the lower modes, which dominate the second factor. The factorisation Eq. (3.48) is an explicit realisation of the separation of scales in Eq. (3.46).

## 3.4 HMC with Fermions Revisited

In the following we consider the case of $N_\mathrm{f} = 2$ mass-degenerate Wilson quarks. We denote their mass by $m_0$ and the Dirac operator by $D = D_\mathrm{w} + m_0$. The partition function is

$$Z = \int \mathscr{D}[U]\, \mathrm{e}^{-S_\mathrm{g}[U]}\, \det(DD^\dagger)\,. \tag{3.49}$$

The integrand is real and positive and can be interpreted as a probability density amenable to Markov chain Monte Carlo methods. The most widely used method to include the fermion determinant is to use the integral representation given in Eq. (3.31) which in the case of Eq. (3.49) is

$$\det(DD^\dagger) = \int \mathscr{D}[\phi]\, \mathrm{e}^{-S_\mathrm{pf}[U,\phi]} \tag{3.50}$$

in terms of a complex-valued field $\phi$ called the pseudofermion field with the action

$$S_\mathrm{pf}[U,\phi] = \langle D^{-1}\phi, D^{-1}\phi\rangle = \langle \phi, (DD^\dagger)^{-1}\phi\rangle\,, \tag{3.51}$$

where the scalar product $\langle\cdot,\cdot\rangle$ is defined in Eq. (A.20).

### *3.4.1 Equations of Motion*

The most widely used method to simulate lattice QCD is the hybrid Monte Carlo algorithm [29] which we discussed in Sect. 2.3 for pure gauge fields. With fermions the starting point is the Hamiltonian

$$H(U,P) = \langle P, P\rangle/2 + S_\mathrm{eff}[U]\,, \tag{3.52}$$

where

$$S_\mathrm{eff}[U] = S_\mathrm{g}[U] + S_\mathrm{pf}[U,\phi]\,. \tag{3.53}$$

We follow Ref. [30], see also the contribution of M. Peardon on algorithms for lattice QCD in [31]. The hybrid Monte Carlo algoritm has three steps.

1. The momenta $P$ are generated according to the probability density proportional to $\exp(-\langle P, P\rangle/2)$ and the pseudofermion $\phi$ according to the probability density proporional to $\exp(-S_{\rm pf}[U,\phi])$ (for fixed gauge field $U$). The latter can be done by generating a normally distributed field $R$ and setting $\phi = D\,R$.
2. The following molecular dynamics equations of motion are solved

$$\dot{P}_\mu(x) = -F_\mu(x)\,, \quad \dot{U}_\mu(x) = P_\mu(x)\,U_\mu(x)\,. \tag{3.54}$$

   The force is defined as $F_\mu(x) = \partial_{x,\mu} S_{\rm eff}[U]$, cf. Equation (A.6). The derivatives are with respect to a fictitious molecular dynamics time $t$ and the equations of motion are integrated numerically from $t = 0$ to $t = \tau$. The initial conditions are $U_0 = U$ and $P_0 = P$. We remark that the pseudofermion field $\phi$ remains unchanged during the integration. The numerical integrator uses a finite step size $h$ and in general it does not preserve the value of the Hamiltonian, i.e.

$$\Delta H(U,P) = H(U_\tau, P_\tau) - H(U_0, P_0) \neq 0\,. \tag{3.55}$$

   This requires a Metropolis acceptance-rejection step.
3. The new gauge field $U'$ is set to the field $U_\tau$ with probability

$$P_{\rm acc}(U,P) = \min\left\{1, \mathrm{e}^{-\Delta H(U,P)}\right\}\,. \tag{3.56}$$

   If the proposal is rejected, $U'$ is set to $U$, which remains unchanged.

The force in Eq. (3.54) has two contributions $F_0 + F_1$. The first originates from the gauge field $(F_0)_\mu(x) = \partial_{x,\mu} S_{\rm g}$ and has been computed in Sect. 2.3.2 for the Wilson gauge action. The second is the contribution of the fermions $(F_1)_\mu(x) = \partial_{x,\mu} S_{\rm pf}$. Using $\left.\frac{\mathrm{d}(DD^\dagger)^{-1}}{\mathrm{d}s}\right|_{s=0} = -(DD^\dagger)^{-1}\left(\left.\frac{\mathrm{d}D}{\mathrm{d}s}\right|_{s=0} D^\dagger + D\left.\frac{\mathrm{d}D^\dagger}{\mathrm{d}s}\right|_{s=0}\right)(DD^\dagger)^{-1}$ and introducing the vectors

$$\psi = D^{-1}\phi\,, \qquad \chi = (D^\dagger)^{-1}\psi = (DD^\dagger)^{-1}\phi\,, \tag{3.57}$$

we arrive at the expression

$$(F_1)^i_\mu(x) = -\langle \chi, \left.\frac{\mathrm{d}D}{\mathrm{d}s}\right|_{s=0} \psi\rangle - \langle \psi, \left.\frac{\mathrm{d}D^\dagger}{\mathrm{d}s}\right|_{s=0} \chi\rangle \tag{3.58}$$

for the Lie algebra components. A calculation of the derivatives shows that

$$\begin{aligned}(F_1)^i_\mu(x) = &+\frac{1}{2}\chi^\dagger(x)T^i U_\mu(x)(1-\gamma_\mu)\psi(x+\hat{\mu}) \\ &-\frac{1}{2}\chi^\dagger(x+\hat{\mu})U^{-1}_\mu(x)T^i(1+\gamma_\mu)\psi(x) \\ &+\frac{1}{2}\psi^\dagger(x)T^i U_\mu(x)(1+\gamma_\mu)\chi(x+\hat{\mu}) \\ &-\frac{1}{2}\psi^\dagger(x+\hat{\mu})U^{-1}_\mu(x)T^i(1-\gamma_\mu)\chi(x)\,. \end{aligned} \tag{3.59}$$

Adding together the first and the fourth terms on the right hand side of Eq. (3.59) gives

$$2\mathrm{Re}\,\frac{1}{2}\mathrm{tr}_{\,\sigma,c}[T^i U_\mu(x)(1-\gamma_\mu)\psi(x+\hat{\mu})\chi^\dagger(x)]\,. \tag{3.60}$$

Here, $\mathrm{tr}_{\,c}$ means the trace over colour indices and $\mathrm{tr}_{\,\sigma}$ the trace over spin indices. Adding together the second and the third terms on the right hand side of Eq. (3.59) gives

$$-2\mathrm{Re}\,\frac{1}{2}\mathrm{tr}_{\,\sigma,c}[U^{-1}_\mu(x)T^i(1+\gamma_\mu)\psi(x)\chi^\dagger(x+\hat{\mu})]\,. \tag{3.61}$$

Finally, summing Eqs. (3.60) and (3.61) yields the result

$$(F_1)^i_\mu(x) = -2\mathrm{Re}\langle\chi\,,\,\delta^i_{x,\mu}D\psi\rangle \tag{3.62}$$

with

$$\begin{aligned}\left(\delta^i_{x,\mu}D\psi\right)(y) = &-\delta_{y,x}\frac{1}{2}(1-\gamma_\mu)T^i U_\mu(x)\psi(x+\hat{\mu}) \\ &+\delta_{y,x+\hat{\mu}}\frac{1}{2}(1+\gamma_\mu)U^{-1}_\mu(x)T^i\psi(x)\,. \end{aligned} \tag{3.63}$$

The computation of $F_1$ requires two inversions of the Wilson–Dirac operator.

We discuss now the modifications that occur when determinant factorisations discussed in Sect. 3.3.2 are used. In the case of even-odd preconditioning the Wilson–Dirac operator is written as in Eq. (3.19) and its determinant factorises according to Eq. (3.45). The effective action Eq. (3.53) in the Hamiltonian becomes

$$S_{\mathrm{eff}}[U] = S_{\mathrm{g}}[U] - 2\mathrm{tr}\,\ln(D_{oo}) + \langle\hat{D}^{-1}\phi_e\,,\,\hat{D}^{-1}\phi_e\rangle\,, \tag{3.64}$$

where the pseudofermion field $\phi_e$ is now defined on the even-sites of the lattice only. The contribution of $-2\mathrm{tr}\,\ln(D_{oo})$ to the fermionic force can be calculated exactly. The force orginating from the even-odd preconditioned operator $\hat{D}$ is $-2\mathrm{Re}\langle\chi_e\,,\,\delta^i_{x,\mu}\hat{D}\psi_e\rangle_e$, where $\psi_e = \hat{D}^{-1}\phi_e$ and $\chi_e = (\hat{D}^\dagger)^{-1}\psi_e$. Introducing the fields $\psi = (\psi_e\ \psi_o)^T$ and $\chi = (\chi_e\ \chi_o)^T$ which are defined on the complete lattice,

we can rewrite the force of $\hat{D}$ with the same expression as in Eq. (3.62) by setting $\psi_o = -D_{oo}^{-1} D_{oe} \psi_e$ and $\chi_o = -(D_{eo} D_{oo}^{-1})^\dagger \chi_e$. In this way implementing the even-odd preconditioning does not require to write a new program. We remark that for the O($a$) improved Wilson operator, $\delta^i_{x,\mu} D$ in Eq. (3.63) receives an additional contribution from the derivative of the Sheikholeslami–Wohlert term, see Eq. (1.147). We refer to [32] for details of this calculation.

In the case of the factorisation Eq. (3.47), the pseudofermion action Eq. (3.51) is replaced by

$$S_{\text{split}} = \langle \tilde{D}^{-1} \phi_1, \tilde{D}^{-1} \phi_1 \rangle + \langle (\tilde{D} D^{-1} \phi_2, \tilde{D} D^{-1} \phi_2 \rangle \tag{3.65}$$

in terms of two pseudofermion fields $\phi_1$ and $\phi_2$ used to represent the two determinant factors in Eq. (3.47). The original idea was to define $\tilde{D}$ such that $\tilde{D}$ and $D\tilde{D}^{-1}$ are better-conditioned matrices. This leads to quark forces which have less fluctuations along the molecular-dynamics trajectories and the step-size can be increased by a factor two [33] for a fixed Metropolis acceptance. Another idea is to define $\tilde{D}$ such that the forces originating from the two terms in Eq. (3.65) are hierarchical and benefit from multi-rate integration schemes (see the next subsection) [34].

A final remark concerns numerical simulations based on the twisted mass factorisation given in Eq. (3.48) [35]. Only the first factor $\det(DD^\dagger + \mu^2)$ is included in the molecular dynamics time evolution. The reason is that it is safe from small eigenvalues of the Dirac operator due to the cut-off parameter $\mu$. The second factor in Eq. (3.48) is included in the measurement of the observables as a reweighting factor [24].

### 3.4.2 Multi-rate Integration Schemes

If the forces deriving from the Hamiltonian are hierarchical and the larger forces turn out to be cheap to compute, the integration of molecular dynamics can be accelerated by means of multi-rate schemes. This is the situation for the Hamiltonian in Eq. (3.52). The gauge force is cheap and is the largest, the fermionic force is expensive but is smaller, see for example Fig. 3 in [23].

In addition, techniques discussed so far in the previous sections often introduce a multirate behaviour in the system that can be exploited by multi-rate schemes, although these techniques originally did not intend to do so: even-odd preconditioning, domain decomposition and determinant splitting. All these methods introduce a splitting of the action of the pseudofermionic field into $M$ different forces:

$$S_{\text{pf}}[U, \phi] = \sum_{m=1}^{M} S_k[U, \phi],$$

and hence the Hamiltonian reads

$$H(U,\,P) = \langle P,\,P\rangle/2 + S_{\mathrm{g}}[U] + \sum_{m=1}^{M} S_k[U,\phi].$$

If the actions are ordered such that computational costs are increasing, while at the same time the strength of the forces is decreasing, a multi-rate integration based on the leap-frog scheme with macro step size $h_0$ and micro step size $h_1 = h_0/m_1$ due to Sexton and Weingarten [36] proceeds as follows:

$$V_H(h_0) = V_{H_2}(h_0/2)\left(V_{H_1}(h_1)\right)^{m_1} V_{H_2}(h_0/2),$$

with $H_1(U,\,P) = \langle P,\,P\rangle/2 + S_{\mathrm{g}}[U] + \sum_{m=1}^{M-1} S_k[U,\phi]$ and $H_2(U,\,P) = S_M[U,\phi]$. This scheme can be nested, by introducing a next finer step size $h_2 = h_1/m_2$ and further splitting $H_1$ into

$$H_1(U,\,P) = H_{11}(U,\,P) + H_{12}(U,\,P)$$

with $H_{11}(U,\,P) = \langle P,\,P\rangle/2 + S_{\mathrm{g}}[U] + \sum_{m=1}^{M-2} S_k[U,\phi]$ and $H_{12}(U,\,P) = S_{M-1}[U,\phi]$ in order to replace $V_{H_1}(h_1)$ above by

$$V_{H_1}(h_1) = V_{H_{12}}(h_1/2)\left(V_{H_{11}}(h_2)\right)^{m_2} V_{H_{12}}(h_1/2).$$

This procedure can be applied recursively to obtain $M$ different step size ratios at the end, corresponding to the activity levels of the $M$ actions $S_k[U,\phi]$.

### *3.4.3 A Single Dynamical Quark Flavour: The RHMC Algorithm*

So far, we have discussed techniques useful for pairs of flavours of mass-degenerate fermions. This is a close approximation to the real world, where the up- and down-quarks both have similar, small masses. The strange quark has no such partner, so to treat its dynamics in a simulation requires techniques built on molecular dynamics that can handle single (or more generally odd numbers of) flavours. Using an exact algorithm in the sense that there are no finite integrator-step-size errors is an advantage. Perhaps the best exact method for these one-flavour simulations is the *Rational Hybrid Monte Carlo* (RHMC) method [37, 38].

#### 3.4.3.1 Rational Approximations to the Square Root and Its Inverse

Evaluating the fermion path integral for one flavour yields the familiar result, $\det M[U]$ and we have seen for simulating two flavours we use $\det M^{\dagger}[U]M[U]$ as part of the probability measure on the gauge fields. The single flavour Wilson

fermion determinant is real, but not necessarily positive so it is not suitable in an importance sampling density. We can use $|\det M|$ instead, adding the sign of the determinant into observables. This could introduce a sign problem where the variance of our Monte Carlo estimator is too large but experience in QCD simulations at zero temperature shows the problem is mild, at least for the strange quark mass. Now writing $|\det M| = \sqrt{\det M^\dagger M} = \det \sqrt{M^\dagger M}$, suggests a method for simulation, providing we can deal with matrix functions such as $\sqrt{M^\dagger M}$. One way to build an approximation to a matrix function, is to write a polynomial in $M^\dagger M$ but Ref. [37] notes that convergence with increasing polynomial order can be slow compared to rational approximations, which take the form $r(x) = p(x)/q(x)$ where $p$ and $q$ are low-order polynomials. Reference [39] gives an example of an optimised rational approximation with degrees for $p$ and $q$ of (3, 3)

$$\frac{1}{\sqrt{x}} \approx 0.3904603901 \times \frac{(x + 2.3475661045)(x + 0.1048344600)(x + 0.0073063814)}{(x + 0.4105999719)(x + 0.0286165446)(x + 0.0012779193)}. \tag{3.66}$$

This approximation is accurate to roughly 3 significant figures in the range $x \in [0.003, 1]$. Notice that all the monomial shifts are real and positive.

### 3.4.3.2 The RHMC Algorithm

Now the approximation to the single-flavour determinant can be translated into a bosonic path-integral following a similar recipe to the two-flavour pseudofermions. With a rational approximation $r(x) \approx \sqrt{x}$, writing

$$\begin{aligned} |\det M[U]| &\approx \det\ r(M^\dagger[U]M[U]), \\ \det\ r(M^\dagger M) &= \int \mathscr{D}\phi \mathscr{D}\phi^*\ \ e^{-\phi^*[r(M^\dagger M)]^{-1}\phi}, \end{aligned} \tag{3.67}$$

gives a representation that can be handled on the computer in a Monte Carlo simulation. At first sight, it looks like a cumbersome task to apply the operator $1/r$ to the lattice pseudofermion $\phi$. To start, note that since $r(x) = p(x)/q(x)$ we have $1/r(x) = q(x)/p(x)$, which is another rational approximation. If $p$ and $q$ have degrees $(n, d)$ with $d < n$, this can be written as a partial fraction sum;

$$\frac{1}{r(x)} = \sum_{k=1}^{n} \frac{\alpha_k}{x + \beta_k}, \tag{3.68}$$

where $\{-\beta_k\}$ are the $n$ zeroes of $p(x)$. Returning to the simple example of Eq. (3.66) (for which the degrees of $p$ and $q$ are equal, so an extra constant is required along with the partial sum) would give

$$\frac{1}{\sqrt{x}} \approx 0.3904603901 + \frac{0.0511093775}{x + 0.0012779193} + \frac{0.1408286237}{x + 0.0286165446} + \frac{0.5964845033}{x + 0.4105999719}. \tag{3.69}$$

Two observations are worth making here; first all the coefficients $\alpha_k$ are positive, giving numerical stability to the algorithm and the smaller values of $\alpha_k$ coincide with the smaller shifts, $\beta_k$. These seem to be helpful accidental properties of the rational approximations of interest here. Now for the pseudofermion action, the partial fraction gives

$$\det\ f(M^\dagger M) = \int \mathscr{D}\phi \mathscr{D}\phi^*\ \ e^{-S_{\mathrm{RHMC}}}, \tag{3.70}$$

with

$$S_{\mathrm{RHMC}} = \sum_{k=1}^{n} \alpha_k\ \phi^* \left[M^\dagger M + \beta_k\right]^{-1} \phi. \tag{3.71}$$

There are efficient algorithms [40] to find the $n$ vectors $\{\underline{v}_1, \underline{v}_2, \ldots \underline{v}_n\}$ which solve the set of linear systems

$$(M^\dagger M + \gamma_k)\ \underline{v}_k = \underline{b}, \tag{3.72}$$

with common right-hand side $\underline{b}$. These methods again build the Krylov space $\mathscr{K}_n(M^\dagger M, \underline{b})$ to find solutions. Since the shifts $\{\beta_k\}$ are all positive for the functions needed here, the multi-shift solver requires about the same number of applications of the matrix $M^\dagger M$ as would a standard conjugate-gradient solution of the simpler system $M^\dagger M \underline{x} = \underline{b}$.

Reference [41] noted an important consequence of the seemingly accidental feature of the partial fraction sum described above; the small values of the weights $\alpha$ coincide with small values of $\beta$. Small values of $\beta$ lead to more expensive inversions, but the resulting contribution to the force is compensated by the small value of $\alpha$.

This action can be used in a sampling measure by defining a molecular dynamics force and making use of the Hybrid Monte Carlo algorithm with the resulting combination called RHMC. The determination of the force term coming from each partial fraction term is computed straightforwardly once the force from a simple two-flavour pseudofermion has been evaluated. This determination starts from observing the simulation-time dependence of the action

$$\frac{dS_{\mathrm{RHMC}}}{d\tau} = -\sum_{k=1}^{n} \alpha_k\ Y_k^* \left[\frac{dM^\dagger}{d\tau} M + M^\dagger \frac{dM}{d\tau}\right]^{-1} Y_k, \tag{3.73}$$

with the auxiliary fields

$$Y_k = \left[M^\dagger M + \beta_k\right]^{-1} \phi. \tag{3.74}$$

## 3.5 The Quark Propagator from a Point Source

As we saw already, the fermion fields in the path integral can not be manipulated so easily on a computer and the first step to getting physics results is usually to explicitly carry out the integral over these fields. Having discussed the fermion determinant and how it can be included in the importance sampling, let us now consider techniques for computing observables that include quark propagation. Dealing with the quark propagator has essentially defined the limitations of what observables were accessible to lattice QCD computations since their beginning. The starting point for the discussion is the propagator from a single origin point.

### *3.5.1 Quark Observables from a Single Point Source*

A range of physically relevant observables can be computed using solely a quark propagator from a fixed origin. The reason for this is the translational invariance of the QCD vacuum, which enables us to relate many diagrams with quark lines to one-another. Consider a path integral, including $N_f$ flavours of quarks

$$\langle O \rangle = \frac{1}{Z} \int \mathscr{D}U \prod_f^{N_f} \mathscr{D}\bar{\psi}_f \mathscr{D}\psi_f \quad O[\bar{\psi}, \psi, U]\, e^{-\sum_f \bar{\psi}_f M_f[U]\psi_f - S_G[U]}. \tag{3.75}$$

Now suppose we have some symmetry operation $\mathscr{G}$, that we can apply to the lattice fields $\{\bar{\psi}, \psi, U\}$ giving new fields $\{\bar{\psi}^{\mathscr{G}}, \psi^{\mathscr{G}}, U^{\mathscr{G}}\}$ which preserves the action and integration measure then it follows

$$\langle O \rangle = \langle O^{\mathscr{G}} \rangle \text{ where } O^{\mathscr{G}}[\bar{\psi}, \psi, U] = O[\bar{\psi}^{\mathscr{G}}, \psi^{\mathscr{G}}, U^{\mathscr{G}}]. \tag{3.76}$$

In infinite volume or with boundary conditions which do not violate translation invariance, one such symmetry operator is translation invariance, so if we consider an observable $O_1$ which depends only on the quark fields at two lattice sites $\psi(\underline{x}_1, t_1)$ and $\bar{\psi}(\underline{x}_2, t_2)$ (for simplicity, we hide the gluon field dependence) then its expectation value has the property

$$\langle O_1[\psi(\underline{x}_1, t_1), \bar{\psi}(\underline{x}_2, t_2)] \rangle = \langle O_1[\psi(\underline{0}, 0), \bar{\psi}(\underline{x}_2 - \underline{x}_1, t_2 - t_1)] \rangle, \tag{3.77}$$

so evaluating the quark propagator from the origin alone still enables us to estimate this observable in spite of its apparent dependence on the co-ordinates of two sites. Similarly if an observable has two spatial sums including an arbitrary momentum projection, translation invariance enables the diagram to be related to a single sum

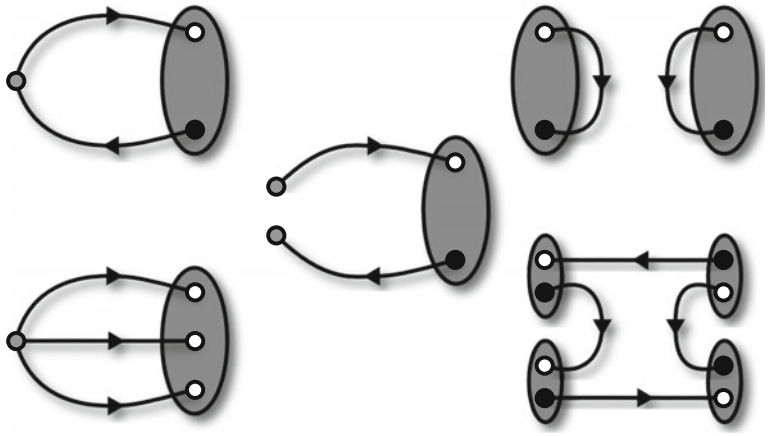


**Fig. 3.1** Quark observables, classified according to the simplest method they can be computed with

$$\sum_{\underline{x}_1,\underline{x}_2} e^{i\underline{p}\cdot(\underline{x}_1-\underline{x}_2)}\langle O_1[\psi(\underline{x}_1,t_1),\bar{\psi}(\underline{x}_2,t_2)]\rangle = L^3\sum_{\underline{y}} e^{i\underline{p}\cdot\underline{y}}\langle O_1[\psi(\underline{0},0),\bar{\psi}(\underline{y},t_2-t_1)]\rangle. \quad (3.78)$$

Hadrons involve more than one quark field, so consider the case where a diagram includes two $\psi$ and two $\bar{\psi}$ fields. Now we see

$$\langle O_2[\psi(x_1),\psi(x_2),\bar{\psi}(x_3),\bar{\psi}(x_4)]\rangle = \langle O_2[\psi(0),\psi(x_2-x_1),\bar{\psi}(x_3-x_1),\bar{\psi}(x_4-x_1)]\rangle. \quad (3.79)$$

If $x_3 - x_1 = 0$ and the flavour structure means the Wick contractions yields only a single quark-line diagram (such as would occur for an isovector light meson, or a kaon) then another symmetry, $\gamma_5$ hermiticity enables this diagram once again to be computed from just a point source. This very fortunately enables the pion, the Goldstone boson of QCD to be studied using just a simple point source.

Translation invariance also enables us to compute the two-point correlation function for simple baryons from a point-like source. We see that with a single origin point, many computations of two-point correlation functions can be constructed using the translational invariance trick, however diagrams where both source and sink involve spatial structure or where the "all-to-all" diagrams of Fig. 3.1 is needed are inaccessible. These states include flavourless mesons or states made up of two mesons, needed for scattering calculations. Spatial structure can usually be added with a small number of extra source points, but the "all-to-all" diagrams will need a completely separate technology.

Reducing two spatial sums to a single one using translation invariance yields a simpler diagram with the same expectation value but remember we will compute this diagram in a Monte Carlo calculation and while these two measurements have the same expectation value, the variance of these estimators may differ significantly.

Usually taking a single origin gives an estimator with larger variance. A number of methods to maintain the flexibility of the point source while reducing this variance have been developed.

### 3.5.2 Reducing Variance in Point Propagator Calculations

Eigenvectors play an important role in a useful method to augment the precision of the point-to-all technique through *Low-mode averaging* [42, 43]. The idea is to partially expand a point-source propagator in terms of low modes and then exploit translation invariance to sum over the lattice volume for these modes alone. This improves the variance of the estimator. This has been used effectively in a number of situations where low noise is important but having access to all elements of the quark propagator is not required.

Consider again a simple example with a single $\psi\bar{\psi}$ insertion, which we showed earlier just depends on $\delta$, the separation between the insertion points. Here, we write this explicitly as a bilinear on the fields, which is independent of $x_1$

$$c(\delta) = \langle \bar{\psi}(x) \Gamma[U](x, x+\delta)\psi(x+\delta)\rangle, \tag{3.80}$$

with $\Gamma$ an operator dependent on the gauge fields alone. Now suppose $P_0$ is a projection operator into the vector space spanned by the lowest $n_V$ eigenvectors of the Dirac operator. We see

$$\begin{aligned} c(\delta) &= \langle \bar{\psi}(x)\Gamma\psi(x+\delta)\rangle \\ &= \langle \bar{\psi}(x)P_0\Gamma P_0\psi(x+\delta)\rangle + \langle \bar{\psi}(x)(\Gamma - P_0\Gamma P_0)\psi(x+\delta)\rangle \\ &= \frac{1}{V}\sum_x \langle \bar{\psi}(x)P_0\Gamma P_0\psi(x+\delta)\rangle + \langle \bar{\psi}(0)(\Gamma - P_0\Gamma P_0)\psi(\delta)\rangle. \end{aligned} \tag{3.81}$$

Translation invariance enables the last step, where the first term constructed in the vector space of low modes has a sum over the lattice volume. Since we have the eigenvectors everywhere, we can compute this term and the resulting estimator should have a low variance. In the second term, translation invariance is used again to shift to the origin and a point propagator is used to build the Monte Carlo estimator. If the physics is dominated by the low-mode term, this should be a small correction that does not add too much noise.

More complicated examples with more quark field insertions can be constructed. An extension of this idea, called the covariant averaging approximation is presented and tested in Refs. [44, 45].

## 3.6 All-to-All Quark Propagators

As we will see in Chap. 4 when making measurements that involve quark fields, it is useful even essential to have access to all or at least most elements of the propagator on a gauge configuration. The fermion matrix is too large to find all elements of its inverse directly, so the task seems daunting. Fortunately, since we are using the quark propagator as an ingredient in a Monte Carlo calculation, it usually suffices to build an unbiased stochastic estimator on each gauge configuration and carry out a "Monte Carlo within a Monte Carlo".

### *3.6.1 Stochastic Estimators*

Consider a vector $\underline{\eta} \in \mathbb{C}^N$, whose components are random numbers, $\eta_i$ which obey

$$E[\eta_i] = 0, \quad E[\eta_i \ \eta_j^*] = \delta_{ij}, \tag{3.82}$$

and so a stochastic representation of the identity in $\mathbb{C}^N$ can be made from this vector by writing the outer-product;

$$E[\underline{\eta} \ \underline{\eta}^\dagger] = I. \tag{3.83}$$

There are different vectors that have this simple property; a popular choice is to draw each $\eta_i$ from an independent normal distribution. Other options have advantages that we will make use of later. Consider drawing the entries in $\underline{\eta}$ from independent samples of a random number $\eta_i \in Z_4 = \{1, i, -1, -i\}$ which take these four values with equal probability. This clearly satisfies the requirements given in Eq. 3.82 but notice $\eta^*\eta = 1$ holds for any of the four elements of $Z_4$ before taking the expected value which would not hold for normally distributed random numbers. To see what difference this makes, consider the stochastic evaluation of the trace of a matrix, $A$ using both these types of noise. For both choices the estimator is the inner product;

$$\mathrm{Tr}\ A = E[\eta^* \cdot A\eta], \tag{3.84}$$

with this result following straightforwardly from Eq. 3.82. To compute the variance of the estimator, we need the result

$$E[\eta_i^* \eta_j \eta_k^* \eta_l] = \begin{cases} \delta_{ij}\delta_{kl} + \delta_{il}\delta_{jk}, & \text{for normally distributed noise} \\ \delta_{ij}\delta_{kl} + \delta_{il}\delta_{jk} - \delta_{ijkl}, & \text{for } Z_4 \text{ noise,} \end{cases} \tag{3.85}$$

with

$$\delta_{ijkl} = \begin{cases} 1 & \text{when } i = j = k = l \\ 0 & \text{otherwise.} \end{cases} \tag{3.86}$$

We find the variance of our estimator,

$$\sigma^2_{\mathrm{Tr\ A}} = E[\left(\eta^* \cdot A\eta\right)\left(\eta^* \cdot A^\dagger \eta\right)] - |\mathrm{Tr}\ A|^2 \tag{3.87}$$

is given by

$$\sigma^2_{\mathrm{Tr\ A}} = \begin{cases} \mathrm{Tr}\ A^\dagger A, & \text{for normally distributed noise} \\ \mathrm{Tr}\ A^\dagger A - \sum_i A^*_{ii} A_{ii} & \text{for } Z_4 \text{ noise,} \end{cases} \tag{3.88}$$

and from this we observe that for estimating a trace, using $Z_4$ noise never has a larger variance. Note the second term in the $Z_4$ case is an unusual one; it means that while the variance in the normally distributed estimator is invariant under a unitary transformation, the corresponding estimator for the $Z_4$ case is not. In fact, if $A$ is diagonal, it is easy to see the estimator has zero variance. This observation can be used to construct effective variance reduction algorithms.

The cost of computational evaluations is substantially reduced by replacing the rank-$N$ identity operator by the rank-1 stochastic matrix, $\underline{\eta}\ \underline{\eta}^\dagger$. Any element of a matrix $A$ describing a linear operator in $\mathbb{C}^N$ can now be written

$$A_{ik} = A_{ij}\ E[\eta_j\ \eta_k^*] = E[\psi_i\ \eta_k^*],$$

and a Monte Carlo algorithm to estimate all elements of $A$ is now introduced; after drawing a sample $\eta$, the vector $\underline{\psi} = A\underline{\eta}$ is computed and the product $\underline{\psi}\ \underline{\eta}^\dagger$ is an unbiased estimator for $A$. Notice how *all* elements of $A$ are accessible after a single matrix-vector operation is performed.

In this simple form, the method usually has too high a variance to be useful. Of course, a larger sample of $N_\eta$ independent and identically distributed random vectors $\{\underline{\eta}^{(1)}, \underline{\eta}^{(2)}, \underline{\eta}^{(3)}, \ldots \underline{\eta}^{(N_\eta)}\}$ can be taken to build a rank-$N_\eta$ estimator

$$E[\frac{1}{N_\eta}\sum_{i=1}^{N_\eta} \underline{\eta}^{(i)}\ \underline{\eta}^{(i)\dagger}] = \delta_{ij}, \tag{3.89}$$

by simple averaging and this has a smaller variance. Usually this is not the most cost-effective choice. The variance of this estimator falls in proportion to $1/N_\eta$ but note that a finite set of $N$ orthonormal vectors can be used to represent the identity *exactly*, giving a clear example where just gathering more statistics is not the optimal choice.

#### 3.6.1.1 Noise Dilution

Rather than spending our computing budget on more sampling, an alternative is to first break $\mathbb{C}^N$, the vector space in which we are trying to construct our estimator into smaller sub-spaces. The use of this technique for lattice calculations was first

introduced by Bernardson et. al. [47]. After decomposing a vector space $V$ into $D$ sub-spaces, $V = V^{[1]} \oplus V^{[2]} \oplus \cdots \oplus V^{[D]}$ a stochastic identity operator in each sub-space is written by first taking a random linear combination of $N^{[s]}$ orthonormal basis vectors in the set $\{\underline{e}_1, \underline{e}_2, \ldots, \underline{e}_{N^{[s]}}\}$ which spans $V^{[s]}$,

$$\underline{\eta}^{[s]} = \sum_{q=1}^{N^{[s]}} \eta_q \ \underline{e}_q,$$

where $\eta_q$ are the random numbers drawn. The benefit is those entries in the stochastic representation of the identity which connect components in different sub-spaces have explicitly been set to zero. The expected value of the outer product of this random vector is

$$E[\underline{\eta}^{[s]}\underline{\eta}^{[s]\dagger}] = \sum_{q=1}^{N^{[s]}} \underline{e}_q \ \underline{e}_q^{\dagger} = I^{[s]}, \tag{3.90}$$

with $I^{[s]}$ the identity operator acting only in sub-space $V^{[s]}$. Since $\underline{\eta}^{[s]}$ only has support in $V^{[s]}$, there is by construction no component of this random matrix in any of the orthogonal sub-spaces and this holds for any sample, before taking the expected value. A stochastic representation of the identity can now be defined by constructing one of these random vectors in each sub-space and summing them all. The identity becomes

$$E[\sum_{s=1}^{D} \underline{\eta}^{[s]} \ \underline{\eta}^{[s]\dagger}] = I. \tag{3.91}$$

At a glance, this resembles the expression of Eq. 3.89 but notice that when the dilution is high enough to ensure all the vector spaces are one-dimensional (a limit often jokingly referred to as homeopathic, since further dilution means there is less than one atom of randomness left in each sample) the stochastic identity becomes exact when $Z_N$ noise is used for each component of $\eta$. While reaching this limit is not usually practical, this argument serves to demonstrate that a *noise-free, finite-cost* representation exists, again emphasising there are better methods than accumulating statistics.

Let us illustrate this point explicitly here; consider a toy example where the vector space to be computed has just four components. A single vector $\eta$ can be drawn from the set of random $Z_2$ vectors, which has just $2^4 = 16$ elements. Suppose the sample we draw is $\eta^T = (+1, -1, -1, -1)$. Now consider the four projectors that would allow us to reach the homeopathic limit applied in turn to $\eta$. The result is then

$$\eta = \begin{pmatrix} +1 \\ -1 \\ -1 \\ -1 \end{pmatrix} \text{ so } \eta^{[1]} = \begin{pmatrix} +1 \\ 0 \\ 0 \\ 0 \end{pmatrix}, \eta^{[2]} = \begin{pmatrix} 0 \\ -1 \\ 0 \\ 0 \end{pmatrix}, \eta^{[3]} = \begin{pmatrix} 0 \\ 0 \\ -1 \\ 0 \end{pmatrix}, \eta^{[4]} = \begin{pmatrix} 0 \\ 0 \\ 0 \\ -1 \end{pmatrix},$$

and then it follows straightforwardly that

$$\eta^{[s]}\eta^{[s]\dagger} = I_4,$$

for this particular sample. It is easy then to see that since this holds for all samples, the estimator must have zero variance.

Now let us apply these ideas to the task of estimating all elements of the quark propagator. For Dirac fermions, on each lattice site the spinor for a single flavour contains twelve complex components, corresponding to the spin and colour degrees of freedom. These indices form a natural starting point for dilution. From a *single* noise source, $\eta_{\beta,j}(\underline{x})$ where $\beta$ denotes Dirac spin index, $j$ colour index and $\underline{x}$ indicate the lattice site, the diluted source vectors (each distinct source is labelled by a superscript $[\cdot]$) are

$$\begin{array}{rcll} \eta^{[i]}_{\beta,j}(\underline{x}) & = & \delta_{ij}\eta_{\beta,j}(\underline{x}) & \text{colour} \\ \eta^{[\alpha,i]}_{\beta,j}(\underline{x}) & = & \delta_{\alpha\beta}\delta_{ij}\eta_{\beta,j}(\underline{x}) & \text{spin–colour.} \end{array} \tag{3.92}$$

Further dilution can be achieved by partitioning space-time into sub-sets, such as an even-odd decomposition. A general spatial partitioning breaks the lattice into $N_\sigma$ sub-sets, $\{\Lambda_1, \Lambda_2, \ldots \Lambda_{N_\sigma}\}$ and introduces a partitioning function on each site

$$\delta_\sigma(\underline{x}) = \begin{cases} 1 & \text{if } \underline{x} \in \Lambda_\sigma \\ 0 & \text{otherwise,} \end{cases} \tag{3.93}$$

The diluted sources, labelled now by indices $[\alpha, i, \sigma]$ become

$$\eta^{[\alpha,i,\sigma]}_{\beta,j}(\underline{x}) = \delta_{\alpha\beta}\delta_{ij}\delta_\sigma(\underline{x})\eta_{\beta,j}(\underline{x}) \qquad \text{spin–colour–space-time.} \tag{3.94}$$

Next, these source vectors are used to form a diluted stochastic identity, following Eq. 3.91 and subsequently the quark propagator is represented as

$$\Delta_{ij,\alpha\beta}(\underline{x},\underline{y}) = E\left[\psi^{[s]}_{i\alpha}(\underline{x})\eta^{[s]}_{j\beta}(\underline{y})\right], \tag{3.95}$$

with

$$\psi^{[s]}_{i\alpha}(\underline{x}) = \left[M^{-1}\right](\underline{x},\underline{y})_{ij,\alpha\beta}\ \ \eta^{[s]}_{j\beta}(\underline{y}). \tag{3.96}$$

In practise, the expressions we must evaluate in physics calculations often combine many quark propagators from all the constituents within a hadron. In this case, independent samples of random noise vectors must be taken for each quark line.

#### 3.6.1.2 Using Low-Precision Polynomials for Variance Reduction

The goal is to write a stochastic representation with as low a variance as possible given some computing budget. One other means of approaching the problem is to split the inverse in two by simply writing

$$M^{-1} = \bar{M} + \left(M^{-1} - \bar{M}\right),$$

and noting that if $\bar{M}$ is an approximation to $M^{-1}$ that is cheap to compute, a cost-efficient all-to-all propagator can be formed by estimating $\bar{M}$ with a low variance method such as dilution and computing the small correction term in a simpler manner that requires just a few, more expensive full solutions to the linear system.

One option is to make use of the hopping parameter expansion [46]. Writing $M = I + \kappa\Delta$, the truncated Taylor expansion about $\kappa = 0$ yields

$$(I + \kappa\Delta)^{-1} \simeq \sum_{k=0}^{N} (-1)^k \kappa^k \Delta^k$$

and this expression converges as $N \to \infty$ provided the spectral radius of $\kappa\Delta$ is small enough (i.e. for sufficiently heavy quarks). The hopping parameter expansion does not converge rapidly for light quarks and so the method can be improved upon by working with alternative polynomials with better convergence. Bali et al. [48] describe another effective alternative that is easy to implement and similarly constructs a low-order polynomial approximation. $\bar{M}$ is taken to be the inverse of the fermion matrix computed using an iterative solver but with the sequence truncated before convergence to high precision is achieved. Care must be taken to ensure the choice of $\bar{M}$, which can depend on the noise source, does not bias the estimator.

#### 3.6.1.3 Estimating More than One Propagator in an Observable and the "One-End Trick"

So far, we have restricted our discussion to writing a stochastic representation of a single quark propagator. In many cases, we would like to estimate something that contains more than one propagator, such as a connected meson two-point correlation function. In general, on a particular gauge background, this would take the form

$$c_{ab} = \mathrm{Tr}\, M^{-1} \Gamma^{(a)} M^{-1} \Gamma^{(b)}, \tag{3.97}$$

where the matrices $\Gamma^{(a)}$ describe the creation and annihilation operators for the meson and can be applied to a vector for a very modest computational cost. Usually, we are interested in computing this for a set of many different choices of $\Gamma$, for example we might want to compute the correlation function for a range of time-separations and in this case, index $b$ indicates the supporting time-slice on which the meson creation

operator was inserted while $a$ is the time-slice of the corresponding annihilation operator. We postpone our discussion of these matrices to the next chapter.

With this requirement, inserting a single stochastic identity operator into the product is restrictive; for every $\Gamma^{(a)}$ we add, two calls to our linear solver must be made. A more flexible solution is to draw two independent random vectors $\underline{\eta}^{[1]}$, $\underline{\eta}^{[2]}$ and for two distinct stochastic identities to be injected between the two fermion matrix inverses. Two solver calls are then needed to compute $\underline{\psi}^{[a]} = M^{-1}\underline{\eta}^{[a]}$, a = 1, 2. A simple estimator for $c_{ab}$ follows from

$$c_{ab} = E\left[\mathrm{Tr}\ \underline{\psi}^{[1]}\underline{\eta}^{*[1]}\ \Gamma^{(a)}\underline{\psi}^{[2]}\underline{\eta}^{*[2]}\ \Gamma^{(b)}\right] = E\left[\kappa_a^{[1,2]}\kappa_b^{[2,1]}\right], \tag{3.98}$$

with

$$\kappa_a^{[1,2]} = \underline{\eta}^{*[1]}\Gamma^{(a)}\underline{\psi}^{[2]} \ \text{ and } \ \kappa_b^{[2,1]} = \underline{\eta}^{*[2]}\Gamma^{(b)}\underline{\psi}^{[1]} \tag{3.99}$$

Notice that the estimator is the product of two random numbers $\kappa_a^{[1,2]}$ and $\kappa_b^{[2,1]}$, which are formed from inner products of vectors with meson creation or annihilation operators inserted. These are simple objects to manipulate on the computer. As with the trace estimator the simplest estimator has too high a variance to be useful in practise. The techniques we discuss in the preceding sections are useful again. In particular, if the two-point function is time-separated, then use of a time-dilution scheme is very effective.

A widely used and convenient recipe to measure this meson two-point function is the "one-end trick" [49]. If a noise vector is spin-diluted, and a simple operator (with no spatial structure) is introduced as a meson source, then

$$M^{-1}\Gamma^a M^{-1} = M^{-1}\Gamma^a P^b P^{b\dagger} M^{-1} = E\left[M^{-1}\Gamma^a P^b \eta\eta^\dagger P^{b\dagger}\right] \tag{3.100}$$

and the matrix $\hat{P}^{a,b}$ can be found such that

$$M^{-1}\Gamma^a P^b \eta = \hat{P}^{a,b} M^{-1}\eta \tag{3.101}$$

so with a limited set of inversions, all spin elements in the propagator can be computed *post-hoc*. Notice this expression has a single noise source but includes two quark line evaluations for this single set of inversions. The variance of the resulting expression is significantly reduced. The method is very effective for simple hadron operators but does not generalise well when a more extensive, fully all-to-all method is needed.

### *3.6.2 Exploiting Low Eigenmodes of the Dirac Operator*

For light quarks, the physical signal in the propagator is dominated by contributions from a small subset containing the eigenvectors of the fermion matrix with the smallest eigenvalues. This again hints at possible techniques to improve the accuracy of

estimators if we have a reliable algorithm to find some low-lying eigenvectors of the lattice Dirac operator. To simplify the discussion, we work here with the hermitian version of the fermion matrix, $Q = \gamma_5 M$. Since $\gamma_5$ is an involution, $M^{-1} = Q^{-1}\gamma_5$. Suppose we computed the lowest $N_V$ eigenvectors of $Q$, finding the column matrix $V$ such that $QV = VD$ with $D$ a diagonal $N_V \times N_V$ matrix. Now write

$$Q^{-1} = Q^{-1}\left(VV^\dagger + I - VV^\dagger\right) = \underbrace{VD^{-1}V^\dagger}_{\bar{Q}_0} + \underbrace{Q^{-1}P_V}_{\bar{Q}_1},$$

with $P_V = I - VV^\dagger$, a hermitian, idempotent projection operator into the vector space spanned by the large eigenvectors that have not been computed. This representation hints at an effective way to build an all-to-all propagator. The first term makes use of the known eigenvectors and the second contribution can be estimated stochastically using the methods defined above, including variance reduction tricks such as dilution. If the signal is dominated by the low modes, the term we estimate stochastically will be a smaller correction, with correspondingly smaller variance. When estimating $\bar{Q}_1$, start by recognising that since $P_V^2 = P_V$ (i.e. $P_V$ is idempotent) a useful estimator can be defined from

$$\bar{Q}_1 = E[Q^{-1}P_V\ \underline{\eta}\ \underline{\eta}^\dagger\ P_V] = E[\underline{\hat{\psi}}\ \underline{\hat{\eta}}^\dagger], \tag{3.102}$$

with $\hat{\eta} = P_V\eta$ and $\underline{\hat{\psi}} = Q^{-1}\hat{\eta}$. The stochastic vectors $\hat{\eta}$ and $\underline{\hat{\psi}}$ do not have support in the vector space spanned by the computed eigenvectors.

In Appendix A of Ref. [50], useful improvements are described that avoid the expensive computations of exact eigenvectors. If a set of $N_V$ approximate eigenvectors is found, they still span a small vector space and a corresponding large, orthogonal vector space in which the physics contribution is smaller. Now however, since we no longer have exact eigenvectors, the solution to $Q^{-1}\underline{\eta}$ has support in both these spaces and the extra contributions must be taken into account. The precision with which eigenmodes are generated gives extra freedom to optimise the efficiency of this method. This paper also describes how even-odd preconditioning can be exploited in constructing stochastic all-to-all propagators.

## 3.7 Summary and Further Reading

In this chapter the techniques to handle fermions on the lattice have been reviewed. Due to their nature as Grassmann (anti-commuting) variables, an exact integration over the fermions is performed in the path integral before it can be solved by numerical methods. The rules of integration, in particular Wick contractions are constructed by explicit examples.

An essential numerical calculation in simulations of lattice QCD is the solution of Dirac's equation. It involves the fermion matrix, which in the case of the

Wilson–Dirac operator is a sparse matrix. Mathematical techniques for handling large sparse matrices are crucial and significant improvements have been recently achieved. Iterative solvers based on Krylov subspace methods and suitable ways to precondition the Wilson–Dirac operator are explained. In addition methods to compute eigenvalues and evaluate matrix functions are discussed.

After Grassmann integration the partition function is an integral over gauge fields only with a determinant factor accounting for the fermions. The techniques to estimate this determinant using pseudofermions are explained. The Hybrid Monte Carlo algorithm is reviewed to include the determinant factor in the case of two mass-degenerate quarks and for a single quark. Multi-rate integration schemes which exploit a hierarchy of forces in Hamilton's equations of motion are discussed.

The propagator is an essential component of field theory calculations involving fermions and its role in physics measurements will be developed in the next chapter. In many computations all (or most) elements of the quark propagator are required for a robust evaluation. This chapter introduced a number of reliable and useful tools to estimate the quark propagator stochastically with as small a variance as practical. These techniques usually work by breaking apart the quark propagator into blocks acting in physically distinct sub-spaces. Most importantly, given the range of techniques at hand, it is very unlikely the best means of reducing the variance of our stochastic estimator with a limited computer budget is to pile up more statistics and use the very slow convergence of simple averaging; make only one noise source per configuration and use your computer budget on dilution.

The importance of finding efficient methods for manipulating quark fields is illustrated by the level of active research in the subject, with new ideas being continually developed. These are often closely tied to the physics goal. This chapter is not able to cover all these directions and clear unifying principles have not yet emerged.

Methods in lattice QCD for fermions are reviewed in the lectures by Lüscher in Ref. [30]. The algebraic multi-grid solver for the Wilson–Dirac operator is described by Frommer et al. in Ref. [13].

## References

1. J. Rubow, U. Wolff, Comput. Phys. Commun. **182**, 2530 (2011). doi:10.1016/j.cpc.2011.07.010
2. M. Lüscher, JHEP **07**, 081 (2007). doi:10.1088/1126-6708/2007/07/081
3. L. Giusti, C. Hoelbling, M. Luscher, H. Wittig, Comput. Phys. Commun. **153**, 31 (2003). doi:10.1016/S0010-4655(02)00874-3
4. L. Del Debbio, L. Giusti, C. Pica, Phys. Rev. Lett. **94**, 032003 (2005). doi:10.1103/PhysRevLett.94.032003
5. R.G. Edwards, U.M. Heller, R. Narayanan, Nucl. Phys. B **540**, 457 (1999). doi:10.1016/S0550-3213(98)00694-4
6. J. van den Eshof, A. Frommer, T. Lippert, K. Schilling, H.A. van der Vorst, Comput. Phys. Commun. **146**, 203 (2002). doi:10.1016/S0010-4655(02)00455-1
7. W. Arndoli, Q. Appl. Math. **9**, 17 (1951)
8. C. Lanczos, J. Res. Natl. Bur. Stan. **45**, 255 (1950)

9. Y. Saad, H. Schultz, SIAM J. Sci. Stat. Comput. **7**, 856 (1986)
10. A. Greenbaum, V. Ptak, Z. Strakos, SIAM J. Matrix Anal. Appl. **17**(3), 465 (1996)
11. M. Hestenes, Stiefel, J. Res. Natl. Bur. Stan. **49**, 409 (1952)
12. M. Lüscher, Comput. Phys. Commun. **156**, 209 (2004). doi:10.1016/S0010-4655(03)00486-7
13. A. Frommer, K. Kahl, S. Krieg, B. Leder, M. Rottmann, SIAM, J. Sci. Comput. **36**, A1581 (2014). doi:10.1137/130919507
14. J. Brannick, A. Frommer, K. Kahl, B. Leder, M. Rottmann, A. Strebel, Numer. Math. **132**(3), 463 (2015). doi:10.1007/s00211-015-0725-6
15. Y. Saad, Linear Algebra Appl. **34**, 269 (1980)
16. M. Eiermann, O.G. Ernst, SIAM J. Numer. Anal. **44**, 2481 (2005)
17. A. Frommer, S. Güttel, M. Schweitzer, SIAM J. Matrix Anal. Appl. **35**, 661 (2014)
18. J. Finkenrath, F. Knechtli, B. Leder, Nucl. Phys. B **877**(441), 2013 (2014). doi:10.1016/j.nuclphysb.2013.10.019. Corrigendum Nuclear Physics, Section B, pp. 574–575
19. J. Finkenrath, Ph.D. thesis (2015), http://elpub.bib.uni-wuppertal.de/edocs/dokumente/fbc/physik/diss2015/finkenrath
20. A. Hasenfratz, R. Hoffmann, S. Schaefer, Phys. Rev. D **78**, 014515 (2008). doi:10.1103/PhysRevD.78.014515
21. B. Leder, J. Finkenrath, F. Knechtli, PoS **LATTICE2013**, 035 (2014)
22. A. Hasenfratz, A. Alexandru, Phys. Rev. D **65**, 114506 (2002). doi:10.1103/PhysRevD.65.114506
23. M. Lüscher, Comput. Phys. Commun. **165**, 199 (2005). doi:10.1016/j.cpc.2004.10.004
24. M. Lüscher, F. Palombi, PoS **LATTICE2008**, 049 (2008)
25. L. Del Debbio, L. Giusti, M. Lüscher, R. Petronzio, N. Tantalo, JHEP **0602**, 011 (2006). doi:10.1088/1126-6708/2006/02/011
26. J. Finkenrath, F. Knechtli, B. Leder, Comput. Phys. Commun. **184**, 1522 (2013). doi:10.1016/j.cpc.2013.01.020
27. M. Hasenbusch, Phys. Lett. B **519**, 177 (2001). doi:10.1016/S0370-2693(01)01102-9
28. M. Hasenbusch, K. Jansen, Nucl. Phys. B **659**, 299 (2003). doi:10.1016/S0550-3213(03)00227-X
29. S. Duane, A. Kennedy, B. Pendleton, D. Roweth, Phys. Lett. B **195**, 216 (1987). doi:10.1016/0370-2693(87)91197-X
30. M. Lüscher, in *Modern perspectives in lattice QCD: quantum field theory and high performance computing. Proceedings, International School, 93rd Session, Les Houches, France, Aug 3–28, 2009* (2010), pp. 331–399, https://inspirehep.net/record/846344/files/arXiv:1002.4232.pdf
31. A. Borici, A. Frommer, B. Joo, A. Kennedy, B. Pendleton, Monte Carlo Simulations of Lattice QCD. (2005)
32. K. Jansen, C. Liu, Comput. Phys. Commun. **99**, 221 (1997). doi:10.1016/S0010-4655(96)00128-2
33. M. Della Morte et al., Comput. Phys. Commun. **156**, 62 (2003). doi:10.1016/S0010-4655(03)00436-3
34. C. Urbach, K. Jansen, A. Shindler, U. Wenger, Comput. Phys. Commun. **174**, 87 (2006). doi:10.1016/j.cpc.2005.08.006
35. M. Lüscher, S. Schaefer, Comput. Phys. Commun. **184**, 519 (2013). doi:10.1016/j.cpc.2012.10.003
36. J. Sexton, D. Weingarten, Nucl. Phys. B **380**, 665 (1992)
37. A.D. Kennedy, I. Horvath, S. Sint, Nucl. Phys. Proc. Suppl. **73**, 834 (1999). doi:10.1016/S0920-5632(99)85217-7
38. M.A. Clark, A.D. Kennedy, Nucl. Phys. Proc. Suppl. **129**, 850 (2004). doi:10.1016/S0920-5632(03)02732-4.[,850(2003)]
39. A.D. Kennedy, Nucl. Phys. Proc. Suppl. **128C**, 107 (2004). doi:10.1016/S0920-5632(03)02466-6.[,107(2004)]
40. A. Frommer, B. Nockel, S. Gusken, T. Lippert, K. Schilling, Int. J. Mod. Phys. C **6**, 627 (1995). doi:10.1142/S0129183195000538
41. M.A. Clark, P. de Forcrand, A.D. Kennedy, PoS **LAT2005**, 115 (2006)

42. T.A. DeGrand, S. Schaefer, Comput. Phys. Commun. **159**, 185 (2004). doi:10.1016/j.cpc.2004.02.006
43. L. Giusti, P. Hernandez, M. Laine, P. Weisz, H. Wittig, JHEP **04**, 013 (2004). doi:10.1088/1126-6708/2004/04/013
44. T. Blum, T. Izubuchi, E. Shintani, Phys. Rev. D **88**(9), 094503 (2013). doi:10.1103/PhysRevD.88.094503
45. E. Shintani, R. Arthur, T. Blum, T. Izubuchi, C. Jung, C. Lehner, Phys. Rev. D **91**(11), 114511 (2015). doi:10.1103/PhysRevD.91.114511
46. C. Thron, S. J. Dong, K. F. Liu, H. P. Ying, Pade - Z(2) estimator of determinants. Phys. Rev. D **57**, 1642–1653 (1998). doi:10.1103/PhysRevD.57.1642
47. S. Bernardson, P. McCarty, C. Thron, Comput. Phys. Commun. **78**, 256 (1993). doi:10.1016/0010-4655(94)90004-3
48. G.S. Bali, S. Collins, A. Schafer, Comput. Phys. Commun. **181**, 1570 (2010). doi:10.1016/j.cpc.2010.05.008
49. C. McNeile, C. Michael, Phys. Rev. D **73**, 074506 (2006). doi:10.1103/PhysRevD.73.074506
50. B. Blossier, M. Della Morte, N. Garron, G. von Hippel, T. Mendes, H. Simma, R. Sommer, JHEP **05**, 074 (2010). doi:10.1007/JHEP05(2010)074

# Chapter 4
# Calculating Observables of Quantum Fields

In this chapter, the task of computing hadron properties is outlined. We write path-integral representations of the relevant quantum-mechanical expectation value and then describe the best current method to compute this in a Monte Carlo calculation. Many of the mathematical tools and ideas introduced earlier will be important in writing efficient algorithms for these computations.

## 4.1 Symmetry Properties of Creation and Annihilation Operators

We have seen in Sect. 1.4.2 that determining the quantum mechanical expectation value of a two-point function gives information on the spectrum and some matrix elements of the theory. Three point functions are used to compute more involved matrix elements of operators inside particular quantum states, such as distributions of the quarks inside a nucleon, the response of a hadron to an external probe such as a photon or the transitions between two different hadrons when a quark changes flavour through the weak interaction.

To make contact with physics, the link between computations made on a lattice and the continuum must be established carefully. Eigenstates of the QCD Hamiltonian, $\hat{H}$ are simultaneously eigenstates of any operator that commutes with $\hat{H}$ and thus generates a *symmetry*. In particular, the symmetries of QCD identify states but the lattice with a finite grid spacing has a smaller set of symmetries with the full set usually being recovered only as the cut-off is removed formally. It is particularly important to understand properties of lattice states under symmetry transformations to carefully identify what physical hadron we have built in our lattice calculation.



F. Knechtli et al., *Lattice Quantum Chromodynamics*,
SpringerBriefs in Physics, DOI 10.1007/978-94-024-0999-4_4

### 4.1.1 Gauge-Invariant Observables

Section 1.4.4 shows the lattice representation of the path integral preserves a version of gauge symmetry. Natural hadron observables are invariant under these transformations and examples were seen when the action was introduced. More general functions of gauge and fermion fields can be introduced. When these are defined for a single time-slice of the lattice, they make candidate *creation operators* for the physical states of interest. Some simple examples of gauge-invariant observables are shown in Fig. 4.1. For gauge fields alone, the simplest observables are traces of path-ordered products along a closed circuit, usually called *Wilson loops*

$$W_{\mathscr{C}} = \mathrm{Tr} \prod_{\{\sigma,x\}\in\mathscr{C}} U_\sigma(x), \tag{4.1}$$

where a loop $\mathscr{C}$ is a list of links such that two adjacent entries end and start at a common site. The next example in the middle of the figure is the *fermion bilinear*, where $U_{\mathscr{P}}$, a string of gauge fields along a path $\mathscr{P}$ starting at $x$ and ending at $y$ is needed for gauge invariance when the fermion fields occupy different lattice sites;

$$O_{\mathscr{P}} = \bar{\psi}(x) U_{\mathscr{P}}(x, y) \psi(y) \quad \text{with} \quad U_{\mathscr{P}}(x, y) = \prod_{\{\sigma,z\}\in\mathscr{P}} U_\sigma(z). \tag{4.2}$$

Operators involving more fermion fields can be formed, one important example for gauge group $SU(3)$ is the baryon-like operator

$$B = \varepsilon_{ijk} \psi_i(x) \psi_j(x) \psi_k(x). \tag{4.3}$$

If the fields are at a common site, this epsilon-contraction can be seen to be gauge invariant; when the fermions are at different sites a gluon string is needed again, following a similar recipe to the bilinear and the right-hand panel of Fig. 4.1 gives an example. Another example, important for studies of quantum fields at finite temperature is the *Polyakov loop*, the trace of a path-ordered product of link variables that wraps around a compact lattice dimension.

### 4.1.2 Charge Conjugation, Isopin and Flavour Symmetry

The action and measure in the path integral are invariant under charge conjugation, which maps the independent fields $\psi$ and $\bar{\psi}$ into one-another. In the continuum Euclidean theory, these transformations are

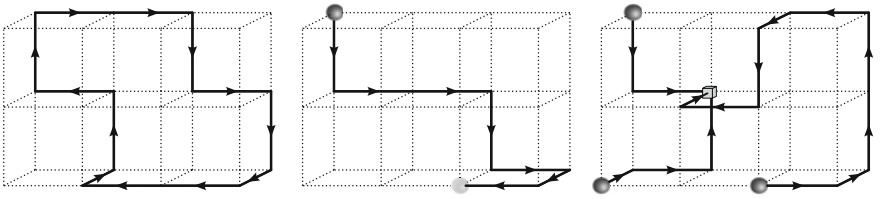

**Fig. 4.1** Examples of *gauge invariant* functions of gluon and quark fields. Quarks and anti-quarks are indicated as *dark* and *light* spheres, with lattice gluon link variables appearing as directed lines. The *cube* in the *right-hand panel* represents an antisymmetric contraction over the three colour indices, using the three-index Levi-Civita tensor

$$\begin{aligned}\psi(x) &\to \psi^c(x) = C\bar{\psi}^T(x)\\ \bar{\psi}(x) &\to \bar{\psi}^c(x) = -\psi^T(x)C^{-1}\\ A_\mu(x) &\to A^c_\mu(x) = -A^T_\mu(x)\end{aligned} \tag{4.4}$$

where making the action invariant requires $-\gamma^*_\mu = C^{-1}\gamma_\mu C$. For lattice gauge fields, the natural transformation leaving the Wilson gauge action invariant is to replace

$$U_\mu(x) \to U^c_\mu(x) = U^*_\mu(x). \tag{4.5}$$

Note the transformed fields are still in the gauge group and the Haar measure is invariant under this transformation. It is easy to see the real part of the trace of any closed loop is invariant under this transformation, while the imaginary part picks up a minus sign. On the lattice, charge conjugation for Wilson, domain wall and overlap fermions looks the same and also a natural link to staggered fermions can be made.

In Nature, the up- and down-quarks can be considered to be mass-degenerate to a good approximation. This introduces an $SU(2)$ symmetry familiar as *isospin*. Many lattice formulations preserve isospin (or other flavour symmetries) exactly and so analysis is straightforward and an irreducible representation on the lattice maps directly to its continuum counterpart. As an example, recall the difference between a pion and the $\eta'$ meson, which are both pseudoscalar mesons ($J^{PC} = 0^{-+}$) but have different transformation properties under isospin rotations. The three pions $\pi^{\pm}, \pi^0$ form the triplet of the vector representation of $SU(2)$ isospin while the $\eta'$ meson is an isoscalar. This has important consequences for measurement of the appropriate two-point function in a spectrum calculation and the Wick contraction gives more terms in the case of the $\eta'$ meson. This distinction will be reviewed again later in this chapter.

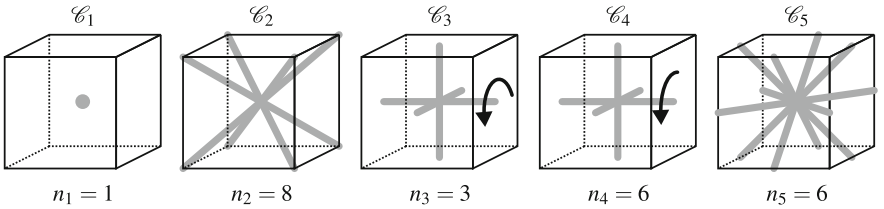


**Fig. 4.2** Conjugacy classes of $O$, the group of proper rotations of the cube with the number of elements in each class

### *4.1.3 Spin and Parity*

When a Hamiltonian is defined, a rest-frame is also implicitly chosen and the little group that leaves its time axis invariant defines a set of symmetries. For a state at rest, this group is $SO(3)$, the proper spatial rotations and its irreducible representations give the *spin* of the rest state, $J = 0, 1, 2, \ldots$. Spatial parity inversion is another discrete little group. For most lattice actions, parity remains a good symmetry and the link with the continuum is simple.

The lattice regulator breaks $SO(3)$ down to a discrete subgroup. For states at rest, this group is $O$ the 24 proper rotations of the cube. When parity is added, the group is $O_h$ which has 48 elements. As a consequence, quantum states in a lattice calculation are classified according to the irreducible representations (irreps) of $O_h$ and the link with the continuum spin needs to be established. The five conjugacy classes of $O$ are shown in Fig. 4.2 and so $O$ has five irreps, commonly labelled $A_1$, $A_2$, $E$, $T_1$ and $T_2$. To link lattice irreps to continuum spins, the *subduced* representations with given spin in $O$ are constructed, then decomposed into irreps. The irreducible content of the first few continuum spins is given in Table 4.1. As an example, consider the spin-two representation, which is a traceless, symmetric tensor $T_{ij}$, with five distinct components. These entries make up two distinct basis sets with elements which can not be mapped into each other through lattice rotations, $\omega_E = \{T_{11}, T_{22}\}$ and $\omega_{T_2} = \{T_{12}, T_{23}, T_{31}\}$ and so the subduced representation spin-two is reducible into $E \oplus T_2$. A spin-two state appears in a lattice calculation as two states in the $E$ and $T_2$

**Table 4.1** The subduced representations of $SO(3)$ of spin J in $O$ up to $J = 12$

| | Spin J | | | | | | | | | | | | |
|---|---|---|---|---|---|---|---|---|---|---|---|---|---|
| | 0 | 1 | 2 | 3 | 4 | 5 | 6 | 7 | 8 | 9 | 10 | 11 | 12 |
| $A_1$ | 1 | | | | 1 | | 1 | | 1 | 1 | 1 | | 2 |
| $A_2$ | | | | 1 | | | 1 | 1 | | 1 | 1 | 1 | 1 |
| $E$ | | | 1 | | 1 | 1 | 1 | 1 | 2 | 1 | 2 | 2 | 2 |
| $T_1$ | | 1 | | 1 | 1 | 2 | 1 | 2 | 2 | 3 | 2 | 3 | 3 |
| $T_2$ | | | 1 | 1 | 1 | 1 | 2 | 2 | 2 | 2 | 3 | 3 | 3 |

irreps, which are degenerate in the continuum limit and the absence of states at the same energy level in other irreps. Identifying this pattern cleanly from Monte Carlo data can be a challenge, in particular since a pattern of near-degenerate states of spin 0, 1 and 2 is almost indistinguishable from a single spin-4 state. Unfortunately, exactly this situation occurs in the spectrum of charmonium with the $\chi_{c0}$, $\chi_{c1}$ and $\chi_{c2}$ quark-model P-wave triplet all being resonances close in energy. More information from lattice calculations has been seen to provide useful extra input in making reliable spin identification [1].

Lattice operators must transform according to irreps of $O_h$ to create eigenstates of the hamiltonian with well-defined quantum numbers. The first step in a lattice calculation involving hadrons is to choose suitable irreducible operators. As an example, consider the smallest non-trivial gauge invariant gluon operator on the lattice, the plaquette. This is the trace of a path-ordered product of links around a $1 \times 1$ square on the lattice and is constructed purely from gluon fields. In the Yang-Mills theory, it creates a glueball state while in QCD with quarks, it would be a mesonic creation operator with isoscalar quantum numbers but the set of states it can couple to is much larger. Summing the real part of these traces over all the squares lying in each of the three spatial planes {[23], [31], [12]} of a three-dimensional time-slice gives three functions, $\phi_1(U)$, $\phi_2(U)$ and $\phi_3(U)$, with

$$\phi_1 = \sum_x \mathrm{ReTr}\left(U_2(x)U_3(x+\hat{2})U_2^\dagger(x+\hat{3})U_3^\dagger(x)\right). \tag{4.6}$$

The choice of orientation of the product around the loop is not significant since the real part of the trace is taken, which sums both clockwise and anti-clockwise combinations. Consider evaluating the three functions on two gauge fields, $U$ and $U'$ where $U'$ is constructed by applying $\sigma_z$, which rotates all links on the cubic lattice by $\frac{\pi}{2}$ about the z-axis. Consequently,

$$\begin{array}{l}\phi_1(U') = \phi_2(U) \\ \phi_2(U') = \phi_1(U) \\ \phi_3(U') = \phi_3(U)\end{array} \quad \text{or} \quad \begin{pmatrix}\phi_1' \\ \phi_2' \\ \phi_3'\end{pmatrix} = \underbrace{\begin{pmatrix}0&1&0\\1&0&0\\0&0&1\end{pmatrix}}_{R_\square(\sigma_z)} \begin{pmatrix}\phi_1 \\ \phi_2 \\ \phi_3\end{pmatrix}. \tag{4.7}$$

The action of rotating the gauge field about the z-axis has been encoded in matrix $R_\square(\sigma_z)$ and so the plaquette forms a $3 \times 3$ *matrix representation* of $\sigma_z \in O_h$. All elements of the group can clearly be represented this way. $R_\square$, the resulting representation of $O_h$ is reducible. The irreducible content of $R_\square$ can be computed using the orthogonality rule which shows

$$R_\square = A_1 \oplus E\,. \tag{4.8}$$

This computation will be reviewed later in this chapter.

### 4.1.4 Translation Invariance and Momentum

The Hamiltonian commutes with a displacement of the lattice fields by any spatial off-set when periodic boundary conditions are imposed on all variables in the path integral and the lattice has toroidal topology. This symmetry is linked with the conserved quantum number of momentum and in the absence of gauge fields the eigenstates of the shift operator are plane waves. For a cubic lattice the allowed values of each component of momentum are multiples of $\frac{2\pi}{L}$ and with a finite lattice spacing, there is an upper bound to the largest value this multiple can take. Note that for a moving quantum state, the classification of the spin and momentum becomes more complicated. This complication arises since the generators of shifts and rotations do not necessarily commute and so an eigenstate of the hamiltonian can not simultaneously be classified by both a momentum and a spin. This situation is familiar in the continuum as moving states are classified by their helicity. On the lattice, the classification is made more complicated as the little group of rotations that preserve a given momentum axis will depend on that axis. For example, the momentum axis $p = (0, 0, 1)$ is left unchanged by any of the symmetries of a square in the X-Y plane which is given by the little group $C_{4v}$ while the lattice axis $p = (1, 1, 0)$ has a smaller symmetry little group, given just by reflections in the $Z$ direction and in the plane normal to $(1, -1, 0)$.

### 4.1.5 Reducing Representations of Symmetries

A consequence of Schur's lemma is that summing the representation matrices over a conjugacy class yields a matrix that would be diagonal for an irreducible representation, but which is not necessarily diagonal if the representation can be reduced. This provides a practical method for reducing a general representation. For a reducible representation, when a non-trivial matrix is found on summing over a conjugacy class, then the corresponding similarity transformation that diagonalises this sum goes at least part way towards reducing the representation. This can be repeated until the representation has been fully decomposed into diagonal, irreducible blocks. Consider again the plaquette introduced in the previous section. Choosing $\mathscr{C}_2$, the conjugacy class of body-diagonal rotations, the resulting $3 \times 3$ matrix obtained from summing the plaquette representations over this class is

$$\Sigma = \begin{pmatrix} 0 & 1 & 1 \\ 1 & 0 & 1 \\ 1 & 1 & 0 \end{pmatrix}.$$

$\Sigma$ has eigenvalues $\lambda = \{2, -1, -1\}$. After taking account of the degenerate eigenvalues, a matrix can be found that diagonalises $\Sigma$ and for this example, completely reduces the representation into two sets,

$$\Phi^{(A_1)}(U) = \frac{1}{\sqrt{3}}\left(\phi_1(U) + \phi_2(U) + \phi_3(U)\right)$$
$$\Phi^{(E)}(U) = \begin{cases} \frac{1}{\sqrt{2}}\left(\phi_1(U) - \phi_2(U)\right) \\ \frac{1}{\sqrt{6}}\left(\phi_1(U) + \phi_2(U) - 2\phi_3(U)\right) \end{cases} \tag{4.9}$$

Notice there have to be two distinct operators for the two-dimensional $E$ irrep. The choice of operators for the $E$ irrep is only defined up to a similarity transformation.

## 4.2 Techniques for Hadron Spectroscopy

A central role for many lattice calculations is studying properties and excitations of hadrons. In this section we review the essentials, focussing on established techniques that have proved effective for studying the lowest few states in the spectrum. Hadrons are composite objects, built up from constituent quarks and gluons. The confined quark and gluon fields are emergent degrees of freedom, generated from the fields in the path integral through strongly-coupled interactions and so good creation operators must reflect this dynamical effect. To study a state we need operators with a strong overlap onto that state; this exposes the physics at earlier time-separations, reduces systematic uncertainties from unknown excited state contributions and offsets the signal-to-noise problem we have in our Monte Carlo computations.

The best known method to expose modes that describe quarks and gluons inside hadrons so effective creation operators can be made is *smearing*. Smearing filters out the short-distance fluctuations from the fields in the path-integral, leaving just confinement-scale modes. These are the essential degrees of freedom needed to construct hadrons. Once we define smeared fields, gauge-invariant functions made by following the symmetry rules described in the previous section give the best possible creation operators. Smearing gluon and quark fields is described in Sects. 4.3.1 and 4.4.1.

If our physics goals extend beyond the study of hadrons in their ground-states, a systematic means of investigating excitations is needed. A widely used technique is the *variational method*, described in the following section. The technique is also helpful for reducing contamination in ground-state correlation functions.

Most states in the spectrum of QCD are unstable against strong decays and are seen in experiments as resonant scattering of long-lived particles in beams or from a target. As described in earlier chapters, the basis for lattice computations is importance sampling Monte Carlo, which demands we study QCD in a Euclidean space-time. Direct contact with dynamical features like scattering is lost as stated in the Maiani-Testa No-go theorem. A framework to study scattering exists, known as the Lüscher method and it has become an active research area.

### 4.2.1 Variational Methods

Consider a two-point matrix correlation function in Euclidean space

$$C_{ij}(t) = \left\langle O_i(t) O_j^*(0) \right\rangle - \left\langle O_i(t) \right\rangle \left\langle O_j^*(0) \right\rangle , \quad i, j = 1, \ldots, N \tag{4.10}$$

of $N$ lattice time-slice fields $O_i(t)$. We assume that the fields $O_i$ have definite symmetry transformations, for example under parity, spin and charge conjugation. Under the assumption of the existence of a hermitian, positive transfer matrix, which is guaranteed for the standard Wilson gauge theory [2, 3], the matrix Eq. (4.10) has a spectral decomposition (cf. Eq. (1.54))

$$C_{ij}(t) = \sum_{n=1}^{\infty} \mathrm{e}^{-E_n t} \psi_{ni} \psi_{nj}^* , \quad \psi_{ni} = \langle 0 | \hat{O}_i | n \rangle . \tag{4.11}$$

The operators $\hat{O}_i$ corresponds in the Hamiltonian formulation to the fields $O_i$. The states $|n\rangle$ are the eigenstates of the Hamiltonian $\hat{H}$, defined as the logarithm of the transfer matrix with energy eigenvalues $E_n$:

$$\hat{H} |n\rangle = E_n |n\rangle , \quad E_n < E_{n+1} . \tag{4.12}$$

We assume that the energy eigenvalues are ordered and non-degenerate. The decomposition Eq. (4.11) is valid in the limit of an infinite Euclidean time extent $T$ of the lattice. The effects of a finite extent $T$ are discussed in [4]. The energy eigenvalues $E_n$ can be extracted from the *generalized eigenvalue problem* (GEVP) defined by

$$C(t) v_n(t, t_0) = \lambda_n(t, t_0) C(t_0) v_n(t, t_0) , \tag{4.13}$$

where the correlation matrix at times $t$ and $t_0$ appears on the left and right hand side respectively. After determining the generalized eigenvalues $\lambda_n(t, t_0)$ define the effective energies

$$E_n^{\mathrm{eff}}(t, t_0) = -\frac{1}{a} \ln \left\{ \frac{\lambda_n(t + a, t_0)}{\lambda_n(t, t_0)} \right\} . \tag{4.14}$$

It can be shown that the energy levels $E_n, n = 1, \ldots, N$ can be computed as [5]

$$E_n = \lim_{t \to \infty} E_n^{\mathrm{eff}}(t, t_0) . \tag{4.15}$$

We denote the corrections by $\varepsilon_n(t, t_0) = E_n^{\mathrm{eff}}(t, t_0) - E_n$. At fixed $t_0$ and for large $t$ the corrections are given by [5]

$$\varepsilon_n(t, t_0) = \mathrm{O}\left(\mathrm{e}^{-\Delta E_n t}\right) , \quad \Delta E_n = \min_{m \neq n} |E_m - E_n| . \tag{4.16}$$

If the distance $\Delta E_n$ to the next energy level is small, the corrections are large and in order to suppress them one has to go to larger values of $t$. This usually turns out to be impractical because the noise-to-signal ratio increases with $t$. An example where the situation just described occurs is string breaking, see Sect. 4.4.4. A faster convergence in Eq. (4.15) can be achieved if the condition

$$t_0 \geq \frac{t}{2} \tag{4.17}$$

is satisfied. This can be realized for example by keeping the difference $t - t_0$ constant or the ratio $t/t_0$ equal to a constant smaller than 2 while taking $t_0$ large. Then it can be shown that [6]

$$\varepsilon_n(t, t_0) = \mathrm{O}\left(\mathrm{e}^{-\Delta E_{N+1,n} t}\right) , \quad \Delta E_{N+1,n} = E_{N+1} - E_n . \tag{4.18}$$

The corrections are exponentially suppressed with the difference of the energy level one wants to extract and the energy $E_{N+1}$. Thus smaller values of $t$ are required than in the situation in Eq. (4.16). The proof of Eq. (4.18) proceeds by splitting

$$C_{ij}(t) = \sum_{n=1}^{N} \mathrm{e}^{-E_n t} \psi_{ni} \psi_{nj}^* + \sum_{n=N+1}^{\infty} \mathrm{e}^{-E_n t} \psi_{ni} \psi_{nj}^* = C_{ij}^{(0)}(t) + C_{ij}^{(1)}(t) . \tag{4.19}$$

The contribution from the states $n > N$ is suppressed at large $t$ and can be treated as a perturbation. The analysis in [6] shows that, in order to suppress the perturbative contributions to $\varepsilon_n(t, t_0)$ beyond the first order, the condition Eq. (4.17) has to be fulfilled. Then the first order contribution to $\varepsilon_n(t, t_0)$ dominates and yields Eq. (4.18). Note that in [6] interpolating fields which approximate the exact eigenvectors $|n\rangle$ of the Hamiltonian with small corrections are constructed. At fixed $t - t_0$ the size of the corrections is $\mathrm{O}\left(\mathrm{e}^{-\Delta E_{N+1,n} t_0}\right)$.

### 4.2.2 Scale Setting

The Wilson lattice action for QCD with $N_\mathrm{f}$ flavors of quarks is given by (cf. Eqs. (1.70) and (1.79))

$$S_\mathrm{QCD} = \frac{\beta}{3} \sum_x \sum_{\mu<\nu} \mathrm{Re\,Tr}\,[1 - P_{\mu,\nu}(x)] + \sum_f a^4 \sum_x \bar{\psi}_f(x)(D_\mathrm{w} + m_{0f})\psi_f(x) . \tag{4.20}$$

The lattice parameters are the gauge coupling $g_0$, which is related to $\beta$ in Eq. (1.112) by $g_0^2 = 6/\beta$, and the quark masses $m_{0f}$, $f = 1, \ldots, N_\mathrm{f}$. The lattice spacing $a$ is not an input parameter. When Eq. (4.20) is simulated on the computer we input dimensionless numbers for $g_0$ and the masses $am_{0f}$ in lattice units. When

there are no non-zero quark masses, there is only one parameter $g_0$ in Eq. (4.20). The renormalization group equation Eq. (1.118) establishes a relation $a(g_0)$ which determines the lattice spacing as a function of the only parameter $g_0$. In order to determine the lattice spacing in physical units, we need to match a physical observable computed on the lattice, such as a glueball mass $am_{\mathrm{g}}$, to its experimental value $m_{\mathrm{g,phys}}$

$$a = \frac{am_{\mathrm{g}}}{m_{\mathrm{g,phys}}} \,. \tag{4.21}$$

This is called *scale setting*. Alternatively one says that the glueball mass is used to set the scale. The value of the lattice spacing depends on the choice of the scale. Any dimensionless ratio

$$R_i = \frac{am_i}{am_{\mathrm{g}}} = \frac{m_{i,\mathrm{phys}}}{m_{\mathrm{g,phys}}} + \mathrm{O}(a^2) \tag{4.22}$$

of a hadron mass $m_i$ to the scale $m_{\mathrm{g}}$ is a prediction of Eq. (4.20). The second equality in Eq. (4.22) follows from Eq. (1.120). It implies that the continuum limit $a \to 0$ of $R_i$ exists and is equal to the value of the ratio of the physical masses.

For non-zero quark masses, there are additional parameters in Eq. (4.20). Interestingly, if we consider the chiral limit in which the quarks are massless, we return to a situation with only one parameter $g_0$ similar to the previous paragraph. In this limit the pions are massless but the proton and rho masses for example are non-zero. Following Eq. (4.22), the ratio of the rho mass to the proton mass is a prediction of the theory with massless quarks.

If the quarks are not massless, we need to fix the mass parameters by matching to experimentally determined quantities. We need one such quantity for each quark mass parameter. Consider for example a theory with only two mass parameters, one for degenerate up and down quark masses and one for the strange quark mass. A natural choice is to take the proton mass $am_{\mathrm{p}}$ to set the scale and use the ratios $m_\pi/m_{\mathrm{p}}$ and $m_{\mathrm{K}}/m_{\mathrm{p}}$ to fix the mass parameters in the action. This is done by requiring that the ratios computed on the lattice, $am_\pi/(am_{\mathrm{p}})$ and $am_{\mathrm{K}}/(am_{\mathrm{p}})$ take their experimentally determined values. Repeating this procedure for several values of the lattice spacing produces points in parameter space along a *line of constant physics*. On this line one can take the continuum limit of other ratios $\lim_{a\to 0} am_i/(am_{\mathrm{p}})$, where $m_i$ is for example the $\Omega$ mass. A recent review of scale setting in lattice QCD is [7]. The choice of the scale used to set the lattice spacing in Eq. (4.21) is arbitrary but it is advantageous to choose a scale which can be accurately measured.

### 4.2.3 The Wilson Flow

We turn now to a discussion of a recent method which can be used to define a scale with high precision, based on the so called Yang–Mills flow. In the continuum the Yang–Mills flow is defined by the equation

$$\frac{\mathrm{d}}{\mathrm{d}t} B_\mu(x,t) = D_\nu G_{\mu,\nu}(x,t) = -\frac{\partial S_{\mathrm{YM}}(B)}{\partial B_\mu(x,t)}\,, \qquad B_\mu(x,t)\big|_{t=0} = A_\mu(x)\,. \quad (4.23)$$

Here $A_\mu(x)$ is the fundamental gauge potential in QCD. $B_\mu(x,t)$ is a Lie Algebra valued field, $D_\mu$ is the covariant derivative defined as in Eq. (1.5) in terms of $B_\mu$, $G_{\mu,\nu} = [D_\mu, D_\nu]$ is the field strength tensor and $S_{\mathrm{YM}}(B)$ is the associated Yang–Mills action defined as in Eq. (1.6). The derivative in Eq. (4.23) is with respect to a new coordinate called the flow time $t$. As can be seen from Eq. (4.23) the flow time has mass dimension equal to $-2$ (since the gauge potential and $D_\mu$ have mass dimension equal to one). The solution of Eq. (4.23) can be expanded in perturbation theory by first scaling the gauge potential by the bare gauge coupling $A_\mu \longrightarrow g_0 A_\mu$ and expanding the field $B_\mu$ in an asymptotic series $B_\mu = \sum_{k=1}^{\infty} g_0^k B_{\mu,k}$. The cofficients $B_{\mu,k}$ obey the constraint $B_{\mu,k}\big|_{t=0} = \delta_{k1} A_\mu$, cf. Eq. (4.23). The equation for the leading-order coefficient $B_{\mu,1}$ is a heat equation with solution

$$B_{\mu,1}(x,t) = \int \mathrm{d}^4 y\, (4\pi t)^{-2} \exp\left\{-(x-y)^2/(4t)\right\} A_\mu(y)\,, \quad (4.24)$$

which shows [8] that the Yang–Mills flow averages the gauge potential over a spherical region of radius $r = \sqrt{8t}$. A consequence is that for $t > 0$, correlation functions built from flow fields are finite at any Euclidean distance [9]. No renormalization beyond that of the gauge coupling and the quark masses is required.

One lattice version of Eq. (4.23), the so called "Wilson flow" [10–12] is defined by the equation

$$\frac{\mathrm{d}}{\mathrm{d}t} V_\mu(x,t) = Z_\mu(x,t) V_\mu(x,t)\,, \qquad V_\mu(x,t)\big|_{t=0} = U_\mu(x)\,. \quad (4.25)$$

Here $U_\mu(x)$ is the fundamental gauge field on the lattice and $V_\mu(x,t)$ is the associated flow. The Lie algebra valued field $Z_\mu(x,t)$ is constructed from the Wilson gauge action $S_{\mathrm{w}}(V)$ in terms of the lattice field $V_\mu(x,t)$ as in Eq. (2.57). The solution to Eq. (4.25) is uniquely defined. The Wilson action $S_{\mathrm{w}}(V)$ in terms of the field $V$ is a monotonically decreasing function of $t$.

The Wilson flow on the lattice Eq. (4.25) smooths the gauge configuration similarly to the gauge link smearing techniques which we will discuss in Sect. 4.3.1. In fact it is equivalent to an infinitesimal stout link smearing. This equivalence is seen by considering the numerical solution of Eq. (4.25) given by the Euler method with a step-size $\varepsilon$ in flow time,

$$V_\mu(x, t+\varepsilon) = \exp\left\{\varepsilon Z_\mu(x,t)\right\} V_\mu(x)\,, \quad (4.26)$$

which is identical to Eq. (4.43).

The Wilson flow can be used to define a physical scale in confining gauge theories. Consider the energy density

$$E(x,t) = \frac{1}{4}\hat{G}^a_{\mu\nu}(x,t)\hat{G}^a_{\mu\nu}(x,t) \tag{4.27}$$

in terms of the Lie algebra components of the lattice field strength tensor $\hat{G}_{\mu\nu}$. The latter is built from the flow field $V$ as in Eq. (1.148). We introduce the dimensionless quantity

$$\mathscr{E}(t) = t^2 \langle E(x,t) \rangle \ . \tag{4.28}$$

The scale $t_0$ is defined through [8]

$$\mathscr{E}(t)|_{t=t_0} = 0.3 \tag{4.29}$$

and the scale $w_0$ through [13]

$$t\mathscr{E}'(t)\big|_{t=w_0^2} = 0.3\,, \tag{4.30}$$

where $\mathscr{E}'(t) = \frac{\mathrm{d}}{\mathrm{d}t}\mathscr{E}(t)$. In lattice simulations one determines numerical values $t_0/a^2$ and $w_0/a$ of the scales in lattice units by solving Eqs. (4.29) and (4.30). These values can be used to fix the lattice spacing. If the scales are known in physical units the lattice spacing can be directly determined, for example as $a = \sqrt{t_{0,\mathrm{phys}}/(t_0/a^2)}$. Alternatively a relative scale setting uses the ratio of a scale computed at two different lattice spacings $a_1$ and $a_2$ to determine the ratio of lattice spacings

$$\frac{a_1}{a_2} = \sqrt{\frac{t_0/a_2^2}{t_0/a_1^2}}\,. \tag{4.31}$$

Scale setting using the flow observables is discussed in [7]. Recent applications of the Yang–Mills flow on the lattice are covered in [14].

The Euler integrator Eq. (4.26) is the simplest. Unlike the integration of the molecular dynamics equations of motion in the context of the Hybrid Monte Carlo algorithm discussed in Sect. 2.4, the integration of Eq. (4.25) does not require simplecticity. In [8] a Runge-Kutta integrator of third order is used. Based on it, an adaptive step-size Runge-Kutta integrator of second order has been constructed in [15].

### *4.2.4 Scattering and the Lüscher Method*

Most hadrons are observed experimentally as resonances; peaks in scattering cross-sections of stable particles or hadrons. There has been significant recent progress in studying the scattering properties of mesons and baryons on the lattice. This is a challenging task, since lattice Monte Carlo studies make use of importance sampling, which requires calculations to be performed on a Euclidean space-time, where dynamical real-time dependence is lost. A formalism [16] to infer scattering

data from the spectrum of QCD in a finite cube was developed almost 30 years ago but only recently have combined advances in both measurement techniques and computing power enabled this formalism to be exploited.

A simple model illustrates how the spectrum of an interacting system in a finite volume can be related to the scattering phase shift. Consider two particles moving in one dimension where after separation, their relative wavefunction $\psi(x)$ with $x$ the distance between the two particles obeys the Schrödinger equation

$$-\frac{d^2\psi}{dx^2} + V(x)\psi(x) = E\psi(x). \tag{4.32}$$

For our model, let us introduce a simple finite-range potential

$$V(x) = V_0\,\delta(|x| - a). \tag{4.33}$$

Solutions to Eq. 4.32 for this potential can be found straightforwardly using an exchange-symmetric ansatz

$$\psi(x) = \begin{cases} A\cos(kx - \delta(k)) & x \leq -a \\ B\cos(kx) & -a < x < a \\ A\cos(kx + \delta(k)) & a \leq x \end{cases} \tag{4.34}$$

where $E = k^2$ and the expression introduces $\delta(k)$, the *scattering phase shift*. If the two particles move in a finite box of length $L > 2a$ with periodic boundary conditions so $\psi(x + L) = \psi(x)$, then only a discrete set of values of $k$ are allowed which maintain periodicity so the system has a spectrum of distinct energy levels. The quantisation condition in one dimension is

$$\frac{kL}{2} + \delta(k) = n\pi \text{ with } n \in \mathbb{Z}. \tag{4.35}$$

Since $\delta(k)$ is determined by the interaction near $|x| = 0$, this quantisation condition links the phase shift to the finite volume directly. With the potential of our toy model, Eq. (4.33), an implicit expression constraining allowed values for $k$ can be found

$$k\sin\frac{kL}{2} - V_0\cos ka\ \cos k(\frac{L}{2} - a) = 0 \tag{4.36}$$

and this can be solved numerically. The limiting cases are instructive; when $V_0 = 0$, the spectrum is given by the non-interacting quantisation condition, $kL = 2\pi n$. In the case $V_0 \to \infty$, the spectrum is found by solving $\cos ka = 0$ or $\cos k(L/2 - a) = 0$, which give the two disjoint spectra associated with disconnected one-dimensional boxes of length $a$ and $L/2 - a$ where the wavefunction vanishes on the ends of the boxes. Avoided level crossings can be seen for finite $V_0$. The right-hand panel of Fig. 4.3 shows the dependence of the discrete spectrum on box size, $L$. For illustration,

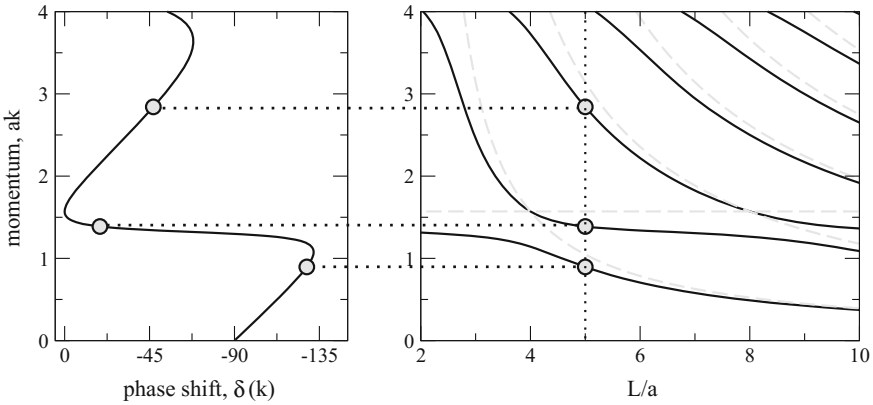


**Fig. 4.3** Relating the quantised spectrum of a one-dimensional toy model to the scattering phase shift. The *right panel* shows the spectrum as a function of box size, with three energy levels shown for $L = 5a$ and $aV_0 = 5$. The corresponding phase shift values are displayed on the *right-hand side* on the phase shift curve

the lowest three energy levels at $L = 5a$ have been used to determine the allowed values of $k_n$ for $n = 0, 1, 2$ and the quantisation condition in Eq. (4.35) directly yields $\delta(k)$ at these values and this is then shown on the phase-shift curve (turned sideways to illustrate the connection) in the right-hand panel.

In a 3+1 dimensional theory, scattering occurs in partial waves as the two interacting hadrons can have relative orbital angular momentum. There is a distinct phase-shift $\delta_l$ for each partial wave. For a scattering state with total momentum $P = 0$, resembling two mesons with mass $m$, the spectrum of energy levels $E_j, j = 0, 1, 2, \ldots$ with the quantum numbers of the channel is found and each energy level is compared its partner in the non-interacting case, computed straightforwardly from a relativistic dispersion relation. In a quantum field theory, inelastic scattering can occur too and the Lüscher formalism is not applicable above this energy scale. The result relating the phase shift in a single elastic scattering partial wave to the spectrum of states in a box of side-length $L$ is given by

$$\cot \delta_l(k) = \mathscr{S}_l(k, L), \tag{4.37}$$

with $\mathscr{S}$ a known function of the partial wave, box size and energy shift. Solving this equation is analogous to solving Eq. (4.36) in our toy model.

An extension to moving frames is presented in Ref. [17] where in a relativistic theory more data on the phase shift curve can be obtained as boosting the system Lorentz contracts the box, giving a different effective value of the size $L$. More recently, the formalism has been applied to coupled channel elastic scattering [18, 19] and extended to three-body interactions [20]. Attempts to model inelastic scattering are an important area, since in real experimental data, almost all interesting resonances are above these thresholds.

## 4.3 Gluons, Wilson Loops and Glueballs

In this section, we consider calculations predominantly concerned with probing the gluon fields. To begin, consider how we can expose the important physical gluon modes through smearing.

### *4.3.1 Gauge Smearing*

For gauge fields, smearing builds a new parallel transporter on each lattice link using neighbouring gluon fields which has the same behavior under gauge transformations as the original link. This technique is used both to build a large basis of operators to improve the extraction of energies (see Sect. 4.2.1) or to construct actions which reduce cut-off effects. Empirically, it seems to be important to build smeared links that are also elements of the gauge group, although this is not a requirement of gauge symmetry.

The simplest form of smearing is the so called APE smearing [21]. The smearing operator $\mathscr{S}$ adds the sum of staples $\Sigma_\mu(x)$ Eq. (2.10) to the original link

$$\mathscr{S}\, U_\mu(x) = \mathscr{P}\left\{(1-\alpha)U_\mu(x) + \frac{\alpha}{6}\Sigma_\mu(x)\right\}, \tag{4.38}$$

with a weight parameter $\alpha$. Here $\mathscr{P}$ denotes the projection on the gauge group. In the case of $SU(3)$ the projection of a smeared link given by a $3 \times 3$ complex matrix $W$ can be approximated by the function [22], defined by replacing

$$W \longrightarrow W/\sqrt{\mathrm{tr}\,(WW^\dagger)/3} \tag{4.39}$$

and applying four iterations of the substitution

$$W \longrightarrow X\left(1 - \frac{i}{3}\mathrm{Im}\,(\det X)\right), \quad \text{with} \quad X = W\left(\frac{3}{2} - \frac{1}{2}W^\dagger W\right). \tag{4.40}$$

Smearing can be iterated $m$ times, resulting in the smeared links $U^{(m)}$ given by

$$U_\mu^{(m)}(x) = \mathscr{S}^m\, U_\mu(x)\,. \tag{4.41}$$

The analysis of smearing in the context of perturbation theory shows that the smearing smooths the gauge field by suppressing high momentum components provided that $0 \leq \alpha \leq 0.75$ [23].

The smeared links of the hypercubic blocking (HYP) [24] are constructed in three steps of a modified APE smearing. In the HYP construction, the smeared link is defined only using links inside the hypercubes attached to the link to be smeared. This can be seen schematically in Fig. 4.4, which shows the two steps required to

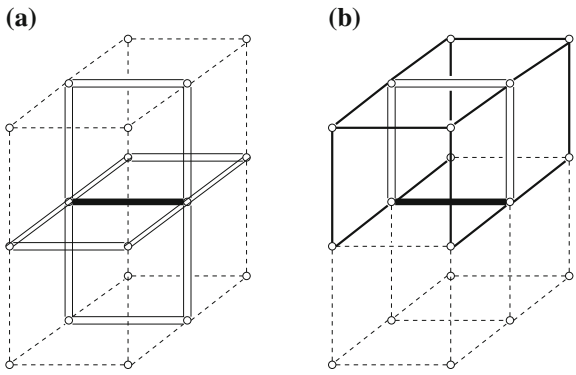


**Fig. 4.4** The hypercubic (HYP) smeared link in three dimensions. Figure taken from [24]

construct the HYP link in three dimensions. The fat HYP link is made from the staples with the doubled-lined links (left figure), which in turn are made from staples of the original links restricted to be inside the hypercubes (right figure). The choice of the HYP parameters depends on the application. The original choice in Ref. [24] minimises the fluctuations of the smallest plaquette and the flavour symmetry violations with staggered fermions. The choice in Ref. [22] minimises the one-loop coefficient $e^{(1)}$ of the static self-energy, see Eq. (4.50) and therefore it approximately maximises the signal-to-noise ratio of correlators with static quarks. The perturbative relation between HYP and original links in momentum space can be found in Ref. [25] and in time-momentum representation in Ref. [26].

Another gauge-field smearing recipe, called the "stout link" [27] is used in current calculations. An important feature is the derivative of a function of stout links with respect to the underlying, unsmeared fields can always be constructed even after applying many levels of stout smearing. This is a useful feature when smearing is to be used in the action appearing in the importance sampling measure and when sampling is carried out using molecular dynamics schemes such as Hybrid Monte Carlo. Stout smearing builds a filter from local staples to remove short-distance structure in a very similar way to the APE and HYP techniques described above except now the link sum is made an element of the Lie algebra of the group. The exponential map from the Lie algebra to the group is then used to construct a new group-valued, smeared link. For $SU(N)$, the Lie-valued variable $Q_\mu(x)$ is constructed starting from the staple sum $\Sigma_\mu(x)$

$$\begin{aligned} \Omega_\mu(x) &= \Sigma_\mu U_\mu^\dagger(x) \quad \text{(no sum over } \mu\text{)}, \\ Q_\mu(x) &= \frac{1}{2}\left(\Omega_\mu(x) - \Omega_\mu^\dagger(x)\right) - \frac{1}{2N}\mathrm{Tr}\left(\Omega_\mu(x) - \Omega_\mu^\dagger(x)\right) . \end{aligned} \tag{4.42}$$

A new $SU(N)$ group-valued smeared link is found, using the exponential mapping,

$$\tilde{U}_\mu(x) = \exp\left\{Q_\mu(x)\right\}\ U_\mu(x). \tag{4.43}$$

The gauge covariance and other symmetry properties of this new link can be shown to be the same as the underlying gauge field. Exponentiation can be evaluated exactly for small matrices by exploiting the Cayley-Hamilton theorem which states every matrix is a zero of its characteristic polynomial. This implies the exponential of a $3 \times 3$ matrix $Q$ can always be written exactly as a short polynomial in $Q$;

$$e^{Q} = f_0 I + f_1 Q + f_2 Q^2$$

where the three scalar functions $f_0$, $f_1$ and $f_2$ depend in turn only on Tr $Q^2$ and Tr $Q^3$. Remember Tr $Q = 0$ when $Q$ is in the Lie algebra of $SU(N)$. Because the exponential map is used to form the stout link, a small change in the gauge fields leads to a small change in the stout links so derivatives are well-behaved. This is a very useful feature for molecular dynamics, where the force term on a link can be computed for an action built from stout links after iteratively applying the procedure $k$ times.

$$U = U^{(0)} \to U^{(1)} \to U^{(2)} \to \cdots \to U^{(k)} \tag{4.44}$$

To compute this force, the first step is to find the change in the action, $S$ with respect to changes in the $k$-th level stout links,

$$\Sigma_{\mu}^{(k)}(x) = \left( \frac{\partial S[U^{(k)}]}{\partial U_{\mu}^{(k)}(x)} \right)^{T} . \tag{4.45}$$

This calculation is the same as would be carried out in analysing molecular dynamics for an action on unsmeared gauge links. The extra step needed when the action contains stout links is a recursion, which works in the opposite direction from Eq. (4.44). At each reverse step, the new force at level $j - 1$ is determined from $\Sigma^{(j)}$ and $U^{(j)}$.

$$\Sigma^{(k)} \to \Sigma^{(k-1)} \to \Sigma^{(k-2)} \to \cdots \to \Sigma^{(0)} \tag{4.46}$$

In this recursion, the form of the action is no longer needed and these steps depend only on the structure of the staple sum used to form each new level of the stout link. The details of can be found in Ref. [27]. The advantages of the HYP staple sum construction can be combined with the exponential mapping in a natural way [28].

### *4.3.2 Glueballs*

Glueballs are integer-spin unflavoured bosons made up predominantly from gluons. In QCD, it is difficult to give a precise definition of a glueball since they will in general mix with states made up of quarks to form the eigenstates of the hamiltonian. In the Yang-Mills theory where the picture is simpler they are the only hadrons in the

spectrum of strongly-interacting gluons. There is a long history of investigating their spectrum in lattice Monte Carlo calculations [29–31].

As with most spectroscopy calculations, the two-point correlation function is used to study glueballs and operators with good overlap onto these states are needed. The Wilson loop is a gauge-invariant function of the gluon fields in the path integral, so makes a good candidate creation operator. Smearing is an essential next step. Section 4.1.3 discusses how to make operators that transform irreducibly under the lattice rotation symmetries, which are needed to probe eigenstates of the spectrum. One property of glueball calculations is the higher statistical noise in the Monte Carlo calculations. The problem is amplified by the large mass of glueballs compared to a standard gluonic reference scale such as the string tension. This means their correlation function falls rapidly for values of the lattice spacing accessible in a typical calculation.

### 4.3.3 The Static Potential and Strong Coupling Constant

The static potential and its excited states are the energies of QCD in presence of a static infinitely massive quark and anti-quark pair. We follow the derivation of the observable for the static potential given in [32]. The potential can be extracted from the path integral expectation value of

$$\langle W(r,t)\rangle = -\frac{1}{2}\Big\langle \overline{\psi}_h(0,\mathbf{0})\,P(0,\mathbf{0};0,r\hat{k})\gamma_5\psi_{\bar{h}}(0,r\hat{k}) \\ \overline{\psi}_{\bar{h}}(t,r\hat{k})\,P^\dagger(t,\mathbf{0};t,r\hat{k})\gamma_5\psi_h(t,\mathbf{0})\Big\rangle_{\psi_h,\,\psi_{\bar{h}},\,\psi_l,\,\ldots}, \tag{4.47}$$

where $\psi_h$, $\overline{\psi}_h$ and $\psi_{\bar{h}}$, $\overline{\psi}_{\bar{h}}$ are the static quark and anti-quark fermion fields respectively and $P(x_0,\mathbf{0};x_0,r\hat{k})$ represents the gauge parallel transporter made from a product of space-like links at time $x_0$. Our conventions for the static quarks are the same as in [33]. After integration over the static fields whose propagator generates the time-like links in the observable, cf. Eq. (2.4) in [22] one recovers the *Wilson loop*

$$\langle W(r,t)\rangle = \Big\langle \mathrm{tr}\,\Big\{P(0,\mathbf{0};0,r\hat{k})\,P(0,r\hat{k};t,r\hat{k})\,P^\dagger(t,\mathbf{0};t,r\hat{k})\,P^\dagger(0,\mathbf{0};t,\mathbf{0})\Big\}\Big\rangle_{\psi_l,\,\ldots}, \tag{4.48}$$

where the path integral expectation value is an integral over the relativistic fermion fields $\psi_l$, $\overline{\psi}_l$ and gauge fields. The Wilson loop in Eq. (4.48) is a rectangular path on the lattice of extension $r/a \times t/a$. Using the transfer matrix formalism, cf. Sect. 1.4.2, it can be shown that the Wilson loop has a spectral decomposition given by [32]

$$\langle W(r,t)\rangle \overset{T\to\infty}{\sim} \sum_n c_n c_n^* \mathrm{e}^{-V_n(r)t}, \tag{4.49}$$

where $T$ is the temporal extent of the lattice. $V_n$ are the static energies measured relative to the vacuum energy. For example $V_0(r) \equiv V(r)$ is the static potential and $V_1(r)$ its first excitation.

Wilson loops suffer from the so called signal-to-noise ratio problem. The expectation value of the trace in Eq. (4.48) is an average of positive and negative numbers which yield a signal which decays exponentially with $t$, cf. Eq. (4.49). Instead, the statistical error is the expectation value of the *variance* $\left\langle W(r,t)^2 \right\rangle - \langle W(r,t) \rangle^2$. The first term in the variance is always positive with a contribution almost independent of $t$ and so the signal-to-noise ratio decays exponentially with $t$. A cure can be found for the pure gauge theory. An exponential reduction of the error with $t$ can be achieved by a technique called one-link integral [34]. It replaces the temporal links in the Wilson loop by their expectation value in the configuration of the other links fixed. The expectation value of the Wilson loop remains unchanged provided that no pair of replaced links belongs to the same plaquette but its variance is reduced exponentially with $t$ [35]. A further improvement is achieved by a multilevel technique which reduces the statistical error exponentially with an exponent approximately proportional to the area of the Wilson loop [36].

The static potential $V(r)$ computed from simulations of the pure $SU(3)$ gauge theory is shown in Fig. 4.5. Data are from Ref. [37]. The quantity plotted is the dimensionless difference $[V(r) - V(r_c)] \cdot r_0$, where $r_c$ and $r_0$ are reference scales defined from the static force, as we discuss below. The static potential contains a contribution $2E_{\text{self}}$ which diverges with the inverse lattice spacing

$$V(r) \sim 2E_{\text{self}} + O(a^0) \sim \frac{1}{a} e^{(1)} g_0^2 + \cdots \tag{4.50}$$

It originates from the combined self-energy of the static quark and anti-quark and depends on the choice of static-quark action in Eq. (4.47). In Ref. [38] a static action

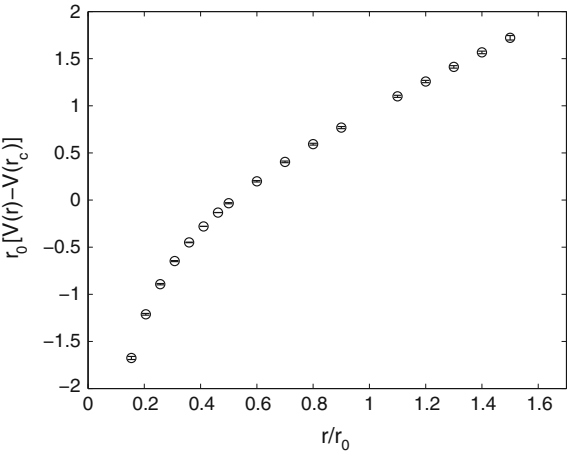


**Fig. 4.5** The static potential $V(r)$ in the continuum limit of the $SU(3)$ pure gauge theory. Data taken from [37]

which uses HYP links [24] in the time covariant derivative was introduced. The use of HYP links reduces the one-loop coefficient $e^{(1)}$ in Eq. (4.50) [22, 25, 26] resulting in an exponential improvement of the signal-to-noise ratio of Wilson loops. In a *difference* of potentials the divergent contribution in Eq. (4.50) is removed.

At small distances $r$ the static potential $V(r)$ can be computed in perturbation theory [39]. At tree level the potential is given by the exchange of one gluon between the static quarks

$$V(r) \overset{r\to 0}{\sim} -C_{\mathrm{F}} \frac{g_0^2}{4\pi r}\,, \tag{4.51}$$

which yields a Coulomb potential. At asymptotically large distances $r \to \infty$ the static potential in the pure $SU(3)$ gauge theory can be described by the form [40, 41]

$$V(r) = \sigma r + \mu + \frac{\gamma}{r} + O(1/r^2)\,, \tag{4.52}$$

which is derived from an effective bosonic string theory [42]. In Eq. (4.52), the coefficient $\sigma$ of the linear term is called the string tension and $\mu$ is a mass parameter. The coefficient $\gamma = -\pi(d-2)/24$ is universal and depends only on $d$, the dimension of space-time. The physical picture behind Eq. (4.52) is that of a flux tube or string fluctuating in $(d-2)$ transverse dimensions. The asymptotic form Eq. (4.52) has been confirmed by very precise Monte Carlo data in [43]. The string broadens as the separation $r$ grows. Its width increases logarithmically with $r$ [44]. This broadening was observed in Monte Carlo simulations [45]. In the presence of dynamical fermions, string breaking occurs, see Sect. 4.4.4.

A physical quantity derived from the static potential is the static force $F(r) = V'(r)$. Taking the derivative of $V$ removes the self-energy contribution. On the lattice, an improved definition of the force [37, 46, 47] is given by

$$F(r_{\mathrm{I}}) = [V(r) - V(r-a)]/a\,. \tag{4.53}$$

The distance $r_{\mathrm{I}}$ is defined by requiring the force evaluated at tree level in perturbation theory obeys

$$F_{\mathrm{tree}}(r_{\mathrm{I}}) = C_{\mathrm{F}} \frac{g_0^2}{4\pi r_{\mathrm{I}}^2}\,. \tag{4.54}$$

It is $r_{\mathrm{I}} = r - a/2 + \mathrm{O}(a^2)$ and reduces the cut-off effects of the force [37] considerably. $r_{\mathrm{I}}$ depends on the static quark action but not on $N_{\mathrm{f}}$, see [32, 37, 46]. From the force a scale $r(c)$ can be defined through [46]

$$r^2 F(r)|_{r=r(c)} = c\,. \tag{4.55}$$

Choosing $c = 1.65$ leads to the scale $r_0 = r(1.65)$ which has a value of about 0.49 fm in QCD [46]. Other choices are $r_1 = r(1.0)$ [48] and $r_c = r(0.65)$ [37],

the latter is used in Fig. 4.5. Computations of the static potential $V(r)$ with $N_\mathrm{f} = 2$ dynamical fermions at distances smaller than the string breaking distance are shown for example in [49].

### 4.3.4 Topological Charge

In the continuum, gauge fields can be classified according to topological sectors. These sectors are characterized by values of the topological charge $Q \in \mathbb{Z}$. First define the topological charge density by

$$q(x) = -\frac{1}{16\pi^2}\mathrm{tr}\left\{F_{\mu\nu}(x)^* F_{\mu\nu}(x)\right\}, \qquad {}^*F_{\mu\nu}(x) = \frac{1}{2}\varepsilon_{\mu\nu\rho\sigma}F_{\rho\sigma}\,. \tag{4.56}$$

The field strength tensor $F_{\mu\nu}$ is defined in Eq. (1.8) and ${}^*F_{\mu\nu}$ is the dual field strength tensor. We note the relation [50]

$$\frac{1}{2}\mathrm{tr}\left\{F_{\mu\nu}(x)^* F_{\mu\nu}(x)\right\} = \partial_\mu \varepsilon_{\mu\nu\rho\sigma}\mathrm{tr}\left\{A_\nu \partial_\rho A_\sigma + \frac{2}{3}A_\nu A_\rho A_\sigma\right\}, \tag{4.57}$$

which shows the topological charge density is a total derivative. The topological charge is defined by the integral over the density $q$

$$Q = \int \mathrm{d}^4x\; q(x)\,. \tag{4.58}$$

Equation (4.57) implies the topological charge only receives non-zero contributions from surface terms, related to the topology of the gauge field. The surface at infinity is given by the sphere $S^3$, which is isomorphic to the group $SU(2)$. First consider the case of an $SU(2)$ gauge field. It can be shown (see [51]) that the integral over $S^3$ of the surface terms can be expressed as the integral of an $SU(2)$ field over the $S^3$ sphere with the Haar measure. The $SU(2)$ field thus defines a mapping $S^3 \longrightarrow S^3$ of the $S^3$ sphere at infinity on the $S^3$ sphere in group space. This mapping is classified according to the homotopy group $\Pi_3(SU(2)) = \mathbb{Z}$. It means that the integral over the surface terms is non-zero if the sphere at infinity covers the group $SU(2)$ a non-zero integer number of times $n$, called the winding number. One arrives at the relation

$$Q = -n \in \mathbb{Z}\,, \tag{4.59}$$

which shows that the topological charge is an integer. For larger gauge groups $SU(N)$ with $N > 2$, Eq. (4.59) still holds. This can be seen by embedding $SU(2)$ subgroups into $SU(N)$ and repeating the arguments given above.

An important quantity is the topological susceptibility, formally defined as

$$\chi_{\text{top}} = \frac{1}{V} \int \mathrm{d}^4x \int \mathrm{d}^4y \ \langle q(x)q(y)\rangle = \frac{\langle Q^2\rangle}{V} \,. \tag{4.60}$$

This quantity has a physical interpretation as the Witten-Veneziano formula [52, 53] relates $\chi_{\text{top}}$ in the pure gauge theory to the mass of the $\eta'$ meson, which is much larger than the mass of the pions due to the axial anomaly [54]. The problem with $\chi_{\text{top}}$ defined in Eq. (4.60) is it is ill-defined due to non-integrable singularities. Using translation invariance we can write $\chi_{\text{top}} = \int \mathrm{d}^4x \ \langle q(x)q(0\rangle$. The integrand diverges in the limit $x \to 0$ as $(x^2)^{-4}$ up to logarithms which results in a singularity of $\chi_{\text{top}}$.

On the lattice there are several possibilities to define topological susceptibility in a way that possesses a well-defined continuum limit. We refer to a recent work [55] and mention here only the definition given in terms of fields generated by the Wilson flow of Eq. (4.25):

$$q(x,t) = -\frac{1}{32\pi^2}\varepsilon_{\mu\nu\rho\sigma}\,\mathrm{tr}\left\{\hat{G}_{\mu,\nu}(x,t)\hat{G}_{\mu,\nu}(x,t)\right\} \,, \tag{4.61}$$

where $\hat{G}_{\mu,\nu}(x,t)$ is the lattice field strength tensor, cf. Eq. (1.148). As the continuum limit is taken, the flow time $t$ is kept fixed in physical units for example by choosing $t = t_0$ defined in Eq. (4.29). Then

$$Q(t) = a^4 \sum_x q(x,t) \,, \qquad \chi_{\text{top}} = \frac{\langle Q^2\rangle}{V} \,. \tag{4.62}$$

This definition of $\chi_{\text{top}}$ holds for periodic boundary conditions. Due to the smoothing properties of the Wilson flow it does not require renormalization. Its continuum limit is independent of $t$. Reference [55] explains how to modify the definition of $\chi_{\text{top}}$ for the case of open boundary conditions.

Finally we remark that there is a relation, called the *index theorem* between the topological charge and the number of zero modes of the massless Dirac operator. This link is valid in the continuum [56] and for a class of Dirac operators which obey the Ginsparg–Wilson relation [57] it also holds at finite lattice spacing. We refer for example to [54] for a discussion of the index theorem.

## 4.4 Quarks and Hadron Physics

The success of the quark model tells us most experimentally observed hadrons are built predominantly from constituent quarks, so for studying mesons and baryons it is essential to have good techniques for building effective operators from the quark fields in the path-integral.

### 4.4.1 Quark Smearing

Smearing aims to expose the long-range degrees of freedom that best create physical states. Since quark fields are not manipulated directly on the computer, one practical constraint on quark smearing is to ensure it is a *linear operator* on the constituent fields so smearing does not generate new Wick contractions. Quark smearing introduces a new field, derived from the underlying one according to

$$\tilde{\psi}(x) = \sum_{y} \Box[U](x, y)\psi(y). \tag{4.63}$$

The operator can be gauge-covariant or it might be defined in a fixed, smooth gauge, such as Coulomb gauge. One well-known example of a gauge covariant smearing method is to use

$$\Box(n; \alpha) = \left(1 + \frac{\alpha\nabla^2}{n}\right)^n \tag{4.64}$$

with

$$\nabla^2(\underline{a}, \underline{b}; t) = -6\delta_{\underline{a},\underline{b}} + \sum_{k=1}^{3} \left(U_k(\underline{a}, t)\delta_{\underline{a}+\hat{\underline{k}},\underline{b}} + U_k^{\dagger}(\underline{a}, t)\delta_{\underline{a}-\hat{\underline{k}},\underline{b}}\right) \tag{4.65}$$

the three-dimensional gauge-covariant Laplace operator and $\alpha$ is a free parameter. Larger values of $\alpha$ lead to broader smearing profiles. The Euler limit tells us

$$\lim_{n\to\infty} \Box(n; \alpha) = e^{\alpha\nabla^2}. \tag{4.66}$$

One useful observation about the gaussian-smearing operator is for the choices of $\alpha$ used to make physical hadrons, it is effectively a very low-rank operator which removes almost all modes from the vector space of fields on a time-slice. This can be exploited to make an efficient smearing with computational advantages, such as enabling all-to-all quark propagation measurements. The resulting technique is called *distillation* [58]. First, the $N_D$ eigenvectors with smallest eigenvalues of the gauge-covariant Laplace operator of Eq. (4.65) are found so $-\nabla^2 V = VD$. Since this operator is hermitian and non-negative, this is numerically stable. Now smearing is defined as projection into this $N_D$-dimensional vector space

$$\Box_{ab}(x_1, x_2; t) = V(x_1; t)_a^{(p)}\ V^{\dagger}(x_2; t)_b^{(p)}. \tag{4.67}$$

with $a, b$ being colour indices, and $p = 1 \ldots N_D$ the distillation space index. If $N_D$ is sufficiently small, all matrix elements in this space can be determined although at some expense. This means the smearing algorithm has enabled all the elements of the quark propagator needed for hadron physics to be computed.

Now let us review an example computation of a two-point function for an isovector meson, constructed from distilled fields and with an arbitrary extended creation operator $\Gamma(x_1, x_2)$ at the source and sink. Details of these creation operators will be revisited in the next section. The correlation function is

$$C_\Gamma(t_1, t_0) = \left\langle \bar{u}(x_1, t_1)\Gamma(x_1, x_2; t_1)d(x_2, t_1) \quad \bar{d}(y_1, t_0)\Gamma(y_1, y_2; t_0)u(y_2, t_0) \right\rangle. \tag{4.68}$$

If the fields in this expression are distilled, the Wick contraction yields

$$C(t_1, t_0) = \left\langle \mathrm{Tr}_D \; \Phi_\Gamma(t_1)\, \tau(t_1, t_0)\, \Phi_\Gamma(t_0)\, \tau(t_0, t_1) \right\rangle,$$

where $\Phi_\Gamma$ gives the representation of the operator $\Gamma$ in the distillation space;

$$\Phi_\Gamma(t) = V^\dagger(x_1, t)\Gamma(x_1, x_2, t)V(x_2, t), \tag{4.69}$$

and similarly $\tau$, the *perambulator* represents a quark propagator connecting distillation spaces on two time-slices;

$$\tau(t_1, t_0) = V^\dagger(x_1, t_1)M^{-1}(x_1, t_1; x_0, t_0)V(x_0, t_0). \tag{4.70}$$

These are $N_D \times N_D$ matrices, so are of a manageable size for lattice volumes up to about 2fm. The full correlation function factorises into a product of matrices and these can be used as building blocks for more complicated diagrams generated in Wick contractions.

In practice, while $N_D$ is small for modest lattice sizes, keeping the effect of smearing constant means $N_D$ must grow in proportion to the spatial volume. This makes the method expensive for large volumes. One solution [59] is to use a stochastic representation of the identity operator in the $N_D$ dimensional "distilled" vector space, following the dilution methods introduced in Sect. 3.6.1.1.

### 4.4.2 Hadron Physics with Quarks

Central to most lattice QCD computations are the hadrons seen in collider experiments. To study energies of states, two-point correlation functions are computed however if we are interested in the interactions of quarks inside hadrons with other probes such as an electroweak current or a possible new particle outside the standard model, three-point correlation functions are needed. The technical issue of manipulating quark fields makes these computationally challenging tasks. Having defined operators on the quantum fields, the quarks are integrated out using Wick's theorem, leaving functions of the gauge fields alone. In this section, we review the construction of hadronic states including the quark fields.

#### 4.4.2.1 Mesons

The simplest colourless combinations of quark fields are creation operators for mesons; bound states of a quark and an anti-quark in a quark model. Mesons made of degenerate up and down quarks form two different irreducible representations of $SU(2)$ isospin symmetry, called the *isovector* ($I = 1$) and *isoscalar* ($I = 0$) mesons. These different symmetry channels have different spectra. At first sight, their different representation under isospin transformation seems a small matter but the extra diagrams generated in Wick contraction make the cost of studying isovector and isoscalar mesons very different.

A general gauge-invariant operator to create a meson from a quark bilinear on a lattice time-slice can be written in full as

$$\Phi^{\dagger(I,R)}(\underline{p}, t) = d^{(I)}_{f_1 f_2} \sum_{\underline{x},\underline{y}} \exp\left(i\,\underline{p}\cdot\frac{\underline{x}+\underline{y}}{2}\right) \left[\bar{\psi}^{\alpha}_{f_1 a}(\underline{x}, t)\ \Gamma^{\alpha\beta(R)}_{ab}(\underline{x}, \underline{y}; t)\ \psi^{\beta}_{f_2 b}(\underline{y}, t)\right] \tag{4.71}$$

A state with a particular $I$, $I_z$ is made from the choice of $d^{(I)}$. The total momentum of the state is $\underline{p}$ and the cubic group representation, or helicity for non-zero momentum, is defined by the choice of $\Gamma^{(R)}$. To make a gauge-invariant object requires $\Gamma$ is either a point-like operator, $\Gamma \propto \delta_{\underline{x},\underline{y}}$ or it depends on the link variables explicitly. A simple example is a creation operator for the pion at rest, for which a simple choice is $\Gamma^{\alpha\beta}_{ab}(\underline{x}, \underline{y}) = \delta_{ab}\ \delta_{\underline{x}\underline{y}}\ [\gamma_5]^{\alpha\beta}$. Note that there are arbitrarily many choices of operators which create a given set of quantum numbers.

If the flavours of the two fields in the bilinear are the same, as for example for the $\pi^0$, the meson is electrically neutral and an eigenstate of charge conjugation can be constructed. G-parity is a generalisation of charge conjugation over isospin multiplets for which all three pions are eigenstates. The G-parity of a multiplet is then $\eta_G = \eta_C(-1)^I$ where $\eta_C$ is the eigenvalue of the neutral part of the multiplet and $I$ is its isospin.

In the continuum, the corresponding colourless creation operator for a meson at rest could be written by inserting $d$ gauge-covariant derivatives in the bilinear

$$\Phi^{\dagger}(t) = C^{J}_{i_1,i_2,\ldots i_d} \int d^3\underline{x}\ \ \bar{\psi}(\underline{x}, t)\Gamma D_{i_1} D_{i_2} \ldots D_{i_d}\psi(\underline{x}, t) \tag{4.72}$$

where the spin, colour and flavour indicies are suppressed here. $C^J$ are the Clebsch-Gordan co-efficients that make a state with well-defined total angular momentum. Since covariant derivatives are non-commuting, one interesting example is the operator with the commutator of two derivatives, $D_a D_b - D_b D_a$. This operator vanishes in the absence of a gauge field so in a constituent picture the resulting bilinear creates a constituent gluon. In this model, these states are called *hybrid mesons*. They are of particular interest in experiment, since some $J^{PC}$ quantum numbers such as $1^{-+}$ are inaccessible to a quark-model state made up solely of a quark and an anti-quark. Details of constructing meson operators and their link to the continuum can be found in Ref. [1].

#### 4.4.2.2 Baryons

Baryons are the bound-states of QCD with half-integer spin. They are parity eigenstates but charge-conjugation relates the masses of the baryons to those of the anti-baryons and is not a relevant label for states. A general creation operator for a baryon at rest on the lattice with isospin $I$ and transforming irreducibly according to representation $R$ can be written

$$\Psi^{(I,R)} = \sum_{\underline{x}} d^{(I)}_{f_1 f_2 f_3} C^{(R)\alpha\beta\gamma} \varepsilon_{abc} \times \left[ \sum_{\underline{x}_1} \Gamma_1(\underline{x}, \underline{x}_1) \psi_{f_1}(\underline{x}_1) \right]^{\alpha}_{a} \left[ \sum_{\underline{x}_2} \Gamma_2(\underline{x}, \underline{x}_2) \psi_{f_2}(\underline{x}_2) \right]^{\beta}_{b} \left[ \sum_{\underline{x}_3} \Gamma_3(\underline{x}, \underline{x}_3) \psi_{f_3}(\underline{x}_3) \right]^{\gamma}_{c} \tag{4.73}$$

The coefficients $d^{(I)}$ make states of definite isospin. The operators $\Gamma_{1,2,3}$ act on the spin and colour indices and can parallel transport the quark fields in a gauge covariant manner. As with the mesons, if $\underline{x} \neq \underline{x}_j$ then $\Gamma_j$ must depend on the gauge background on the time-slice. The three fields are then anti-symmetrically contracted at site $\underline{x}$. The irreducible representation of the cubic group that the operator transforms under is set by choosing $C^{(R)}$. The colour indices are antisymmetrised to make a singlet by construction, leaving the spin, flavour and spatial structures which must be combined into a totally symmetric combination to maintain anti-symmetry overall. $S_3$, the group of permutations of three objects has two one-dimensional representations (labelled S,A) and a two-dimensional representation (with rows labelled MS and MA) and the projection into these three sets can be carried out using the Schur lemma idea given above. The construction of operators is presented in Ref. [60] and reviewed for lattice calculations in Refs. [61, 62].

Monte Carlo estimates of baryon two- and three-point functions generally suffer more from high statistical variance than their counterparts in the meson sector. An expression for the variance of an estimator can be written [63] which contains six quark propagators and these can be rearranged to look like the correlation function of three pions. At physical quark masses and large volume, this state has a lower energy (approximately $3m_\pi$) than a proton of mass $m_N$ or any other baryon. An approximate expression for the signal-to-noise ratio is

$$\rho_B \propto e^{-(m_N - \frac{3}{2}m_\pi)t}, \tag{4.74}$$

which shows the signal-to-noise falls exponentially and rapidly for a baryon. For nucleon physics calculations, extracting a reliable signal at small time-separations becomes a priority.

#### 4.4.2.3 Tetraquarks and Beyond

Over the past fifteen years, collider experiments found a number of puzzling resonances that are not easily explained in a quark model. One hypothesis is these are *tetraquarks*, bound-states of two quarks and two anti-quarks.

A lattice study requires building local operators that can excite these four constituents close together in a colour singlet. The colour contraction of the four fields decomposes as

$$3 \otimes 3 \otimes \bar{3} \otimes \bar{3} = 1 \oplus 1 \oplus 8 \oplus 8 \oplus 8 \oplus 8 \oplus 10 \oplus \bar{10} \oplus 27. \tag{4.75}$$

Relevant for this discussion is the appearance of two copies of the trivial representation. The two ways of combining four Grassmann fields into colour singlets are

$$\begin{aligned} T_1 &= \left(\delta_{ac}\delta_{bd} + \delta_{ad}\delta_{bc}\right) \phi_a \lambda_b \bar{\chi}_c \bar{\psi}_d \\ T_2 &= \left(\delta_{ac}\delta_{bd} - \delta_{ad}\delta_{bc}\right) \phi_a \lambda_b \bar{\chi}_c \bar{\psi}_d \end{aligned} \tag{4.76}$$

The spin and flavour groups must similarly be combined into irreducible representations. We will not present the details here. The resulting operator would create four constituents at a point. Fierz identities can be used to re-write these as products of two bilinears that are familiar as meson creation operators, although since these are localised this is a distinct operator from one that would have a good overlap onto two meson final states with well-defined momentum at the operator level.

The group theory requirements for making colour-singlet operators allow for an arbitrary number of constituent fields, so these construction can be extended to make pentaquark, hexaquark, etc. operators. The pentaquarks have a long, controversial history although recent experimental data has seen a revival of interest.

### *4.4.3 Hadron Scattering in Lattice Monte Carlo Calculations*

As discussed earlier, Lüscher's method relates the scattering phase shift to the spectrum of states in a finite volume. Many states in this spectrum predominantly resemble two separated hadrons and if the scattering channel contains a resonance, there is an extra state which broadly resembles a single, excited hadron in the box. This is a simplified view of the dynamics; the eigenstates of the Hamiltonian in the finite volume are mixtures of these components. One important observation which seems to be confirmed empirically is the overlap of a local quark bilinear onto one of the two-meson-like states is small. A simple model predicts this falls in inverse proportion to the three-dimensional volume of the box. If states are missed in a spectrum calculation, the determination of scattering parameters is unreliable. Phase shift calculations therefore need to include a broad basis of operators, including ones with

good overlap onto the resonance as well as the two-hadron scattering states. Since details of a few of the lowest states in the spectrum are usually needed, variational calculation forms an essential part of the construction.

Recall also the Lüscher method is only valid for scattering up to inelastic thresholds. In QCD, the light pion mass and dense spectrum means these thresholds are reached for low scattering energies and so the technique is restricted to rather low energies.

Consider the best-studied resonance in QCD, the scattering of two-pions in isospin-1, P-wave ($J = 1$) which leads to the $\rho$ resonance. In the finite volume spectra at rest, P-wave states first appear in the $T_1$ irrep, so let us build a basis of operators with these quantum numbers. Begin with the quark bilinears that create the $\rho$ meson at rest and a single pion with momentum $p$

$$\begin{aligned}\rho_i^+ &= \sum_x \bar{d}(x)\gamma_i u(x)\\ \pi^+(p) &= \sum_x e^{ip\cdot x}\ \bar{u}(x)\gamma_5 d(x)\\ \pi^0(p) &= \frac{1}{\sqrt{2}}\sum_x e^{ip\cdot x}\ \Big(\bar{u}(x)\gamma_5 d(x) - \bar{d}(x)\gamma_5 u(x)\Big).\end{aligned} \tag{4.77}$$

Now symmetrise to form a two-pion operator with definite $I, I_z$ and zero total momentum;

$$\chi_{\pi\pi}(p) = \frac{1}{\sqrt{2}}\Big(\pi^+(p)\pi^0(-p) - \pi^+(-p)\pi^0(p)\Big). \tag{4.78}$$

Note this operator vanishes when $p = 0$; there is no S-wave scattering in the $I = 1$ channel. This operator has different irreducible content under $O$ for different values of $p$, so the last step when building a basis to study the $\rho$ is using the reduction techniques given in Sect. 4.1.5 to make the $T_1^-$ irrep of $O_h$. This gives a basis of the form

$$\begin{aligned}\phi_1 &= \rho_1^+\\ \phi_2 &= \chi_{\pi\pi}(1,0,0)\\ \phi_3 &= \frac{1}{2}\Big(\chi_{\pi\pi}(1,1,0) + \chi_{\pi\pi}(1,0,1) + \chi_{\pi\pi}(1,-1,0) + \chi_{\pi\pi}(1,0,-1)\Big)\\ \phi_4 &= \frac{1}{2}\Big(\chi_{\pi\pi}(1,1,1) + \chi_{\pi\pi}(1,-1,1) + \chi_{\pi\pi}(1,-1,1) + \chi_{\pi\pi}(1,-1,-1)\Big)\end{aligned} \tag{4.79}$$

when relative $\pi$ momentum values up to $p = (1,1,1)$ are included. The next step is to use the Wick contraction rules to determine the two-point functions between all combinations of these operators in terms of quark propagators.

### 4.4.4 The Static Potential with Light Quarks: String Breaking

In Sect. 4.3.3 we introduced the potential between a static quark and anti-quark pair. In pure $SU(3)$ gauge theory, the static potential $V(r)$ rises linearly with the distance $r$, see Fig. 4.5. In QCD, where there are dynamical quark fields in the fundamental representation of $SU(3)$, the potential flattens at asymptotically large distance $r$, a phenomenon called *string breaking*. Around the string breaking distance $r_\mathrm{b}$, the energy in the flux tube between the static sources is sufficient to form a pair of static-light mesons, bound states of a static and a light quark. String breaking in lattice QCD has been observed in Monte Carlo simulations [64] and was previously demonstrated in $SU(2)$ gauge theory with scalar matter fields in four [65, 66] and three dimensions [67].

To see the flattening of the potential due to string breaking, it is not enough to consider Wilson loops for the extraction of the potential. Their overlap to the broken string state is tiny and impractically large temporal separations $t$ are needed to extract the correct ground state energy from the spectral decomposition in Eq. (4.49) as $|c_0| \ll 1$. Instead a mixing analysis based on a $2 \times 2$ correlation matrix $C(r,t)$ is needed, including the Wilson loop, off-diagonal elements representing the transition from a string to a pair of static-light mesons (and vice versa) and a diagonal element representing the transition between states made of two static-light mesons. For $N_\mathrm{f}$ mass-degenerate flavors the correlation matrix is schematically (diagrams are taken from [64])

$$C(r,t) = \left( \quad \sqrt{N_\mathrm{f}} \quad \right) \tag{4.80}$$

Explicit formulae are given in [64]. Solving the generalized eigenvalue problem as explained in Sect. 4.2.1 yields two energy eigenvalues which corresponds to the ground state and first excited state potential. The extraction can be improved by increasing the size of the correlation matrix using for example smearing of the spatial Wilson lines, see Sect. 4.3.1, and of the light quarks, see Sect. 4.4.1.

The mixing analysis can be understood with a simple model of Eq. (4.80) given by

$$C(r) = \begin{pmatrix} \sigma r & g \\ g & 2E_\mathrm{stat} \end{pmatrix}, \tag{4.81}$$

where $\sigma r$ represent a linearly rising energy level, $2E_\mathrm{stat}$ the energy of a static-light meson pair and $g$ the mixing. If $g = 0$, the matrix is diagonal and yields two energy levels which cross at a distance which corresponds approximately to the string breaking distance $r_\mathrm{b}$. If $g \neq 0$ the energy levels repel each other in the string

breaking region where $\sigma r \approx 2E_{\text{stat}}$ and are approximately given by

$$2(E_{\text{stat}} \pm g). \tag{4.82}$$

This phenomena is often referred to as an "avoided level crossing".

The string breaking distance has been calculated from simulations of $N_{\text{f}} = 2$ dynamical fermions in [64] and a first estimate in the $N_{\text{f}} = 2 + 1$ theory is given in [68]. The continuum limit and quark mass dependence of string breaking are still open issues in lattice QCD.

## 4.5 Statistical Data Analysis

Since the Monte Carlo method relies on repeated sampling of a random number to estimate an integral, careful statistical analysis is crucial and a good understanding of statistics is important. In this section, we give a short overview of these ideas but detailed descriptions and a more complete introduction can be found in [69]. We briefly review the main ideas regarding sampling and the statistical analysis of sampled data, mainly to introduce notation.

$\bar{X}$, the *sample mean* of $\Omega = \{X_1, X_2, \ldots X_n\}$, an ensemble of $n$ independent, identically distributed random numbers with expected value $E[X_k] = \mu_X$ and finite variance $\sigma_X^2 = E[X_k^2] - E[X_k]^2$ is defined as

$$\bar{X} = \frac{1}{n} \sum_{k=1}^{n} X_k, \tag{4.83}$$

and the linear property of expectation values gives $E[\bar{X}] = \mu_X$. The laws of large numbers states the sample mean converges almost surely to $\mu_X$ as the size of the ensemble increases. In practise we work with a finite ensemble so our results must be quoted as a confidence interval. To determine this, we need to know $\sigma_{\bar{X}}^2$, the variance of the sample mean which is related simply to the variance of the underlying random number, $X$ by

$$\sigma_{\bar{X}}^2 = E[\bar{X}^2] - E[\bar{X}]^2 = \frac{\sigma_X^2}{n}. \tag{4.84}$$

This result follows from the definition of $\bar{X}$ and noting that for *independent* random samples, $E[X_i X_j] = E[X_i]E[X_j]$ when $i \neq j$. To give a confidence interval for the true value of $\mu_X$ requires understanding something about the distribution of $\bar{X}$. The *central limit theorem* helps (CLT) simplify the discussion immensely. The CLT tells us the sample mean of $n$ independent and identically distributed random numbers obeys

$$\lim_{n\to\infty} P\left(\frac{-a\sigma}{\sqrt{n}} < \bar{X} - \mu_X < \frac{a\sigma}{\sqrt{n}}\right) = \frac{1}{\sqrt{2\pi}} \int_{-a}^{a} e^{-x^2/2} dx. \tag{4.85}$$

Note the right-hand-side is dependent only on $a$, the size of the confidence interval defining the probability on the right side of Eq. (4.85). The CLT means that we can give reliable confidence intervals by treating the sample mean as a normally distributed random number for $n$ large enough. In practise, $n \approx 50$ is often sufficient, although ensembles with extreme outliers give counter-examples.

### 4.5.1 Controlling Bias, Covariance and Autocorrelations in Data from a Markov Chain

In most lattice physics projects, more than one expectation value is estimated on a given Monte Carlo ensemble and functions of these sample averages are taken. A well-used example is the *effective mass* of a state, computed from the ratio of expectation values of the two-point correlation function for two different time-separations. In an example such as this, care is needed to determine a confidence interval from the data. Often this pays off as correlations in statistical fluctuations can lead to better statistical precision.

Usually, taking a function of a sample mean and using it to estimate the result of the function applied to the true expectation value leads to a *biased estimator* and the size of this bias should be understood and corrected for, if possible. Suppose as an example we want to compute $y = f(x)$ where we can construct $X$, a random number that is an unbiased estimator for $x$ but cannot do the same for $y$. A simple recipe would be to sample $X$ many times and compute the mean $\bar{X}$ on an ensemble of $n$ independent samples. Evaluating the stochastic variable $\bar{Y} = f(\bar{X})$ yields an estimator which converges to $y$ under some assumptions but for which there is a bias in general so $E[\bar{Y}] \neq y$ for finite $n$. It can be seen that

$$E[\bar{Y}] = y + \frac{\sigma_X^2 f''(x)}{2n} + \mathcal{O}(n^{-2}) \tag{4.86}$$

with $\sigma_X^2$ the variance of $X$. The bias falls in inverse proportion to $n$. This is a faster fall-off than the standard deviation for a sample average, so bias is a particular problem for small samples.

#### 4.5.1.1 Jack-Knife Resampling

The *jack-knife* method provides both a robust means of estimating and partially correcting for the bias and also estimating the variance of our Monte Carlo sample average. This enables a reliable confidence interval to be given. The procedure is simple to carry out on a computer and widely used. With an ensemble of $n$ independent

sample data, $\Omega = \{X_1, X_2, \ldots X_n\}$, consider the $n$ ensembles each with $n-1$ data where the $j$-th such ensemble consists of all the entries of $\Omega$ *excluding* $X_j$;

$$\Omega^{(j)} = \left\{X_1, X_2, \ldots X_{j-1}, X_{j+1} \ldots X_n\right\}. \tag{4.87}$$

The *jack-knife mean* on $\Omega^{(j)}$ is then defined in the obvious way;

$$\bar{X}^{(j)} = \frac{1}{n-1} \sum_{k \neq j} X_k. \tag{4.88}$$

Suppose again we want to estimate $y = f(x)$ from our data. We have already seen that in general $\bar{Y} = f(\bar{X})$ is a biased estimator for $y$ with a bias that usually falls in inverse proportion to the sample size. Also, we have no robust estimate for the uncertainty or size of a confidence interval. Relying on linear propagation of errors can give unreliable answers. The jack-knife provides an easy-to-use method that circumvents both these issues. Define an estimator for $y$ on each jack-knife ensemble,

$$\bar{Y}^{(j)} = f(\bar{X}^{(j)}), \tag{4.89}$$

and first compute

$$\bar{Y} = \frac{1}{n} \sum_j \bar{Y}^{(j)}. \tag{4.90}$$

Now defining

$$\Sigma_Y^2 = \frac{n}{n-1} \sum_j (\bar{Y} - \bar{Y}^{(j)})^2, \tag{4.91}$$

gives an estimate of the variance of $\bar{Y}$. An estimator with no $\mathcal{O}(1/n)$ bias is

$$\hat{Y} = nf(\bar{X}) - (n-1)\bar{Y}. \tag{4.92}$$

The bias cancellation is seen from Eq. (4.86) and by noting that each jack-knife estimate is just a sample average with $n-1$ data points and so has the same bias expression as the full average, $\bar{Y}$ with this change. The linear combination in Eq. (4.92) removes the $\mathcal{O}(n^{-1})$ bias, leaving the leading term proportional to $n^{-1} - (n-1)^{-1} = \mathcal{O}(n^{-2})$. The jack-knife also provides an easy means of estimating and correctly dealing with *covariance*. Suppose now we sample two random numbers $A$ and $B$ with expected values $\mu_A, \mu_B$ from our underlying Monte Carlo data set. It is very likely that on a given configuration, $A_k$ and $B_k$ are not independent. If we would like to use this data to estimate $\mu_G = g(\mu_A, \mu_B)$ for some choice of $g$, then the jack-knife again provides a simple, robust means of estimating a confidence interval. The jack-knife estimates

$$\bar{G}^{(j)} = g(\bar{A}^{(j)}, \bar{B}^{(j)}), \tag{4.93}$$

are first generated, where a common pair of data-points $A_j$ and $B_j$ are simultaneously removed. Then once again generating

$$\bar{G} = \frac{1}{n}\sum_j \bar{G}^{(j)} \text{ and } \Sigma_G^2 = \frac{n}{n-1}\sum_j (\bar{G} - \bar{G}^{(j)})^2, \tag{4.94}$$

provides a reliable estimate for $\mu_G$ and the variance of this estimate.

#### 4.5.1.2 Statistical Analysis of Data from a Markov Chain

So far, we have assumed that samples in the ensemble are independent. Unfortunately, this is not the case for most lattice calculations where the importance sampling ensemble is a Markov chain. To assess the impact of this requires studying the autocorrelation and again the sample ensemble provides the data we need.

The *autocorrelation time* measures the efficiency of approximating $E[O]$ with $\bar{O}$. Assuming we have reached the fixed point distribution, we can estimate

$$\sigma_{\bar{O}}^2 = \frac{\sigma^2}{n}\left(1 + 2\sum_{j=1}^{n-1}\left(1 - \frac{j}{n}\right)\sigma_j\right) \approx \frac{\sigma^2}{n}\left(1 + 2\sum_{j=1}^{\infty}\sigma_j\right) \tag{4.95}$$

with the autocorrelation function given by

$$\sigma_j = E\left[O(U^{(k)})O(U^{(k+j)})\right] - \mu_O^2. \tag{4.96}$$

Defining now the *autocorrelation time* $\tau_O$ of $O$ by

$$\tau_O = \frac{1}{2} + \sum_{j=1}^{\infty}\sigma_j, \tag{4.97}$$

gives $n\sigma_{\bar{O}} \approx 2\tau_O\sigma^2$. The autocorrelation time defines approximately how many configurations have to be computed to get independent samples. It links the variance of the estimate to the variance of the underlying observable when there are correlations in the chain.

A simple way to determine the influence of autocorrelations on the sample variance is to analyse bins of data from the Markov chain. Starting with the original chain, take adjacent pairs of values and average them, which leads to a sequence of values of half the length. Now analyse this data in the usual way. If there were no autocorrelations, the expectation value of the sample variance would be unchanged but autocorrelations lead to a larger estimate. This process can be repeated with increasingly large bin sizes and if the sample variance stabilises to a value independent of the bin size, it is reasonable to suggest the autocorrelation time is smaller than the bin size. Of course

this assumes there are enough samples in the original data to reach this limit in a robust way, which is often difficult to ascertain.

### 4.5.2 Comparing Monte Carlo Data to a Model

In most calculations a theoretical model for data, often including how a range of expectation values should depend on some parameters, is provided and we would like to both test this model and perhaps find the *best-fit* parameters suggested by the data. The starting point for such an analysis is to determine the $\chi^2$ statistic, which in its simplest (uncorrelated) form is

$$\chi^2 = \sum_{a=1}^{m} \frac{(f_a - \bar{F}_a)^2}{\sigma_a^2}, \tag{4.98}$$

with $f_a,\ a = 1 \ldots m$ the model predictions and $\bar{F}_a$ the Monte Carlo data. $\sigma_a^2$ are the variances of our estimators and are usually in turn estimated from the Monte Carlo data using the jack-knife. $\chi^2$ is non-negative and since it depends on sample data, it is itself a random number that is sampled. Smaller values of $\chi^2$ indicate a smaller mis-match between our model and our Monte Carlo data. Since we are sampling to estimate expectation values, there is no reason for $\chi^2$ to be exactly zero when the model is correct. The standard deviation gives the scale for fluctuations in the sample mean and so a reasonable value for $\chi^2$ if the model gives a reliable prediction is $\chi^2 \approx m$. If the statistic is very much larger it is unlikely our data supports the model. More precise statements can be made by computing the *goodness-of-fit*, $Q(\chi^2, m)$ which gives the probability a correct model description would lead to a value of $\chi^2$ at least as big at the value measured. See Ref. [70] for software to evaluate this function. More generally, when $m > 1$ and there are correlations between sample means, the *correlated* $\chi^2$ statistic is needed;

$$\chi^2 = \sum_{a,b=1}^{m} (f_a - \bar{F}_a)[C^{-1}]_{ab}(f_b - \bar{F}_b) \tag{4.99}$$

where $C_{ab}$ is the *covariance matrix* between the $m$ observables.

$$C_{ab} = \frac{E[F_a F_b] - E[F_a]E[F_b]}{n^2}. \tag{4.100}$$

In most cases the entries in this matrix are again estimated from Monte Carlo data. From its definition, $C$ is a positive semi-definite symmetric matrix but for real data, this often comes close to breaking down and $C$ might have very small eigenvalues as a symptom of statistical instability. The solution is to apply a singular value decomposition to $C$ and remove very small eigenvalues before the inversion is computed.

For each singular value removed, the effective value of $m$ is reduced and this must be taken into account when looking at the $\chi^2$ statistic. The appearance of singular values implies there is a measured observable that is statistically indistinguishable from some linear combination of the others in the set.

#### 4.5.2.1 Fitting Model Parameters to Data

Recall there may be situations where the model has a set of $p$ unknown parameters $\lambda_\alpha, \alpha = 1 \ldots p$ that we would like to constrain from the Monte Carlo data. The *best-fit* parameters are those that minimise the $\chi^2$ statistic. In the case the model is linear in these parameters, $f_a = \sum_{\alpha=1}^{p} h_{a,\alpha}\lambda_\alpha$ this minimum is easily found as the solution to a linear system. More generally, finding the minimum of a non-linear model is often a challenge and there are many software packages that attempt to automate this process to the extent possible. A well-known method in model fitting is the *Marquardt-Levenberg* algorithm, which is presented in Ref. [70] and more advanced methods feature in numerical software libraries.

## 4.6 Summary

In this final chapter, we presented a sketch of how to bring together the algorithms discussed in earlier chapters to make contact with physics questions and how to analyse the statistical data that comes from Monte Carlo calculations. As seen earlier, most of the algorithmic and computational costs are from manipulating quark fields, although calculations of gluonic observables are often difficult due to the large variance of Monte Carlo estimators.

This area of research is still developing and changing rapidly, driven by new experimental results, better theoretical frameworks in which to analyse lattice data and advances in both algorithms and computer power available to researchers. Progress in most of the physics topics discussed in this section is reported each year at the lattice symposium and we refer readers to the usually very thorough review articles in the proceedings.

## References

1. J.J. Dudek, R.G. Edwards, M.J. Peardon, D.G. Richards, C.E. Thomas, Phys. Rev. D **82**, 034508 (2010). doi:10.1103/PhysRevD.82.034508
2. M. Lüscher, Commun. Math. Phys. **54**, 283 (1977). doi:10.1007/BF01614090
3. M. Creutz, Phys. Rev. D **15**, 1128 (1977). doi:10.1103/PhysRevD.15.1128
4. N. Irges, F. Knechtli, Nucl. Phys. B **775**, 283 (2007). doi:10.1016/j.nuclphysb.2007.01.023
5. M. Lüscher, U. Wolff, Nucl. Phys. B **339**, 222 (1990). doi:10.1016/0550-3213(90)90540-T

6. B. Blossier, M. Della Morte, G. von Hippel, T. Mendes, R. Sommer, JHEP **04**, 094 (2009). doi:10.1088/1126-6708/2009/04/094
7. R. Sommer, PoS **LATTICE2013**, 015 (2014)
8. M. Lüscher, JHEP **08**, 071 (2010). doi:10.1007/JHEP08(2010071), 10.1007/JHEP03(2014)092. [Erratum: JHEP03, 092 (2014)]
9. M. Lüscher, P. Weisz, JHEP **02**, 051 (2011). doi:10.1007/JHEP02(2011)051
10. R. Narayanan, H. Neuberger, JHEP **03**, 064 (2006). doi:10.1088/1126-6708/2006/03/064
11. M. Lüscher, Commun. Math. Phys. **293**, 899 (2010). doi:10.1007/s00220-009-0953-7
12. R. Lohmayer, H. Neuberger, PoS **LATTICE2011**, 249 (2011)
13. S. Borsanyi et al., JHEP **09**, 010 (2012). doi:10.1007/JHEP09(2012)010
14. A. Ramos, in *Proceedings, 32nd International Symposium on Lattice Field Theory (Lattice 2014)* (2015), https://inspirehep.net/record/1373921/files/arXiv:1506.00118.pdf
15. P. Fritzsch, A. Ramos, JHEP **10**, 008 (2013). doi:10.1007/JHEP10(2013)008
16. M. Luscher, Commun. Math. Phys. **105**, 153 (1986). doi:10.1007/BF01211097
17. K. Rummukainen, S.A. Gottlieb, Nucl. Phys. B **450**, 397 (1995). doi:10.1016/0550-3213(95)00313-H
18. C.B. Lang, D. Mohler, S. Prelovsek, M. Vidmar, Phys. Rev. D **84**(5), 054503 (2011). doi:10.1103/PhysRevD.89.059903, 10.1103/PhysRevD.84.054503. [Erratum: Phys. Rev. D89, no. 5, 059903 (2014)]
19. D.J. Wilson, R.A. Briceno, J.J. Dudek, R.G. Edwards, C.E. Thomas, Phys. Rev. D **92**(9), 094502 (2015). doi:10.1103/PhysRevD.92.094502
20. M.T. Hansen, S.R. Sharpe, Phys. Rev. D **90**(11), 116003 (2014). doi:10.1103/PhysRevD.90.116003
21. M. Albanese et al., Phys. Lett. B **192**, 163 (1987). doi:10.1016/0370-2693(87)91160-9
22. M. Della Morte, A. Shindler, R. Sommer, JHEP **0508**, 051 (2005)
23. C.W. Bernard, T.A. DeGrand, Nucl. Phys. Proc. Suppl. **83**, 845 (2000). doi:10.1016/S0920-5632(00)91822-X
24. A. Hasenfratz, F. Knechtli, Phys. Rev. D **64**, 034504 (2001). doi:10.1103/PhysRevD.64.034504
25. A. Hasenfratz, R. Hoffmann, F. Knechtli, Nucl. Phys. Proc. Suppl. **106**, 418 (2002). doi:10.1016/S0920-5632(01)01733-9 [418 (2001)]
26. A. Grimbach, D. Guazzini, F. Knechtli, F. Palombi, JHEP **03**, 039 (2008). doi:10.1088/1126-6708/2008/03/039
27. C. Morningstar, M.J. Peardon, Phys. Rev. D **69**, 054501 (2004). doi:10.1103/PhysRevD.69.054501
28. S. Capitani, S. Durr, C. Hoelbling, JHEP **11**, 028 (2006). doi:10.1088/1126-6708/2006/11/028
29. B. Berg, A. Billoire, Nucl. Phys. B **221**, 109 (1983). doi:10.1016/0550-3213(83)90620-X
30. G.S. Bali, K. Schilling, A. Hulsebos, A.C. Irving, C. Michael, P.W. Stephenson, Phys. Lett. B **309**, 378 (1993). doi:10.1016/0370-2693(93)90948-H
31. C.J. Morningstar, M.J. Peardon, Phys. Rev. D **60**, 034509 (1999). doi:10.1103/PhysRevD.60.034509
32. M. Donnellan, F. Knechtli, B. Leder, R. Sommer, Nucl. Phys. B **849**, 45 (2011). doi:10.1016/j.nuclphysb.2011.03.013
33. R. Sommer, (2010)
34. G. Parisi, R. Petronzio, F. Rapuano, Phys. Lett. B **128**, 418 (1983). doi:10.1016/0370-2693(83)90930-9
35. G.S. Bali, K. Schilling, C. Schlichter, Phys. Rev. D **51**, 5165 (1995). doi:10.1103/PhysRevD.51.5165
36. M. Lüscher, P. Weisz, JHEP **09**, 010 (2001). doi:10.1088/1126-6708/2001/09/010
37. S. Necco, R. Sommer, Nucl. Phys. B **622**, 328 (2002). doi:10.1016/S0550-3213(01)00582-X
38. M. Della Morte, S. Durr, J. Heitger, H. Molke, J. Rolf, A. Shindler, R. Sommer, Phys. Lett. **B581**, 93 (2004). doi:10.1016/j.physletb.2005.03.017
39. P. Weisz, Nucl. Phys. B **212**, 1 (1983). doi:10.1016/0550-3213(83)90595-3
40. M. Lüscher, K. Symanzik, P. Weisz, Nucl. Phys. B **173**, 365 (1980). doi:10.1016/0550-3213(80)90009-7

41. M. Lüscher, Nucl. Phys. B **180**, 317 (1981). doi:10.1016/0550-3213(81)90423-5
42. Y. Nambu, Phys. Lett. B **80**, 372 (1979). doi:10.1016/0370-2693(79)91193-6
43. M. Lüscher, P. Weisz, JHEP **07**, 049 (2002). doi:10.1088/1126-6708/2002/07/049
44. M. Lüscher, G. Münster, P. Weisz, Nucl. Phys. B **180**, 1 (1981). doi:10.1016/0550-3213(81)90151-6
45. F. Gliozzi, M. Pepe, U.J. Wiese, Phys. Rev. Lett. **104**, 232001 (2010). doi:10.1103/PhysRevLett.104.232001
46. R. Sommer, Nucl. Phys. B **411**, 839 (1994). doi:10.1016/0550-3213(94)90473-1
47. M. Guagnelli, R. Sommer, H. Wittig, Nucl. Phys. B **535**, 389 (1998). doi:10.1016/S0550-3213(98)00599-9
48. C.W. Bernard, T. Burch, K. Orginos, D. Toussaint, T.A. DeGrand, C.E. DeTar, S.A. Gottlieb, U.M. Heller, J.E. Hetrick, B. Sugar, Phys. Rev. D **62**, 034503 (2000). doi:10.1103/PhysRevD.62.034503
49. B. Leder, F. Knechtli, PoS **LATTICE2011**, 315 (2011)
50. M. Lüscher, R. Narayanan, P. Weisz, U. Wolff, Nucl. Phys. B **384**, 168 (1992). doi:10.1016/0550-3213(92)90466-O
51. M. Creutz, Acta Phys. Slov. **61**, 1 (2011). doi:10.2478/v10155-011-0001-y
52. E. Witten, Nucl. Phys. B **156**, 269 (1979). doi:10.1016/0550-3213(79)90031-2
53. G. Veneziano, Nucl. Phys. B **159**, 213 (1979). doi:10.1016/0550-3213(79)90332-8
54. C. Gattringer, C.B. Lang, Lect. Notes Phys. **788**, 1 (2010). doi:10.1007/978-3-642-01850-3
55. M. Bruno, S. Schaefer, R. Sommer, JHEP **08**, 150 (2014). doi:10.1007/JHEP08(2014)150
56. M.F. Atiyah, I.M. Singer, Annals Math. **93**, 139 (1971). doi:10.2307/1970757
57. P. Hasenfratz, V. Laliena, F. Niedermayer, Phys. Lett. B **427**, 125 (1998). doi:10.1016/S0370-2693(98)00315-3
58. M. Peardon, J. Bulava, J. Foley, C. Morningstar, J. Dudek, R.G. Edwards, B. Joo, H.W. Lin, D.G. Richards, K.J. Juge, Phys. Rev. D **80**, 054506 (2009). doi:10.1103/PhysRevD.80.054506
59. C. Morningstar, J. Bulava, J. Foley, K.J. Juge, D. Lenkner, M. Peardon, C.H. Wong, Phys. Rev. D **83**, 114505 (2011). doi:10.1103/PhysRevD.83.114505
60. S. Capstick, N. Isgur, Phys. Rev. D **34**, 2809 (1986). doi:10.1103/PhysRevD.34.2809, 10.1063/1.35361 [AIP Conf. Proc. 132, 267 (1985)]
61. S. Basak, R.G. Edwards, G.T. Fleming, U.M. Heller, C. Morningstar, D. Richards, I. Sato, S. Wallace, Phys. Rev. D **72**, 094506 (2005). doi:10.1103/PhysRevD.72.094506
62. R.G. Edwards, J.J. Dudek, D.G. Richards, S.J. Wallace, Phys. Rev. D **84**, 074508 (2011). doi:10.1103/PhysRevD.84.074508
63. G.P. Lepage, in *Boulder ASI 1989: 97–120*, pp. 97–120 (1989), http://alice.cern.ch/format/showfull?sysnb=0117836
64. G.S. Bali, H. Neff, T. Duessel, T. Lippert, K. Schilling, Phys. Rev. D **71**, 114513 (2005). doi:10.1103/PhysRevD.71.114513
65. F. Knechtli, R. Sommer, Phys. Lett. B **440**(345), 1998 (1999). doi:10.1016/S0370-2693(98)01098-3 Erratum-ibid. B454: 399
66. F. Knechtli, R. Sommer, Nucl. Phys. B **590**, 309 (2000). doi:10.1016/S0550-3213(00)00470-3
67. O. Philipsen, H. Wittig, Phys. Rev. Lett. **81**, 4056 (1998). doi:10.1103/PhysRevLett.81.4056 [Erratum: Phys. Rev. Lett. 83, 2684 (1999)]
68. V. Koch, J. Bulava, B. Hrz, F. Knechtli, G. Moir, C. Morningstar, M. Peardon, (2015)
69. U. Wolff, Comput. Phys. Commun. **156**, 143 (2004). doi:10.1016/S0010-4655(03)00467-3, 10.1016/j.cpc.2006.12.001 [Erratum: Comput. Phys. Commun. 176, 383 (2007)]
70. W.H. Press, S.A. Teukolsky, W.T. Vetterling, B.P. Flannery, *Numerical Recipes 3rd Edition: The Art of Scientific Computing*, 3rd edn. (Cambridge University Press, New York, NY, USA, 2007)

# Appendix A
# Notational Conventions

Throughout the book we use Einstein's implicit summation convention: repeated indices in an expression are automatically summed over.

We work in natural units where the Planck constant is $\hbar = 1$ and the speed of light is $c = 1$. In these units, energy and mass have the same mass dimension equal to +1 and time and length have the same mass dimension equal to $-1$. A useful relation is $1 = 197\,\text{MeVfm}$, which allows the conversion between energy in units of MeV[1] and length in units of fm.[2]

In Lattice Quantum Chromodynamics the fields representing the quarks and the gluons are defined on a Euclidean lattice in four dimensions with lattice spacing $a$. The directions on the lattice are labelled by $\mu = 0, 1, 2, 3$. The lattice points have coordinates $x = (x_0, x_1, x_2, x_3)$ which are integer multiples of $a$: $x_\mu = n_\mu a$, $n_\mu \in \mathbb{N}$ for $\mu = 0, 1, 2, 3$. The coordinate $x_0$ is referred to as the Euclidean time and the spatial coordinates are collectively denoted by $\underline{x} = (x_1, x_2, x_3)$. The nearest neighbor of a lattice point x in positive $\mu$ direction is denoted by $x + a\hat{\mu}$, where $\hat{\mu}$ is the unit vector in direction $\mu$. If the lattice has a finite volume $V = T \times L^3$ then the ranges of the coordinates are $x_0/a = 0, 1, \ldots, T/a - 1$ and $x_k = 0, 1, \ldots, L/a - 1$ for $k = 1, 2, 3$. Unless otherwise specified, in finite volume we impose periodic boundary conditions, which mean that the points $x + T\hat{0}$ and $x + L\hat{k}$ for $k = 1, 2, 3$ are identified with $x$.

[1] MeV means Mega electronvolt; 1 eV is the potential energy that an electron aquires when a tension of 1 V is applied.

[2] fm means fermi; $1\,\text{fm} = 10^{-15}\,\text{m}$.



F. Knechtli et al., *Lattice Quantum Chromodynamics*,
SpringerBriefs in Physics, DOI 10.1007/978-94-024-0999-4

## A.1 $SU(N)$ Notation

An $SU(N)$ gauge field on the lattice assign an element $U_\mu(x)$ of $SU(N)$ to the link connecting the point $x + a\hat{\mu}$ with $x$. $SU(N)$ is the special unitary group. In the fundamental representation, the elements $U$ are $N \times N$ complex matrices which satisfy

$$U \in SU(N) \Leftrightarrow U^{-1} = U^\dagger \equiv (U^T)^* \,, \ \det(U) = 1 \,. \tag{A.1}$$

The Lie algebra $\mathfrak{su}(N)$ of $SU(N)$ may be identified with the linear space of all anti-hermitian traceless $N \times N$ matrices $X$:

$$X^\dagger = -X \,, \quad \text{and} \quad \mathrm{tr}\, X = 0 \,. \tag{A.2}$$

We denote the generators (basis) of $\mathfrak{su}(N)$ by $T^i$, $i = 1, \ldots, N^2 - 1$. Any element $X$ of $\mathfrak{su}(N)$ can written as

$$X = X^i T^i \,, \quad X^i = -2\mathrm{tr}\left\{X T^i\right\} \,,$$

in terms of real components $X^i$. The normalisation of the generators is given by

$$\mathrm{tr}\left\{T^i T^j\right\} = -\frac{1}{2}\delta^{ij} \,. \tag{A.3}$$

The natural scalar product in $\mathfrak{su}(N)$ is

$$\langle X, Y\rangle = X^i Y^i = -2\mathrm{tr}\left\{XY\right\} \,. \tag{A.4}$$

The structure constants $f^{ijk}$ defined by the commutation relation

$$[T^i, T^j] = f^{ijk} T^k \tag{A.5}$$

are real and totally anti-symmetric in the indices $i, j, k$. They satisfy $f^{ikl} f^{jkl} = N\delta^{ij}$. The exponential map

$$\mathrm{e}^X = I + \sum_{k=1}^{\infty} \frac{X^k}{k!} \,,$$

maps an element $X \in \mathfrak{su}(N)$ onto the group $SU(N)$. Differentiation of a function of the lattice gauge field $f(U)$ with respect to a link $U_\mu(x)$ is defined by the link differential operators [1]

$$\partial_{x,\mu} f(U) = T^i \partial^i_{x,\mu} f(U) \quad \text{with} \quad \partial^i_{x,\mu} f(U) = \left.\frac{\mathrm{d} f(U_s)}{\mathrm{d}s}\right|_{s=0} \,. \tag{A.6}$$

In the derivative with respect to $s$ the gauge field $U_s$ is given by

$$(U_s)_\nu(y) = \begin{cases} \mathrm{e}^{sT^i} U_\mu(x) & \text{if } (y,\nu) = (x,\mu) \\ U_\nu(y) & \text{otherwise} \end{cases} . \tag{A.7}$$

Useful formulae are

$$\left.\frac{\mathrm{d}(U_s)_\mu(x)}{\mathrm{d}s}\right|_{s=0} = T^i U_\mu(x)\,, \quad \text{and} \quad \left.\frac{\mathrm{d}(U_s)^{-1}_\mu(x)}{\mathrm{d}s}\right|_{s=0} = -U^{-1}_\mu(x) T^i\,,$$

where the second expression follows from $0 = \left.\frac{\mathrm{d}(U_s)^{-1}_\mu(x)(U_s)_\mu(x)}{\mathrm{d}s}\right|_{s=0}$.

## A.2 Fermions

A fermion field assigns Dirac spinors $\psi^\alpha_j(x)$ and $\bar{\psi}^\alpha_j(x)$ to each lattice point $x$. The spinor index is $\alpha = 1, 2, 3, 4$ and the colour index in the fundamental representation of $SU(N)$ is $j = 1, 2, \ldots, N$. The components of the fermion field are Grassmann numbers.

The Grassmann algebra of $q$ Grassmann numbers $\{\eta_1, \eta_2, \ldots, \eta_q\}$ is defined as

$$\{\eta_i, \eta_j\} = 0\,, \quad i, j = 1, 2, \ldots, q\,. \tag{A.8}$$

For a single Grassmann variable, the Berezin integral is

$$\int d\eta = 0, \quad \text{and} \quad \int d\eta\ \eta = 1.$$

These are not integrals in our usual intuitive sense of the area under a curve but should be considered as abstract and simple rules that define the fermion path integral in a physically sensible way in analogy to the bosonic path integral. Since $\eta^2 = 0$ for a Grassmannian, any function of this single variable can be written

$$f(\eta) = f_0 + f_1 \eta,$$

with $f_0$ and $f_1$ two constants and so the integral of any function is then

$$\int d\eta\ f(\eta) = f_1$$

and we see the first peculiar property of a Grassmann variable; integration is equivalent to differentiation. Now consider integrating $q$ Grassmannians. The rules above

apply straightforwardly, but care is needed to take the order of integration appropriately since Grassmann variables anti-commute. We have

$$\int \mathscr{D}[\eta] \;\; \eta_1 \eta_2 \ldots \eta_q = 1 \tag{A.9}$$

with $\mathscr{D}[\eta] = \prod_{k=1}^{q} d\eta_k$. All other integrals, which have at least one of the variables missing, vanish. A function of $q$ Grassmannians will have $2^N$ coefficients in its most general form and can be written in a binary notation. For example, with $q = 3$

$$f(\eta_1, \eta_2, \eta_3) =$$
$$f_{000} + f_{100}\eta_1 + f_{010}\eta_2 + f_{001}\eta_3 + f_{110}\eta_1\eta_2 + f_{101}\eta_1\eta_3 + f_{011}\eta_2\eta_3 + f_{111}\eta_1\eta_2\eta_3,$$

and the integral result follows easily;

$$\int \mathscr{D}[\eta] \;\; f(\eta_1, \eta_2, \ldots, \eta_q) = f_{11\ldots1}.$$

An important role is played by "Gaussian" integrals. The Matthews–Salam formula is

$$\int \mathscr{D}[\eta]\mathscr{D}[\bar{\eta}] \;\; \mathrm{e}^{\bar{\eta}_i M_{ij} \eta_j} = \det(M)\,, \tag{A.10}$$

where $\{\bar{\eta}_1, \bar{\eta}_2, \ldots, \bar{\eta}_q\}$ is a second set of independent Grassmann numbers. Consider a linear transformation of the Grassmann variables $\eta = A\eta'$, where $A$ is a complex matrix. Using the chain of equalities

$$\det(M) = \int \mathscr{D}[A\eta']\mathscr{D}[\bar{\eta}]\mathrm{e}^{\bar{\eta}M(A\eta')} = J(A)\int \mathscr{D}[\eta']\mathscr{D}[\bar{\eta}]\mathrm{e}^{\bar{\eta}(MA)\eta'} = J(A)\det(MA) \tag{A.11}$$

we conclude that the Jacobian of the transformation is $J(A) = \det(A)^{-1}$. Similarly, the transformation $\bar{\eta} = \bar{\eta}'B$ leads to a Jacobian $\mathscr{D}[\bar{\eta}'B] = J(B)\mathscr{D}[\bar{\eta}']$ with $J(B) = \det(B)^{-1}$.

On an infinite lattice we can represent the fermion fields as integrals

$$\psi(x) = \int_{-\pi/a}^{\pi/a} \frac{\mathrm{d}^4 p}{(2\pi)^4} \mathrm{e}^{ipx} \tilde{\psi}(p)\,, \tag{A.12}$$

$$\bar{\psi}(x) = \int_{-\pi/a}^{\pi/a} \frac{\mathrm{d}^4 p}{(2\pi)^4} \mathrm{e}^{-ipx} \tilde{\bar{\psi}}(p)\,. \tag{A.13}$$

The momenta $p = (p_\mu)$ are defined over the Brillouin zone $p_\mu \in [-\pi/a, \pi/a]$. The Fourier components can be computed by Fourier transformation as

$$\tilde{\psi}(p) = a^4 \sum_x \mathrm{e}^{-ipx} \psi(x)\,, \tag{A.14}$$

$$\tilde{\bar{\psi}}(p) = a^4 \sum_x \mathrm{e}^{ipx} \bar{\psi}(x)\,. \tag{A.15}$$

The Wilson–Dirac operator acts on fermion fields according to Eq. (1.83). There, the $4 \times 4$ Dirac matrices $\gamma_\mu$, $\mu = 0, 1, 2, 3$ act in spinor space. They are Hermitian $(\gamma_\mu)^\dagger = \gamma_\mu$ and satisfy the anti-commutation relation

$$\{\gamma_\mu, \gamma_\nu\} = 2\delta_{\mu\nu}\,. \tag{A.16}$$

Since $\gamma_\mu$ is Hermitian, it follows $(\gamma_\mu^*)^{\alpha\beta} = \gamma_\mu^{\beta\alpha}\ \forall \mu$. An explicit choice is given by the chiral representation of the Dirac matrices, where

$$\gamma_\mu = \begin{pmatrix} 0 & e_\mu \\ (e_\mu)^\dagger & 0 \end{pmatrix}. \tag{A.17}$$

A possible choice for the $2 \times 2$ matrices $e_\mu$ is

$$e_0 = -I\,, \qquad e_k = -i\sigma_k\,,\ k = 1, 2, 3\,, \tag{A.18}$$

where $\sigma_k$ are the Pauli matrices

$$\sigma_1 = \begin{pmatrix} 0 & 1 \\ 1 & 0 \end{pmatrix}, \quad \sigma_2 = \begin{pmatrix} 0 & -i \\ i & 0 \end{pmatrix}, \quad \sigma_3 = \begin{pmatrix} 1 & 0 \\ 0 & -1 \end{pmatrix}.$$

We define $\gamma_5 = \gamma_0\gamma_1\gamma_2\gamma_3$ with the properties

$$(\gamma_5)^\dagger = \gamma_5\,, \qquad (\gamma_5)^2 = I\,, \qquad \{\gamma_\mu, \gamma_5\} = 0\ \forall \mu\,. \tag{A.19}$$

In the chiral representation Eq. (A.17) of the Dirac matrices we have

$$\gamma_5 = \begin{pmatrix} I & 0 \\ 0 & -I \end{pmatrix}$$

and for the matrices $\sigma_{\mu\nu} = \frac{i}{2}[\gamma_\mu, \gamma_\nu]$

$$\sigma_{0k} = \begin{pmatrix} \sigma_k & 0 \\ 0 & -\sigma_k \end{pmatrix}, \qquad \sigma_{ij} = -\varepsilon_{ijk} \begin{pmatrix} \sigma_k & 0 \\ 0 & \sigma_k \end{pmatrix},$$

where $\varepsilon_{ijk}$ is the totally anti-symmetric tensor with $\varepsilon_{123} = 1$.

A pseudofermion field is defined like the fermion field to have space $x$, spin $\alpha$ and color $i$ indices but it takes complex values instead of being Grassmann-valued. The scalar product of two pseudofermion fields $\phi$ and $\psi$ is defined as

$$\langle \phi, \psi \rangle = \sum_{x,\alpha,j} \phi_j^{*\alpha}(x)\, \psi_j^{\alpha}(x)\,. \tag{A.20}$$

We remind the useful properties $\langle \phi, \psi \rangle^* = \langle \psi, \phi \rangle$ and $\langle \phi, A\,\psi \rangle = \langle A^\dagger \phi, \psi \rangle$ for any matrix $A$ acting on the pseudofermion fields. The scalar product in Eq. (A.20) can be rewritten as

$$\langle \phi, \psi \rangle = \sum_{x} \mathrm{tr}_{\sigma,c} \left[ \psi(x) \phi^\dagger(x) \right]\,. \tag{A.21}$$

Here, $M = \psi(x)\phi^\dagger(x)$ is a matrix in colour and spinor space with elements $M_{jk}^{\alpha\beta} = \psi_j^{\alpha}(x)\phi_k^{*\beta}(x)$ and $\mathrm{tr}_c$ means the trace over the colour indices and $\mathrm{tr}_\sigma$ the trace over the spinor indices.

## A.3 Probability Spaces

A *probability space* $(\Omega, \mathscr{F}, P)$ consists of a non-empty set $\Omega$, a $\sigma$*-algebra* $\mathscr{F}$ and a *probability measure* $P$ mapping $\mathscr{F}$ onto $[0, 1]$. Hereby a set of subsets of $\Omega$ is called $\sigma$-algebra, if the following three conditions hold:

1. $\Omega \in \mathscr{F}$.
2. $A \in \mathscr{F} \Rightarrow \Omega \setminus A \in \mathscr{F}$.
3. $A_i \in \mathscr{F}$ for $i = 1, 2, \ldots \Rightarrow \cup_{i=1}^{\infty} A_i \in \mathscr{F}$.

For $P$ being a probability measure, $P(\Omega) = 1$ has to hold, as well as $P(\cup_{i=1}^{\infty} A_i) = \sum_{i=1}^{\infty} P(A_i)$ for $A_i$ being pairwise disjoint.

A *random variable* $X : \Omega \to \mathbb{R}^n$ is a measurable function mapping $\Omega$ onto $\mathbb{R}^n$, i.e., $f^{(-1)}(B) \in \mathscr{F}$ for all open sets $B \in \mathbb{R}^n$. Any measurable function $f$ with the property

$$P(A \in \Omega) = \int_{X^{-1}A} dP = \int_A f\, dx$$

for all open set $A \in \mathbb{R}^n$ is called a probability density function.

## Reference

1. M. Lüscher, Commun. Math. Phys. **293**, 899 (2010). doi:10.1007/s00220-009-0953-7